La borsa di dottorato è stata cofinanziata con risorse del
Programma Operativo Nazionale Ricerca e Innovazione 2014-2020 (CCI 2014IT16M2OP005)
FSE REACT-EU, Azione IV.5 “Dottorati di Ricerca su tematiche Green”

UNIVERSITA’ DELLA CALABRIA

Dipartimento di Biologia, Ecologia e Scienze della Terra (DiBEST)

Dottorato di Ricerca in

Life Science and Technology

Con il contributo di

JRS Silvateam Ingredients s.r.l.

CICLO

XXXVII

Studio di sistemi strutturati con fibre alimentari da sottoprodotti della lavorazione di agrumi

Settore Scientifico Disciplinare: ICHI-01/B Principi di Ingegneria Chimica

Coordinatore: Ch.mo Prof. Tommaso Angelone

Firma __ Tommaso Angelone 21.02.2025 18:44:21 GMT+01:00 _____

Supervisore/Tutor: Prof. Domenico Gabriele

Firma_____

Dott.ssa Francesca Romana Lupi, PhD

Firma_____

Dottorando: Dott. Domenico Mammolenti

Firma _____

This thesis presents the results of the research project “Study of structured systems with dietary fiber derived from citrus processing by-products” developed within the framework of the PhD program in Life Science and Technology, XXXVII cycle (Programma Operativo Nazionale Ricerca e Innovazione 2014-2020, risorse FSE REACT-EU, Azione IV.5 “Dottorati di Ricerca su tematiche Green”) from January 1, 2021, to December 31, 2024.

The research was carried out in academic institutions and in an industrial company involved, as partner, in this industrial PhD; particularly, the activities were developed at the laboratory “Reologia e Ingegneria Alimentare” of the University of Calabria (Italy), at the laboratory “Reología Aplicada y Tecnología de Coloides” of the University of Seville (Spain), and at the R&D laboratory of JRS Silvateam Ingredients s.r.l. (Italy).

Study of systems structured with dietary fibers from citrus processing by-products

... to the best of my knowledge ...

ACKNOWLEDGMENTS

I would like to express my gratitude to my wonderful supervisors Prof. Domenico Gabriele and Dr. Francesca Romana Lupi, who with their knowledge and experience have inspired and guided me in this PhD research program. Thank you for encouraging, supporting and helping me to always achieve better results and for giving me the critical judgment skills needed in research.

I would like to extend my special thanks to Prof. José Muñoz for his immense availability during my time at the University of Seville and his contribution in improving my research activity and professionalism, through fruitful discussions.

Thanks also to Dr. Antonio D'Agostino, Dr. Danilo Gaudio and all the other colleges of JRS Silvateam Ingredient s.r.l. for their contribution in broadening my research activity and interests.

I would like to thank Prof. Noemi Baldino for her support during these years and for her contribution in improving the quality of my research work.

Finally, I would like to thank all my colleagues for the special time spent together in the lab, for the chats, the exchange of ideas, for the encouragement and supporting me during these years.

INTRODUCTION

In recent years, due to recent consumers demand, there is a rising interest from both the industry and the academia in developing and applying healthy and naturals ingredients suitable for the formulation of foods products intended for mass marketing. Particularly relevant for their "green" character are the ingredients obtained from the valorization of by-products generated by the food industry itself, such as citrus fiber. Furthermore, it should be highlighted that the growing request by consumers of foods with specific taste and texture has moved researchers to the design of new foods also throughout physicochemical modelling. In light of these observations, the need of a PhD research project on "Study of structured systems with dietary fiber derived from citrus processing by-products" is framed. The research activities were carried out with the aim of providing scientific advancements and contributions concerning the "fundamental research" of systems structured with citrus fiber, from rheological, physicochemical and technological point of view, including process conditions investigation. At the same time, considering the industrial interest of the research program, a part of the research activities had, as a purpose, the improvement of the R&D work linked to products development, by advanced characterization techniques and methods such as rheological and stability analysis.

Specifically, the research activities included both theoretical and experimental studies on systems containing citrus fibers with potential applications in the food field. From a theoretical perspective, a literature analysis was carried out by focusing on the engineering and process aspects of citrus fiber-based systems and on the rheological modeling of composite gels. On the other hand, the experimental activities focused on the preparation and the characterization, by rheological and physicochemical analyses, of hydrogels and emulgels structured with citrus fibers.

The research findings are presented in five chapters. Chapter 1, "Technological advancements of Insoluble Dietary Fiber from food by-product processing: a review," provides an overview of the state of the art and current trends in developing systems containing insoluble dietary fibers (IDFs) from by-products, such as citrus fibers, and the technologies used for their production. Furthermore, selectively introduce the reader to the various general topics covered in the other chapters.

Chapter 2, "Impact of solutes and temperature on rheological and microscopic properties of particle gels from insoluble citrus-derived dietary fiber," discusses experimental results on

monophasic, water-based, systems containing citrus fibers. In particular, the research activities were oriented to deepen the effects of salts on the properties of fiber hydrogels and \to fill the information gap regarding the effects of sweeteners and temperature on the rheology and microstructure of hydrogels structured with insoluble citrus-derived dietary fiber. This chapter was submitted to Food Research International.

Chapter 3, entitled "The rheological modeling of food emulgels: application and insights on the interfacial contribution and estimation of droplets radius", focuses on the preparation and characterization of biphasic systems, specifically emulgels, structured with citrus fiber and on the use of Kerner and Palierne equations for their rheological modeling. Besides the application and validation of Kerner model for food design, the attention was mainly pointed on the contributions of the interfacial properties and on the evaluation of the microstructure.

Chapter 4, entitled "Microfluidized hydrogels and emulgels structured with citrus fiber: effect of processing cycles and channels on rheology and microstructure," reports the study on the connection between microfluidization conditions and rheological properties of monophasic (hydrogel) and biphasic (emulgel) systems containing citrus fiber.

The preparation and characterization of the systems presented in chapters 3 and 4 were carried out in the laboratory "Reología Aplicada y Tecnología de Coloides" of the University of Seville, whereas the study of the model equations, as well as the research which led to chapter 1 and chapter 2, was carried out in the laboratory "Laboratorio di Reologia e Ingegneria Alimentare" of the University of Calabria.

Chapter 5 focused on the potential industrial applications of citrus fiber; this activity was developed at the R&D laboratory of the industrial partner JRS Silvateam Ingredients s.r.l. The chapter is organized in two research units: "Production of homogenized orange juice clean label and source of fiber stabilized by inulin/citrus fiber blends" deals with the application of citrus fiber as a structuring ingredient in monophasic systems; "Assessment of consistency, structuring and stability of clean label vegan mayonnaise stabilized by citrus fiber and plant proteins" discusses the application of dietary fiber in biphasic food systems.

After the conclusions, the thesis ends with the list of conference proceedings and publications to which a contribution was provided during the doctoral period.

CHAPTER 1

Technological advancements of Insoluble Dietary Fiber from food by-product processing: a review

Technological advancements of Insoluble Dietary Fiber from food by-product processing: a review

Domenico Mammolenti, Francesca Romana Lupi*, Noemi Baldino, Domenico Gabriele

Department of Information, Modeling, Electronics and Systems, (D.I.M.E.S.) University of Calabria, Via P. Bucci, Cubo 39C, I-87036 Rende (CS), Italy

Corresponding author

Francesca Romana Lupi, PhD

Department of Information, Modeling, Electronics and System Engineering (D.I.M.E.S.)

Via P. Bucci – Cubo 39C

I-87036 Rende (CS), Italy

Email: francesca.lupi@unical.it

Tel. (+39) 0984 49400

Abstract

Insoluble dietary fibers (IDFs) represent one of the most promising candidates for novel food formulations, since they can be produced from a wide range of food by-products and wastes, have several health benefits, and result in a successful enhancement of the rheology and stability of foods. Recently, the most innovative engineering and processing aspects of these attractive ingredients have received considerable attention. The present work is aimed at enlightening the technological state-of-the-art regarding IDFs (much less investigated than soluble fibers, as discussed in this review). The review begins with a brief but crucial discussion on the definition of this type of dietary fiber by highlighting raw materials, functional properties, physiological activity, and stabilization capacity in food products. The analysis of the rheological methods dedicated to the technical investigations of these ingredients and recent advancements are discussed. Finally, food processing technologies used in the formulation of foods containing insoluble IDFs, such as homogenization techniques, are discussed.

Keywords:

non-starch polysaccharides, food processing, homogenization, rheology, food design

1. Introduction

A particular category of bioactive edible polymers, which has received special attention in recent years for its impact on human nutrition, is dietary fibers (DFs) (Payling et al., 2020). DFs include a large number of biopolymers, not only polysaccharides, with different molecular and supramolecular structures; thus, they exhibit a wide and diversified spectrum of physiological and nutritional features (Payling et al., 2020). It is rather well-known that a proper intake of dietary fiber is associated to positive effects on human nutrition and health, contributing to mitigate the risk of several metabolic diseases, and a number of papers are available in the literature on this topic (Y. He et al., 2022; Quin et al., 2021). From a compositional point of view, DFs are composed of a water-soluble part and a water-insoluble part; therefore, dietary fibers are characterized by two specific fractions, that is, soluble dietary fiber fraction (or "percentage" SDF%) and IDF%, i.e., IDF percentage, yielding as a final result, the total dietary fiber fraction (TDF%) (McCleary, 2003) . The soluble dietary fiber fraction (SDF%) is usually recognized as fermentable, whereas the insoluble dietary fiber fraction (IDF%) is typically non-fermentable or least-fermentable (Quin et al., 2021). The health benefits related to SDF% are a decrease in the cholesterol and glucose levels in the blood and reduction of fat adsorption (Y. He et al., 2022) while that typically associated with IDF% is the improvement of digestion in the gastrointestinal tract (Y. He et al., 2022; Quin et al., 2021).

Different agricultural products, such as cereals, fruit, vegetables, legumes, nuts etc., contain a significant amount of DFs and they are often called "natural source of fibers". People who do not consume enough fruits, vegetables, and cereals are predisposed to follow a low-fiber diet and may incur different health issues (Y. He et al., 2022; Quin et al., 2021). This suggests the possibility of incorporating DFs in foods that do not naturally contain them, that is, foods enriched with fibers, food sources, or advanced foods such as food supplements and nutraceuticals. It is worth noting that there is significant technological interest in using DFs as ingredients in food manufacturing. Indeed, DFs incorporated into foodstuffs may act as texturing agents or more properly as rheological modifiers; for instance, thickening and/or gelling component DFs induce significant enhancement in the consistency and stability of the final products (Fernández-Fernández et al., 2020; Yang et al., 2020). The most attractive raw materials from which DFs can be obtained are typically by-products of the food processing industry (Fernández-Fernández et al., 2020; Pathania and Kaur, 2022). The recovery of functional food components, such as DFs, from food by-products makes a far from negligible contribution to the reduction of food waste, involving economic,

environmental, and ethical upgrading for the food industry worldwide (Pathania and Kaur, 2022).

Dietary fiber incorporation into foods is regulated in the European Union by EU Regulation No. 1129/2011, (European Parliament and Council, 2011) and in the USA by the Code of Federal Regulation Tile 21 parts 172 and 182 (21 CFR Part 172 .Food Additives Permitted for Direct Addition to Food for Human Consumption, 2024). According to EU regulation some dietary fibers like pectin, guar gum and xanthan gum can be considered additives and in most of food preparation and needs to be indicate with an "E number", (European Parliament and Council, 2011) other dietary fibers like wheat fibers, apple fibers and citrus fiber can be considered ingredients and they be simply declared as "fiber" on the nutrition information (European Parliament and Council, 2011), promoting the application of the claim "clean label" (Alexandri et al., 2022) to food products. Typically, DFs designed with E number are rich in SDF% (SDF%/IDF% > 1); therefore, they are typically named soluble dietary fibers (SDFs). On the contrary, DFs that are simply indicated as fibers are typically rich in IDF% (SDF%/IDF% < 1), with some exceptions such as psyllium and inulin, which are almost entirely constituted by SDF% and are typically named insoluble dietary fibers (IDFs). Food with high content of DFs as ingredients not as additives, i.e., with IDFs, inulin or psyllium, can be also claimed as "source of fiber" or "rich in fiber" (European Parliament and Council, 2011). Independently form type of fiber, if SDFs or IDFs, there are several studies and reviews that report the recent advances from a healthy standpoint (Y. He et al., 2022; Payling et al., 2020; Quin et al., 2021). In addition, the sources, extraction, application, and modification methods of the DFs are described in detail (Fernández-Fernández et al., 2020; O'Shea et al., 2012; Pathania and Kaur, 2022).

It is worth mentioning that recently, the technological aspects, such as processing, rheology, and textural properties of SDFs, such as pectin and gums, have been reviewed in detail (Yang et al., 2020). On the contrary, as far as IDFs, such as citrus fiber, wheat fiber, and pea fiber, are concerned, a lack of review work on technological advancements is still present in the literature, although there are a large number of research articles. The present study aims to summarize the most salient technological aspects of IDFs and IDF-based food systems. Specifically, after a general contextualization of IDFs and the due considerations of their composition, source, and role in foods and nutrition, an engineering analysis was proposed by focusing on rheological modification induced by the incorporation of IDFs into foods and on the processing used in the manufacturing of IDF-based food systems.

2. A targeted look at the scientific literature on dietary fiber (DFs)

The theme of dietary fiber has always been a truly interdisciplinary topic, arousing interest in the medical and technological fields. To date, some research areas, such as technology, are becoming more active than others. With the aim of providing a fundamental overview of the state-of-the-art dietary fibers, a simple but targeted bibliometric analysis is proposed. It should be emphasized that the present review is not intended as a systematic literature review or a hybrid review because the preliminary bibliometric analysis is rather general and illustrative, and no specific methodology was used to analyze them in a systematic way. Using Scopus database, a simple query was imposed, "Dietary Fibers" and only research articles and reviews in English language were searched, starting from 1953, date in which the terms "dietary fiber" was first used, to 2025. The number of documents found was more than 54000. By inserting "Insoluble Dietary Fibers" as a query, the total number of documents decreased to approximately 3500, indicating that this subclass of fiber is less investigated. However, other more specific query, for instance linked to fiber type, gives comparable results, in terms of number of documents, such as "Citrus Fiber", "Oat Fiber", "Apple Fiber" which led to approximately 1750, 2800 and 1560 document respectively, or gives even a higher number of papers such as "Wheat Fiber" which gives more than 12000 documents. This indicates that for a more reliable and accurate bibliometric analysis on Insoluble Dietary Fibers the only terms "Insoluble Dietary Fibers" is not a suitable query. This issue is probably mainly due to the widespread practice of using the specific name of the type of dietary fiber rather than general terms, since even by searching for "Soluble Dietary Fibers, only about 5900 documents were found, but also to a lesser extent to the complex matching between the regulations on use and classification and scientific developments. For this reason, the research trends concerning the query "Dietary Fibers" were considered more representative and were used as a rough indicator for the bibliometric analysis of insoluble dietary fibers (IDFs).

In this regard, some specific data on the academic literature are presented in Fig. 1. Looking at Fig.1a, an increase in scientific publications on "Dietary Fibers" appears from 2000 while, form Fig. 1b, it is easy to note that, to date, the most of research works are in "Medicine related subjects" and "Agro-Biology related subjects" while only a few percentages of works concern the "Technology related subject." However, also form Fig.1b, considering different scale of time, 2000-2025, 2015-2025 and 2020-2025 it is possible to observe how the research interest in "Technology related subjects" such as "chemical engineering", "engineering", "chemistry" and "material science" is increasing. From 2000 to 2025 the

whole production of academic literature is around 44216 documents while excluding the research areas not related to technology ("Agricultural and Biological Sciences", "Medicine", "Nursing", "Biochemistry, Genetics and Molecular Biology", "Veterinary", "Immunology and Microbiology" "Pharmacology, Toxicology and Pharmaceutics", "Social Science", "Health Professions", "Neuroscience", "Psychology", "Physics and Astronomy", "Business, Managements and Accounting", "Earth and Planetary Science", "Mathematics", "Economics, Econometrics and Finance", "Dentistry", "Arts and Humanities" and "Decision Science") and by excluding the non-technological keywords ("Animals", "Metabolism", "Animal", "Human", "Nonhuman", "Controlled Study", "Humans", "Male", "Female", "Diet", "Adult", "Intestine Flora", "Nutrition", "Fermentation", "Microbiology", "Genetics", "Animal Experiment", "Gastrointestinal Microbiome", "Physiology", "Mouse", "Mice", "Animal Food", "Middle Aged", "Drug Effect", "Unclassified Drug", "Glucose", "Dietary Intake", "Food Intake", "Feces", "Dietary Supplement", "Dietary Supplements", "Caloric Intake", "Triticum", "Aestivum", "Animal Tissue", "Bacterium", "Aged", "Obesity", "Digestion", "Bacteria", "Enzyme Activity", "Body Weight", "Body Mass", "Blood", "Nutritional Value", "Animal Model", "Pathology", "Rats", "Diet Supplementation", "Cross-sectional Study", "Microbiota", "Fat Intake", "RNA 16S", "Protein Intake", "Mice, Inbred C57BL", "Rat", "Prebiotics", "Growth, Development And Aging", "Swine", "Pharmacology", "Gene Expression", "Nutrients", "Pig", "Microflora", "Microbial Community", "Feeding Behavior", "Mammals", "Cross-Sectional Studies", "Cattle", "Triticum", "Major Clinical Study", "Lipid Diet", "Administration And Dosage", "Drug Effects", "Nutritive Value", "Inflammation", "Cholesterol", "C57BL Mouse", "Biosynthesis", "Young Adult", "Protein Expression", "Animalia", "RNA, Ribosomal, 16S", "Glucose Blood Level", "Probiotics", "Agriculture" and "Bovine") the number of works drastically decrease to 605 documents. However, looking at Fig. 1c it is possible to see that, in proportion the "Effective works on DFs technologies" has a higher percentage of research article with respect to the "General literature on DFs", 91.6% against 84.8% confirming that, nowadays, such fields are the most productive in terms of new research results. Hence, there is a need of new reviews covering the latest advancement.

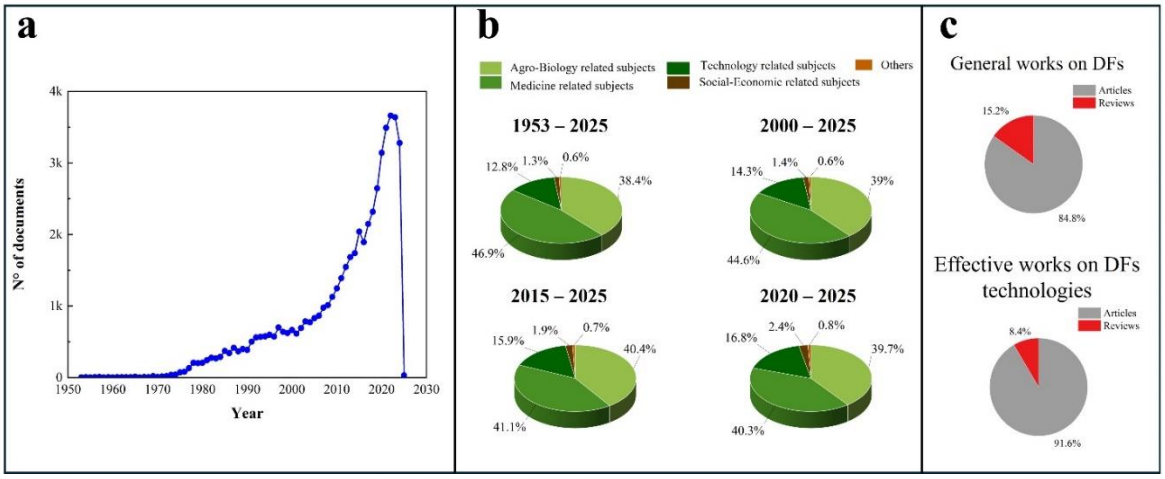

Fig.1. Bibliometric analysis of dietary fibers (a) total paper on DFs, (d) research areas on DFs during years (d) comparison of the ratio of review/article for "General literature on DFs" and for the "Effective works on DFs technologies" in 2000-2025.

3. Insoluble dietary fibers (IDFs) definition: regulatory and scientific background

The term "dietary fiber" was used first by Hipsley (1953) to describe polymeric carbohydrates of the plant cell walls resistant to digestion; this definition received a lot of attention in the following years when it was expanded to include polysaccharides not only coming from cell walls, such as pectin and gums (Lupton, 2010). Despite the concern of both the scientific community and regulatory authorities during the decades, the concept of dietary fiber is still an object of critical reflection (Lupton, 2010).

It is worth noting that it is not easy to define what "dietary fiber" (DF) is because it is not a simple chemical compound, but a combination of different chemical substances (Payling et al., 2020). After a long debate, the "Codex Committee on nutrition and foods for special dietary uses" proposed, in 2009, a comprehensive definition to promote international harmonization for food labelling and to recognize that the definition of "dietary fiber" can be used, independently of the way in which fiber is produced, if physiological benefits are involved (Lupton, 2010). In this definition, the national authorities are given the chance to include carbohydrates from 3 to 9 monomeric units in the fiber definition, and the fractions of lignin and/or other compounds associated with polysaccharides are also considered dietary fiber (foot note of the regulatory of Codex Alimentarius). Other relevant definitions of dietary fibers, more chemically or physiologically detailed, were provided by the European Food Safety Authority (EFSA) and the American Association of Cereal Chemists (AACC), respectively (Board of Directors of the American Association of Cereal Chemists,

2001; EFSA Panel on Dietetic Products, Nutrition, 2016). Although the technological aspects of DFs are connected to SDF%/IDF%, looking at all the definitions of the international authorities, it is possible to see that the distinction between soluble and insoluble fractions of DFs is not considered, which can depend on the method adopted for the determination and they seem not to be strictly related to physiological effects. In light of all these considerations, generally speaking, insoluble dietary fibers (IDFs) can be considered a food ingredient belonging to the dietary fiber category (Board of Directors of the American Association of Cereal Chemists, 2001; Codex Alimentarius, . Guidelines on Nutrition Labelling, CXG 2-1985, 2021; EFSA Panel on Dietetic Products, Nutrition, 2016), characterized by the typical health benefits of IDF% but also, to a lesser extent, by that of SDF% and are often obtained from the revaluation of food processing by-products. In addition, as mentioned above, their usage also promotes the claims "clean label", "source of fiber", and "rich in fiber" (Alexandri et al., 2022; European Parliament and Council, 2011).

4. Source, composition and functionalities of IDFs

Considering the literature, it is interesting to observe how fruit, vegetable, and cereal by-products contain a higher value of IDF% than their respective unprocessed sources (Tejada-Ortigoza et al., 2016). Relevant food processing by-products are peels and pulps from tropical fruits and citrus, tomato and apple pomaces, bran of cereals, and legume hulls because of their high content of IDF% and their commercial volumes (O'Shea et al., 2012). The main fruit, vegetables, cereal, and legume food processing by-products are suitable for IDFs production, i.e., that available on the market due to the large-scale production, and their fractions of soluble (SDF%) and insoluble fiber (IDF%) are reported in Tab.1. Looking at Tab.1, it is interesting to note how the study concerning the extraction techniques, the chemical and functional characterization of IDFs from different commercially relevant sources such as some fruits and citrus processing by-products, were carried out during the first decades of 2000, in agreement with the increasing trend in the number of papers reported in the bibliometric overview disused above. However, other food by-products such as legume hulls received attention more recently (Keskin et al., 2022), indicating that, although deeply investigated and reviewed (Tejada-Ortigoza et al., 2016), the extraction and chemical and functional characterization of IDFs form new food by-products is a still active and attractive research fields. Furthermore, considering Tab.1., it is easy to see that even though the content of IDF% in the plant by-products was higher than that of SDF%, as previously

discussed, IDFs still contained a non-neglectable fraction of soluble biopolymers. From a compositional perspective, IDFs are a complex mixture of macromolecules belonging to the following groups (ordered by relevance): insoluble polysaccharides such as cellulose and hemicellulose, soluble polysaccharides such as pectins, β-glucans, lignin (anchored to the insoluble polysaccharides), and even traces of bioactive compounds (Quin et al., 2021). Concerning the physiological activity of IDFs, the prevalent component is IDF%, but it can also promote secondary liked to SDF% or even to active compounds, such as polyphenol residues in the polymer matrix (Fernández-Fernández et al., 2020). SDF% The IDF% ratio is important for both nutritional and technological properties. As suggested in the literature, to ensure balanced nutritional benefits from both fractions, IDF%/SDF% should be in the range 3:1 to 2:1 (Cui et al., 2019) . The health properties of IDFs, or more generally of DFs, are quite difficult to predict because, on one hand, they are tightly dependent on the physiological actions they exert in diverse levels of the human body; on the other hand, the medical benefits are linked to the complex molecular and supramolecular structure (Payling et al., 2020). Despite these limitations, different simple parameters have been developed with the aim of quantifying some physicochemical behaviors indirectly related to physiological functions (Tejada-Ortigoza et al., 2016). These parameters are commonly known as functional properties. The main functional properties are water-holding capacity (WHC), water-swelling capacity (WSC), and oil-holding capacity (OHC) (Tejada-Ortigoza et al., 2016). The typical values of WHC and WSC are reported in Tab.1, for different categories of IDFs. IDFs can exhibit a quite diversified range of functional properties depending on the kind of vegetable source and the processing they undergo, indeed, for citrus fiber the WHC rages form around 6 to almost 13 mL/g while for cereals by-products it goes from 3 to 3.8 mL/g (Tejada-Ortigoza et al., 2016). Looking at research work in the field of DFs, it is possible to find additional functional properties related to the hydration capacity of DFs, such as the water solubility index (WSI) and bulk density (BD), but the parameters described above (WHC, WSC, and OHC), in agreement with what is reported in the literature, seem to be essential (Tejada-Ortigoza et al., 2016). However, paying attention to the research reported in scientific literature it is worth noting that IDFs are marked with further functional properties more related to their effect on human health and on physiological mechanisms (Y. He et al., 2022). Among these, the glucose adsorption capacity (GAC) and cholesterol adsorption capacity (CAC) deserve mention because of their relevance and effectiveness in mimicking the relative physiological phenomena in vitro (Y. He et al., 2022). Additionally, some authors have reported the functional properties of DFs, such as their gel-forming

capacity and viscosity (Tejada-Ortigoza et al., 2016). Nevertheless, aware of the importance of these properties from a physiological point of view and taking into account the scope of this work, viscosifying and gelling abilities are considered technological properties rather than functional properties, given their key role in food design and manufacturing.

Food by-products	**TDF%**	**SDF%**	**IDF%**	**SDF%/IDF% ratio**	**WHC (g/g)**	**WSC (ml/g)**	**References**
Fruits processing							
Apple pomace var. Royal Gala	78.20	14.33	63.90	1:4.5	1.62	6.59	Figuerola et al. (2005)
Apple pomace var. Granny Smith	60.70	4.14	56.50	1:12.9	1.78	6.89	
Apple pomace var. Liberty	89.8	8.20	81.60	1:9.9	1.87	6.87	
Passion fruit	81.50	35.50	46.00	1:1.3	13.5	7.2	Martínez et al. (2012)
Pineapple	75.80	0.60	75.20	1:125.3	14.6	6.6	
Guava	69.10	11.10	57.70	1:5.2	10.2	1.4	
Mango	70.00	28.20	41.50	1:1.5	6.4	4.6	
Mango peel var. Raspuri	54.90	17.20	37.70	1:2.2	-	-	Ajila and Prasada Rao (2013)
Mango peel var. Badami	72.50	23.00	49.50	1:2.2	-	-	
Cactus pear peel var Rojo San Martìn	45.20	10.60	35.2	1:3.3	-	-	Jiménez-Aguilar et al. (2015)
Cactus pear peel var Verde Villanueva	58.1	17.2	40.9	1:2.4	-	-	
Cactus pear peel var. Rojo Cenizo	50.90	19.3	31.6	1:1.6	-	-	
Cactus pear seed var Rojo San Martìn	93.8	2.60	91.3	1:35	-	-	
Cactus pear seed var	91.2	2.7	88.5	1:33	-	-	

Verde Villanueva							
Cactus pear seed var Rojo Cenizo	86.7	2.4	84.3	1:35	-	-	
Vegetable processing							
Tomato peel	86.10	14.30	71.80	1:5.0	6.86	0.11	Navarro-González et al. (2011)
Carrot pomace	96.20	1.4	94.70	1:67	22.9	-	Yadav et al. (2017)
Sugarcan bagasse	90.82	0.00	90.82	-	17.3	-	
Citrus processing							
Orange bagasse var. Navel	35.40	12.60	22.80	1:1.8	10.02	-	Grigelmo-Miguel and Martín-Belloso (1998)
Orange bagasse var. Salustiana	35.90	13.00	22.90	1:1.8	10.32	-	
Orange bagasse var. Valencia	36.90	11.30	25.50	1:2.3	7.30	-	
Orange peel, bagasse and seed	63.60	17.40	46.20	1:2.7	8.71	-	de Moraes Crizel et al. (2013)
Orange peel	63.70	15.60	48.20	1:3.1	9.63	-	
Lime peel var. C. Aurantifolia	70.40	21.89	48.67	1:2.2	12.84	13.64	Ubando-Rivera, Navarro-Ocaña, and Valdivia-López (2005)
Lime peel var. C. Latifolia	66.70	20.26	46.45	1:2.3	6.96	11.34	
Lemon peel var. Eureka	60.10	9.20	50.90	1:5.5	1.85	7.32	Figuerola et al. (2005)
Lemon peel vat. Fino 49	68.30	6.25	62.00	1:9.9	1.74	9.19	
Oragne peel var. Valencia	64.30	10.28	54.00	1:5.3	1.65	6.11	
Cereal processing							
Wheat bran	45.50	2.80	41.7	1:14.9	-	-	Vitaglione, Napolitano,
Rye bran	35.80	5.30	30.50	1:5.8	-	-	
Oat bran	21.70	4.30	17.40	1:4.0	-	-	

							and Fogliano (2008)
Corn bran	96.54	4.09	92.44	1:22.6	32.8/74.3	-	Yadav et al. (2017)
Wheat bran	92.03	0.00	92.03	-	13.9	-	
Wheat straw	97.55	0.00	97.55	-	23.7	-	
Rice fiber	98.63	0.00	98.63	-	6.4	-	
Barley hulls	102.65	4.15	98.51	1:23.7	13.8	-	
Barley straw	104.41	6.84	97.57	1:14.3	21.4	-	
Legume processing							
Bean hull	77.35	5.56	71.79	1:12.9	3.4	-	Keskin et al. (2022)
Chickpea hull	84.18	6.50	77.61	1:11.9	3.7	-	
Cowpea hull	70.86	1.08	69.78	1:64.6	3.8	-	

Tab.1. Food by-products sources of IDFs: $IDF_{\%}$, $SDF_{\%}$ and $TDF_{\%}$ (the slight differences between the sum of $IDF_{\%}$ and $SDF_{\%}$, and the total quantity $TDF_{\%}$ is due to experimental error), fiber fractions, water holding capacity (WHC) and water swelling capacity (WSC).

5. IDFs as rheological modifiers in food systems

Despite the differences in composition, from a physical point of view, IDFs aqueous systems can be conceptualized as complex heterogeneous mixtures, that is, a suspension of solid hydrated particles dispersed in a continuous matrix buildup of a diluted polymer and/or oligomer solution, where a network of particles and polymer entanglements are also present. Generally, IDFs in water can generate suspensions or particle hydrogels, as shown in Fig.2. depending on the particle size, composition, amount, and processing conditions (Bruno et al., 2021; Gidley and Yakubov, 2019; Wang et al., 2024). In multiphase systems such as O/W systems, IDFs can generate structured emulsions such as emulgels or bigels (Bruno et al., 2024, 2022) if the continuous phase is a particle hydrogel or a Pickering emulsion if the dispersed phase is composed of oil droplets surrounded by adsorbed small particles (He et al., 2020b; Qi et al., 2021). Consequently, in any case, IDFs act as rheological modifiers in the first case by forming a gel network, whereas in the second by surrounding the droplets, making the systems thicker (Fig. 2). The reduction of droplet mobility due to structuring and/or the interfacial action due to the Pickering effect involved in the incorporation of IDFs significantly contributes to the improvement of the physical stability of food (Dickinson, 2013; Yang et al., 2020). The rheological properties of such complex heterogeneous systems

are severely influenced by a wide range of peculiar factors, such as the amount and size of the hydrated dispersed particles (Gidley and Yakubov, 2019) as well as the shape and deformability of the particles (Moelants et al., 2014), oil phase composition, amount, distribution, and rheology (Dickinson, 2013; McClements, 2016). Beyond the classical parameters that typically affect the rheology of heterogeneous materials, that is, shear rate and temperature, all the aforementioned parameters should be considered when describing IDFs as rheological modifiers (Moelants et al., 2014). In this section, after a brief discussion on the stability action due to the rheological modification induced by IDFs incorporation, a basic discussion on rheological measurements and modeling, typically used for the description of food suspensions, hydrogels, and structured emulsions containing IDFs, is proposed. Finally, some significant examples of studies on the viscosity and gelling ability of IDFs are briefly discussed.

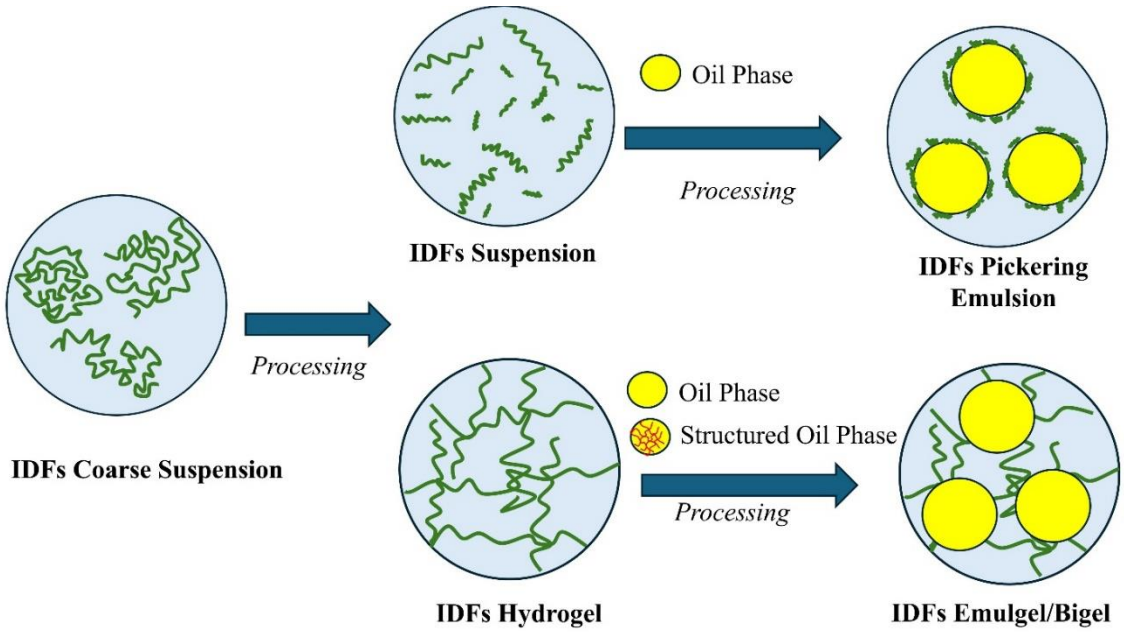

Fig. 2. Structuring/stabilization action of IDFs in O/W systems.

5.1.Stability of food systems structured with IDFs

Since IDFs act as rheological modifiers, their inclusion in foods such as creams, dressings, mayonnaise, or other multiphasic food systems allows an increase in structuring and a consequent improvement in the physical stability of the product (Guo et al., 2021; Pathania and Kaur, 2022). Typically, the methods mainly employed for studying the stability of multiphase food systems range from direct to indirect. For instance, methods ranging from visual assessments at the macroscopic scale to the evaluation of the surface/interface interactions, to the changes in droplet size with time, passing from rheological investigations

and morphological observations (McClements, 2016) can be employed in the study of the stability of emulsion-type systems. To date, scientific research aimed at verifying the suitability of IDFs in enhancing the stability of multiphase food systems has taken advantage of a very large number of characterization techniques and parameters; therefore, it is arduous to summarize in detail singularly. In addition, the stabilization ability of IDFs depends on the dispersed phase volume fraction, pH, temperature, and salts, as well as the fiber concentration and size (He et al., 2020a; Qi et al., 2021). To summarize the most advanced parameters and techniques used for stability assessments of multiphase systems stabilized by IDFs, a guide is provided in Tab.2.

Stability parameters	Symbol	Technique used	References
Surface diameters, over time	$D_{3,2}$	Laser diffraction, Dynamic light scattering	He et al. (2020a)
Volume diameter, over time	$D_{4,3}$	Laser diffraction, Dynamic light scattering	K. He et al., (2020); Qi et al., (2021)
Emulsion index	EI%	Visual inspection	K. He et al. (2020)
Theoretical surface coverage	C	Coupling different methods	K. He et al. (2020)
ζ-potential	ζ	Electrophoretic laser doppler	Qi et al. (2021)
Emulsion stability index	ESI	Dynamic light scattering	Qi et al. (2021)
Interfacial tension	γ	Contact angle, pendant drop	Bruno et al. (2022); Gao et al. (2022)

Tab.2. Parameters typically used in the assessment of physical stability of multiphase systems structured with IDFs.

5.2.Investigation tools in the rheology of food systems structured with IDFs

The study of rheological properties in IDF-based food systems is important for tuning their texture and consistency.

As highlighted by Moelants et al. (2014), rheological tests and modeling represent a successful way to determine the connection between the process, structure, and functionality in IDF-based food systems. The rheological investigation typically adopted to describe the flow properties of such materials is the steady-state flow test, (Barnes et al., 1989) whereas for the viscoelasticity study, dynamic oscillatory shear measurements typically in the small-amplitude regime are used. However, other types of tests are also suitable for particular. The most suitable type of instruments for the rheological characterization of IDF-based systems are rotational rheometers, which are typically equipped with parallel plates (both serrated or

smooth) or cylindrical geometry, or with special geometries, such as vanes, to overcome practical measurement limits connected to intrinsic issues of some samples.

Rheological models are widely used to study food systems structured with IDFs. It was found that several suspensions and hydrogels based on plant tissues, agricultural wastes, by-products, (Huang et al., 2020; Moelants et al., 2014) or more complex food systems, such as pickering emulsions (He et al., 2020a; Qi et al., 2021), and yogurts (Chen et al., 2023; Du et al., 2023), typically exhibit a shear thinning flow behavior that can be described by the power law model, Eq.1 or by the Herschel-Bulkley model (Moelants et al., 2014; Su et al., 2020a), Eq.2, although other equations were used sporadically to describe viscosity (Su et al., 2020a).

$$\tau = K \cdot \dot{\gamma}^n \tag{1}$$

$$\tau = \tau_0 + K \cdot \dot{\gamma}^n \tag{2}$$

where K (Pa sn), n (−), and τ_0 (Pa) are the consistency, flow index, and yield stress, respectively (Barnes et al., 1989). Concerning viscoelastic properties, the rheological characteristics of IDF-based food systems, such as suspensions, hydrogels, pickering emulsions, emulgels, and bigels, can be related to the microstructure of the network through the weak gel model, Eq.3 (Gabriele et al., 2001; Lupi et al., 2020).

$$G^* = \mathrm{A} \cdot \omega^{\frac{1}{z}} \tag{3}$$

where A (Pa sz) and z (-) represent the network strength and the number of rheological units interacting within, respectively (Gabriele et al., 2001). In addition, the viscoelasticity of hydrogels and suspensions structured with IDFs from citrus were recently modelled by a microrheological model already adopted for fats, assuming a fractal microstructure (Bruno et al., 2021; Tang and Marangoni, 2006).

$$G' = \lambda \cdot \phi^{\frac{1}{3-D}} \tag{4}$$

where λ is a constant (Pa) related to the interactions between primary fractal flocs, ϕ (dimensionless) is the particle volume fraction, and D (dimensionless) is the fractal dimension (Bruno et al., 2021). Recently, multiphase systems containing IDFs were modelled from a rheological point of view. Specifically, emulgels and bigels structured with citrus fibers were modelled (Bruno et al., 2024, 2022) using equations derived from the Palierne theory of composite gels by linking the complex viscoelastic modulus (G^*) to the composition and microstructure.

5.3.Viscosifying ability of IDFs

The viscosity improvements induced by the incorporation of IDFs into food depend mainly on fiber type, concentration, processing technology, and conditions. The flow properties of several suspensions of vegetable pulp and dried fibers were studied using cylindrical geometries. The results showed a higher flow index (n) and lower consistency coefficient (K) for dried fibers than for vegetable pulps. Furthermore, K increased with concentration, while n decreased (Bayod et al., 2005). Moelants et al. (2013) studied the flow behavior of carrot pulp suspensions using a six-bladed vane and found that both viscosity and viscoelasticity increase with increasing fiber concentration. They proposed a power-law type relation (Eq.5) for the dependence of yield stress on the pulp content.

$$\sigma_0 = a\ (pulp\%)^b \quad (5)$$

where σ_0 (in Pa) is the yield stress, pulp% is the pulp percentage, and a and b are the fitting parameters. In addition to the effects of concentration, most viscosity investigations are concerned with changes in the flow behavior induced by processing. Redgwell et al. (2011) investigated the viscosity of citrus fiber suspensions by varying the extrusion process parameters (and fiber concentration). Shear-thinning behavior was observed, and an increase in process energy led to a decrease in viscosity. Furthermore, the viscosity of the systems was correlated to the concentration of fibers through an exponential function characterized by a critical concentration value, which is strictly influenced by the process conditions, beyond which the viscosity increases sharply. The effect of pressure, provided by high pressure homogenization, on orange pulp suspensions (4% w/w of dried fiber) was studied by Van Buggenhout et al. (2015) by measuring the viscosity using the coaxial cylinder and vane geometries and modeling them the Herschel-Bulkley model. The authors observed an increase in the yield stress by increasing the homogenization pressure. By studying the effect of pressure on sugar beet pulp (2 g/100 mL), an increase in apparent viscosity, which followed a power law relation with the shear rate, was observed with increasing homogenization pressure (Huang et al., 2020). On the contrary, a decrease in the yield stress and consistency coefficient following the effect of homogenization pressure was found for lily pulp suspensions (Liu et al., 2019). Although the shear-thinning response is the most common behavior of IDFs suspensions and hydrogels, some contrasting results can be found in the literature, as observed by Daou and Zhang (2014). Specifically, they tested the different fractions of fibers extracted from the defatted rice bran and observed a shear thickening behavior for both the total, the insoluble, and the soluble fractions at two levels of concentrations 1 and 3% w/w.

5.4. Gelling ability of IDFs

As for the viscosifying effect, the gelling properties of IDFs are strictly related to the raw material from which the fiber is obtained, the concentration, and the process used to modify and incorporate it into foodstuffs. Bengtsson et al. (2011) investigated the impact of heat treatment on the rheological properties of insoluble dietary fiber (CLDF) suspensions from potato, apple, and carrot, focusing on β-elimination and de-esterification to control pectin content. Using stress sweep tests, they assessed the elastic and viscous moduli and the stress values at specific points in the linear region. All suspensions (3% w/w insoluble material) exhibited solid-like behavior, with results showing that rheological properties were influenced more by the fiber source than by heat treatment. Willemsen et al. (2017) studied the effect of residual pectin in lemon peel fibers on suspension rheology. They sequentially solubilized pectin with various solvents and removed acid, producing four suspensions (2% w/w) with varying pectin content. Frequency sweep tests revealed strong gel behavior with moderate stiffness in high-pectin-depleted suspensions, showing enhanced viscoelasticity compared with the typical weak gel structure. Concerning the dependence of viscoelastic properties on concentration, several interesting results were obtained by different authors, (Huang et al., 2020; Lupi et al., 2020; Moelants et al., 2013) and even an empirical relation was proposed (Moelants et al., 2013). Indeed, in addition to modeling the linear viscoelastic behavior of a carrot suspension using the weak gel model, Moelants et al. (Moelants et al., 2013) proposed a power law correlation (Eq.6) to relate the effect of the pulp content on the dynamic elastic shear modulus, according to a model quite similar to the fractal one.

$$G' = c\ (pulp\%)^d \tag{6}$$

where G' (Pa) is the elastic shear modulus, pulp% is the pulp percentage, and c and d are the fitting parameters. Dynamic oscillatory shear tests have been widely used to assess the effects of processing technology and conditions on the microstructure of IDF-based systems. The effect of high-pressure homogenization on the viscoelasticity of the orange pulp suspension was investigated by measuring the dynamic moduli as a function of strain (strain sweep test) of orange pulp suspensions (Van Buggenhout et al., 2015). A strong correlation between the particle size and viscoelastic properties was found. The effect of process conditions on the rheological properties of citrus fiber particle gels produced via high-speed homogenization has also been extensively studied (Lupi et al., 2020). In particular, increasing the mixing intensity, in terms of power and energy, strengthened the fiber network, although very high values of energy or power did not improve the gel network. The changes in linear viscoelastic behavior due to different types of dispersion methods, that is,

high-speed homogenization and microfluidization, on the linear viscoelastic behavior of citrus fiber hydrogels were also studied, reporting that both rheology (elastic modulus, G', and phase angle δ) and particle size are strictly dependent on the type of technique (Bruno et al., 2021).

Recently, rheological tests in linear region were proven to be effective also in the investigation of the effects of IDFs addition on the viscoelastic properties and gelation process of other food components in complex food formulation, like in IDFs addition to yogurts (Chen et al., 2023; Du et al., 2023). In particular, improvements in viscoelastic properties in terms of G' and G" and in casein gelation mechanism can be obtained by using IDFs form differ sources, however the improvements as well as the drawbacks, such as the hindrance to gelation process, resulted strictly related to composition and to the preparation procedure adopted (Chen et al., 2023; Du et al., 2023).

In addition to rheological investigation in the linear viscoelastic region (small amplitude oscillation test (SAOS)), rheological tests in nonlinear regions (large amplitude oscillatory shear (LAOS)) were used to study IDF-based suspensions. Su et al. (2020b) examined the viscoelasticity of citrus fiber suspensions viscoelasticity through LAOS tests. Using Fourier transform and Chebyshev stress decomposition, they identified two response types (Types I and III), with the third harmonic being stronger than the fifth. Elastic behavior dominated at low strains, transitioning to viscosity dominance at higher strains. Chebyshev analysis showed strain-stiffening at low concentrations, with strain-softening occurring as concentration and strain increased. Homogenization shifted the behavior from shear thinning to shear thickening. Huang et al. (2020) applied a similar approach to sugar beet pulp suspensions, finding that non-homogenized samples exhibited reduced G', while homogenized samples showed a strain overshoot. Lissajous curves revealed that untreated samples were elastic-dominated up to 105% strain, whereas homogenized samples became viscous-dominated at 33% strain. Additionally, processing pressures above 50 MPa shifted the behavior from soft to hard gel, demonstrating how processing affects viscoelastic properties.

6. Processing of food systems with IDFs

Processing methods play a crucial role in the preparation of IDF-based food systems such as suspensions, hydrogels, emulgels, and bigels. They are typically processed using high shear–dispersion methods. The dispersion action beyond suspending food particles may cause

changes in the particle structure. Indeed, many studies have reported the influence of dispersion methods on the properties of the fibers (Gan et al., 2021). For this reason, a given technique can be used to directly prepare IDF-based food, as well as to modify the fiber or even the starting by-product. Therefore, in the first case, it can be considered a self-standing preparation method, whereas in the latter case, it can be considered as a mechanical pretreatment. In light of these assumptions for each processing technology, the dispersion method, strategy, and conditions used are highlighted. According to the literature, it is possible to conclude that among all the high shear dispersion techniques, there are some of greater relevance, as shown in Fig.3.

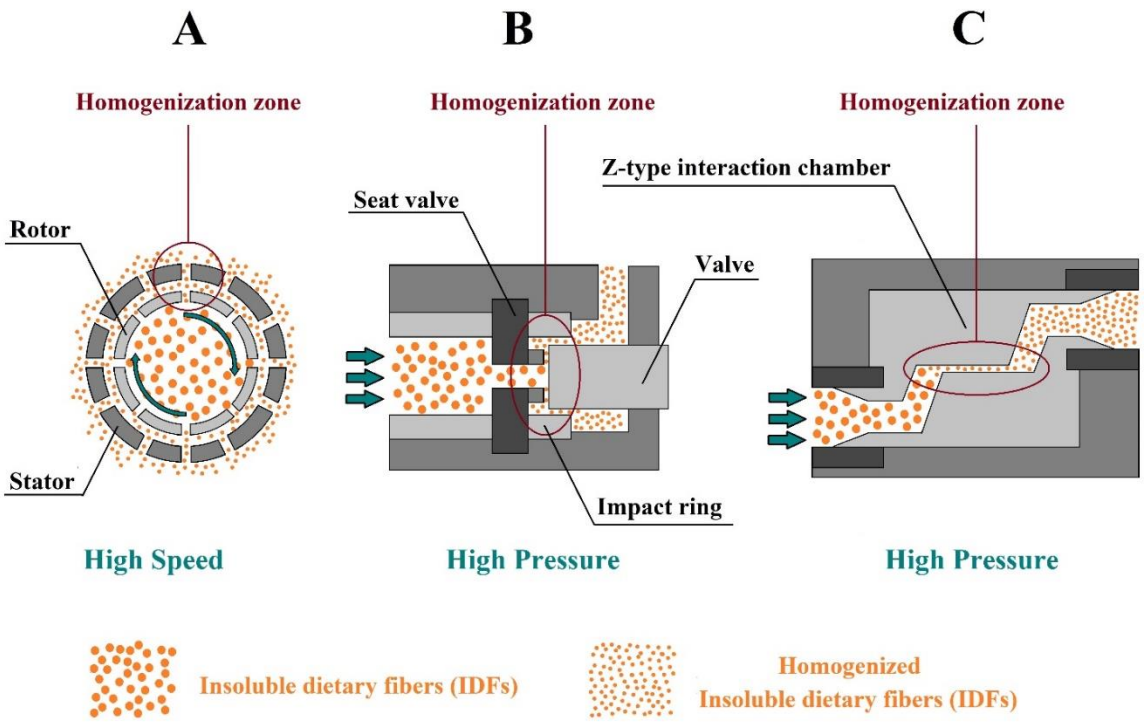

Fig. 3. Working principle of homogenization methods in IDFs processing: (A) high speed homogenizer (HSH), (B) high pressure homogenization (HPH) and (C) dynamic high pressure microfluidizer (DHPM).

In particular, high-speed homogenization (HSH), high-pressure homogenization (HPH), and dynamic high-pressure microfluidization (DHPM) appear to be the most suitable ways to effectively process and modify IDF-based food systems (Gan et al., 2021). Some of these processes can be coupled to achieve optimal preparation, generating a multistep protocol. In addition to the aforementioned homogenizations, extrusion cooking seems to be a more

feasible method for processing IDF-based products (Wolf, 2010). Although less used than homogenization, extrusion cooking of IDFs has received little attention for a long time (Wolf, 2010). In addition, in order to maintain an exhaustive approach, the novel but still pioneering methods of dispersion, successfully adopted for processing IDFs-based systems, will be included in the present section. In the following paragraphs, only some significant recent works, considered particularly representative, will be discussed by highlighting the role of process variables on the properties of IDFs and IDF-based systems. Examples of processing protocols that exploit one or more techniques used for the preparation of IDF-based food systems are reported in Tab.3. From Tab.3, it is easy to observe how IDFs were processed using different methods for a wide range of final food purposes. It is also interesting to note that in addition to nutritional and chemical characterizations, there is a significant tendency to use rheology in both process investigations and product design.

IDFs	**Food product**	**Technological and physiological assessments**	**Processing methods**	**References**
Sugar beet fiber	Meat emulsion model	Viscosity, viscoelasticity, rheological modeling, texture profile	HSH (2250 rpm, 10 s + addition of oil + 5s)	Ağar et al. (2016)
Okara fiber	3D-printed cookies	Viscosity, viscoelasticity, texture analysis, functional properties, stability studies	Ultrasound (400-600 W, 30 min) HPH (5000-15000 rpm, 10 min), 3D-printing	Y. Liu et al. (2021)
Sweet corn Fiber	Whole sweet corn suspension	Viscosity, physical stability, Phenolic compounds, *in-vitro* antioxidant activity	Industry-scale microfluidization (60, 09, 120 MPa)	Guo et al. (2021)
Bamboo, acacia, potato, and citrus fiber	Processed cheese sauces	Viscosity, viscoelasticity, texture analysis,	HSH (1118 g, 2 + 10 min)	Szafrańska and Sołowiej (2020)
Pumpkin, carrot, green pea, and zucchini purees	Fiber-enriched yogurt	Physical-chemical profile, *in-vitro* antioxidant activity, texture analysis	Homogenization + Homogenization for yogurt production (60°C, 50 bar)	Yildiz and Ozcan (2019)
Oat bran	Acid-Milk gel model	Microstructure, functional properties, viscosity, texture	Enzymatic reaction + cooking extrusion + microfluidization + mixing	Rosa-Sibakov et al. (2022)

Grape pomace fiber	Cassava-soy-Gape pomace fiber composite food model	Viscosity, *in-vitro* digestibility studies, phenolic compounds, *in-vitro* antioxidant activity	Extrusion-cooking (60-140°C, 200rpm)	Oladiran and Emmambux (2018)
Apple pomace fiber	Fiber-enriched yogurt	Soluble/insoluble fraction	Mixing/homogenization (conditions not specified)	Issar, Sharma, and Gupta (2017)
Orange Fiber	Ice cream	Physical and functional properties, chemical profile	Homogenization in batch processing plant (conditions not specified)	de Moraes Crizel et al. (2013)
Citrus Fiber	O/W food emulgel model	Viscoelasticity, interfacial properties, modeling of the viscoelastic properties	HSH (5000-10000 rpm, 180-800 s)	Bruno et al. (2022)
Citrus Fiber	O/W food bigel model	Viscoelasticity, modeling of the viscoelastic properties	HSH (2000 rpm, 120-240 s) + HSH (5000 rpm, 180-360 s)	Bruno et al. (2024)
Tomato fiber	Ketchup-like tomato sauce	Viscosity, Viscoelasticity	HSH (3400-14000 rpm, 12 min), HPH (0-10 MPa, 0-10 cycles)	Y. Wang et al. (2018)
Tomato fiber/wheat fiber	Pimento Purée	Viscosity, thixotropy, texture analysis, functional properties	HSH (1500 rpm)	Cepeda and Collado (2014)

Tab.3. Processing and characterizations of IDFs-based foods systems

6.1. High-speed homogenization (HSH)

High-speed homogenization (HSH), also known as rotor-stator homogenization (RSH), is a widely used technique in food processing to disperse, emulsify, and mix food ingredients and vegetable matrices (Håkansson, 2018). Research indicates that HSH is often employed as a pre-dispersion step in the preparation of IDF-based food systems, even if in some cases both suspension-type and emulsion-type food matrices can be prepared solely by HSH, demonstrating satisfactory quality and stability (Tab.3).

The effects of power and energy on the rheological and microstructural properties of citrus fiber suspensions were extensively studied by Lupi et al. (2020). They investigated the relationship between the operational parameters (speed and time) and the power of HSH using calorimetric methods. Homogenization was conducted under isoenergy (16.2 kJ/kg)

and isopower (22 and 54 W/kg) conditions. Rheological and microstructural analyses showed that gel strength increased with both mixing power and energy. The extension of the network seemed largely independent of the process conditions, although a slight reduction was noted with increasing fiber concentration. A subsequent study by the same group used different HSH devices and compared them to dynamic high-pressure microfluidization (DHPM), yielding consistent results and confirming the effectiveness of the approach for dispersing IDFs (Bruno et al., 2021).

Response surface methodology was employed to study the effects of homogenization speed and time on the chemical and physical properties of pulp from bael fruit (Aegle marmelos L.) (Kamble et al., 2022) treated with HSH. Using parameters such as color, total soluble solids, β-carotene, ascorbic acid content, and viscosity, optimal conditions were found to be 10700 rpm and 43 min of homogenization.

Wang et al. (2018) prepared tomato fiber suspensions at varying concentrations (0.1% - 1% w/w) using HSH at speeds ranging from 3400 to 14000 rpm for 12 min. Both HSH and high-pressure homogenization (HPH) at moderate pressure (0-10 passes and 0-10 MPa) improved the physicochemical properties and consistency of the suspensions. HPH was slightly more effective, leading to a tomato sauce comparable in quality to that of commercial ketchup.

High-speed homogenization was particularly effective for the preparation of multiphasic systems structured with IDFs, such as Pickering emulsions, emulgels, and bigels (Bruno et al., 2024, 2022; He et al., 2020a) or processed cheese sauces (Szafrańska and Sołowiej, 2020).

6.2. High-pressure homogenization (HPH)

High-pressure homogenization (HPH) is a nonthermal, continuous process commonly used in the food industry for various purposes (Betoret et al., 2015), including the preparation of IDF-based food systems. It is often employed alone or in combination with mechanical pretreatments, such as high-speed homogenization (HSH), to create refined products. HPH has become the primary method for preparing IDF-based foods, as demonstrated by numerous scientific studies.

Van Buggenhout et al. (2015) examined the effects of different pressures in HPH on the physical, chemical, and functional properties of orange pulp suspensions. They compared samples processed by homogenization at 200 and 800 bar and simple blending. While the homogenized suspensions had a better appearance, the functional properties did not change

significantly compared to the blended samples. However, HPH notably affected the rheological behavior, increasing consistency and reducing the particle size from 409 to 49 μm. J. Liu et al. (2019) improved the stability of lily pulp suspensions by using HPH. After pretreatment of the pulp with a domestic blender and homogenization at various pressures (0 to 100 MPa), they observed reduced particle size, narrower distribution, improved physical stability, and increased total soluble solids. The process also significantly decreased the yield stress and consistency coefficient, while increasing the flow index as the pressure increased. Castro et al. (2013) prepared IDF-based suspensions from yacon roots using HPH after knife milling pretreatment. The HPH process, performed at 90 bar over multiple cycles, produced stable suspensions, demonstrating the effectiveness of the process for treating different fiber sources. Suspensions made from apple, tomato, potato, and carrot fibers were also processed using HPH by Bengtsson and Tornberg (2011). These suspensions, at concentrations of 0.8% and 1.2% w/w, were pretreated with a food processor before HPH at 90 bar. The study showed that different fiber types and concentrations require varying levels of treatment to achieve the desired consistency and particle size.

Many studies highlight the need for a pre-treatment step, especially when starting from solid or pulp-like raw materials, to avoid the blockage of systems and to work with more contracted matrices. High-speed homogenization (HSH) is commonly used before HPH to create treatable food matrices. For example, Su et al. (2019) prepared citrus fiber suspensions using a combination of HSH and HPH. After pretreatment with HSH for 2 min, the suspensions were further processed using HPH at pressures of 90 and 160 MPa over three cycles. Mechanical treatment improved both the microstructural and functional properties of the fibers. Although suspensions were obtained and characterized even bypassing HSH (Su et al., 2020b), some limitations for high (3% w/w) and low (2% w/w) concentrations were observed. Lemon peel fibers obtained through various extraction methods were processed using HSH, followed by HPH (Willemsen et al., 2018, 2017). In these studies, the suspensions were first dispersed with HSH at 8000 rpm for 10 min and then homogenized with HPH at pressures of 20 MPa and 80 MPa. The pretreatment steps, combined with HPH, significantly altered the fiber properties, including their behavior in response to pH and salt. Juric et al. (2019) treated tomato peel suspensions with HSH at 20000 rpm for 5 min and sieved them before homogenization with HPH at 100 MPa over multiple passes. This combination of mechanical treatments was successful in producing suspensions with improved physicochemical properties, leading to tomato-based products with qualities comparable to those of commercial ketchups. Sugar beet pulp suspensions were processed

using HPH after pretreatment with HSH (Huang et al., 2020). The suspensions, with a 2% w/w concentration, were homogenized at various pressures (0 to 100 MPa) for three cycles. The authors observed significant changes in the microstructural and functional properties of the fibers as a function of pressure. Soybean hull residues were used to create IDF-based suspensions using a sequential procedure of HSH, followed by HPH (Colletti et al., 2020). After pre-homogenization, the fibers were treated with HPH at pressures ranging from 300 bar to 1000 bar over three cycles. The study found that varying pressure affected the fiber properties, such as the particle size and functional attributes, leading to suspensions with distinct rheological characteristics.

Ball milling is another common pretreatment method used before HPH to reduce the size of IDFs powders. Yin et al. (2021) processed soybean okara fiber by ball milling before suspending it in water and treating it with HPH. Similarly, Jiang et al. (2022) used ball milling to prepare citrus fibers, which were then homogenized using HPH at 60 MPa and 100 MPa over four cycles. Both studies demonstrated that the combination of ball milling and HPH improved the microstructural and functional properties of the fibers. Van Audenhove et al. (2022) treated tomato fibers using cryogenic ball milling, followed by HSH and HPH. The cryogenic milling process caused a collapse of the fiber microstructure, but the HPH step restored some of the desired properties, such as the re-functionalization of the fibers. Huang et al. (2020) explored the use of two different size reduction methods before HPH for sugar beet pulp fibers. After reducing the particle size with high-speed multifunction milling and micronizing the powder, the suspensions were treated with HPH at pressures ranging from 0 to 100 MPa. The study found that low-pressure treatments led to fiber aggregation, but higher pressures significantly reduced the particle size and improved the rheological properties. Apart from hydrogels and suspensions, HPH is also a particularly suitable technique for the preparation of more complex food systems structured with IDFs such as Pickering emulsions (Qi et al., 2021) or yogurts (Chen et al., 2023; Yildiz and Ozcan, 2019).

6.3. Dynamic high pressure microfluidization (DHPM)

Dynamic high-pressure microfluidization (DHPM), also known as microfluidization, is an advanced homogenization technique in which a fluid is forced through microchannels in an interaction chamber and subjected to high-speed impacts, high-frequency vibrations, cavitation, and instantaneous pressure drops (Guo et al., 2020) (Fig. 3C). This technology is emerging in the food processing industry and shows promise in modifying food

macromolecules and creating fiber-based food products. Although less established than other methods, such as high-pressure homogenization (HPH) or high-shear homogenization (HSH), DHPM has shown significant potential in preparing IDF-based food systems and improving fiber functionality in food products (Guo et al., 2020).

In recent studies, citrus fiber hydrogels were prepared using DHPM, which demonstrated improved consistency and stability compared to other methods (Bruno et al., 2021). Coarse suspensions were initially processed using HSH at 500 rpm for two minutes and then microfluidized through two Z-type microchannels at 1020 and 1700 atm. This process reduced the particle size and improved the hydrogel quality, particularly in terms of the storage modulus, which is a measure of consistency. A comparison of DHPM with HSH alone revealed that DHPM produced samples with a lower phase angle, indicating better dispersion and stability. However, limited processability has been found for concentrated systems. A study by Zhu et al. (2018) demonstrated that the addition of soybean oil during DHPM processing improves the physical properties of citrus fiber powder. After mixing the fibers with oil and water using HSH, the coarse emulsion was processed via DHPM at 90 and 160 MPa for two cycles. This process significantly reduced the particle size and bulk density and increased the porosity of the fibers. Additionally, DHPM preserves the flowability of the modified powder, which is essential for various food applications. Further studies, such as those conducted by Serial et al. (2021), have explored the microstructure and rheological behavior of citrus fiber suspensions processed through DHPM. Using methods such as small-angle X-ray scattering (SAXS) and rheo-MRI, the authors were able to analyze how different process conditions affected the short-range order and microfibrillar network of the fiber. They found that while DHPM influenced the fiber structure at the micro level, the cross-sectional size of the individual microfibrils remained intact, indicating that the integrity of the fibers was preserved even under high pressures of microfluidization. The cooperative flow of microfibril flocs, observed during low-shear conditions, further highlighted the enhanced functional properties introduced by DHPM. Chen et al. (2013) investigated the use of DHPM to enhance the properties of dietary fiber derived from peaches and oats. Both the peach pomace and commercial oat fibers were dispersed in water and processed using DHPM at 120 MPa for a single cycle. The resulting freeze-dried powders exhibited improved physicochemical properties, solubility, and functional characteristics compared to the native fibers. This demonstrates the versatility of DHPM in modifying dietary fibers from various sources, making it more suitable for use in fiber-enriched, low-calorie food formulations. Further studies by Morales-Medina et al. (2020) examined the

effect of microfluidization on pea hull fibers with varying particle sizes. To obtain the desired particle size distribution, the fibers were ground and fractionated before microfluidization. After pre-treating the coarse suspensions with DHPM at pressures of 2000 bar using a Z-type interaction chamber (200 μm), to avoid blockage of channels, the authors found that multiple cycles of microfluidization through a series of two Z-type interaction chambers (200 and 100 μm) significantly improved the nutritional and functional properties of the fibers and the rheological behavior in the optics of food applications.

On a larger industrial scale, DHPM has been used to modify pea fibers in a continuous process, as described by He et al. (2022). An industry-scale microfluidizer equipped with a pre-pulverizing unit processed high volumes of pea fiber suspensions at pressures of 60, 90, and 120 MPa. The final product, freeze-dried for analysis, showed significant improvements in morphology, microstructure, and functional properties. Microfluidization reduced the crystallinity and particle size of the fibers while enhancing their hydration and oil-holding capacities. This suggests that DHPM can be effectively scaled up for industrial food processing, maintaining its capacity to enhance the nutritional and functional qualities of dietary fiber. In addition to enhancing the functional properties, DHPM has been shown to improve the adsorption capacity of rice bran insoluble dietary fibers for heavy metals (Wu et al., 2021). They found that higher pressures (up to 150 MPa) resulted in greater adsorption of heavy metals under physiological conditions. This indicates that microfluidization could also be useful for food safety applications, particularly for removing or reducing harmful substances from food ingredients. In addition, DHPM was successfully employed for the preparation of more complex food-type systems containing IDFs, such as the acid-milk gel model (Rosa-Sibakov et al., 2022).

6.4. Extrusion-cooking

Extrusion is a widely used technology in both polymer processing and the food industry, particularly the latter, which is more commonly known as extrusion cooking (Wolf, 2010). This process combines mechanical energy and heat to modify the feed matrix, which enhances the properties of food products. Most of the research on extrusion cooking focuses on SDFs such as gums; nevertheless, its effects on IDFs have also been explored. Studies have shown that extrusion cooking can increase the soluble fraction and viscosity of IDFs such as citrus fibers, onion residues, and sugar beet pulp, without causing significant thermal degradation. This suggests that extrusion cooking can improve the functional properties of these fibers (Wolf, 2010).

A key study conducted by Redgwell et al. (2011) highlighted the effect of varying the specific mechanical energy (SME) and moisture content on commercial citrus fibers during extrusion. When the SME increased from 201 kJ/kg to 479 kJ/kg, both the viscosity and water retention capacity decreased. At lower moisture levels, machine blockage occurred, whereas a higher SME triggered slight Maillard reactions. Overall, increasing the SME improved the soluble fraction of citrus fibers. Extrusion-cooking has proven effective for processing highly concentrated IDF-based systems, resulting in products that resemble pastes or wet powders rather than suspensions, hydrogels, or structured emulsions. Although extrusion generally increases the solubility and fermentability of IDFs, some studies have reported conflicting results. For example, research on powdered fruit peels from orange, mango, and prickly pear showed that extrusion sometimes reduced the total fiber content and soluble fraction, indicating that the vegetable source plays a significant role in the process outcomes (Tejada-Ortigoza et al., 2022). The same authors carried out a previous study using a factorial experimental design approach with the aim of describing the effects of process parameters on the SDF% and IDF% of orange peel fiber concentrate (Garcia-Amezquita et al., 2019). A similar study on soybean hulls demonstrated that optimal conditions, moisture at 42.58%, screw speed at 182.46 rpm, and temperature at 87.34°C, improved the physicochemical properties and solubility of soybean hull fibers, enhancing their nutritional features (Tabibloghmany et al., 2020). Recently, Schmid et al. (2021) found that extrusion cooking of chokeberry pomace increased the soluble fraction without affecting the total dietary fiber, phenolic acid, or flavonoid content. However, high SME levels negatively affected sugars and anthocyanins.

6.5. Novel processing methods

There are a lot of new and non-conventional techniques suitable to produce IDF-based systems which can be virtually used and proposed for industrial implementation. It is worth noting that, in contrast to conventional methods, novel processing methods are mainly aimed at modifying the properties of IDFs rather than preparing food-type systems.

The high hydrostatic pressure (HHP) between the latest generation technologies in IDFs processing seems to be particularly relevant and attractive owing to its advantages (Balasubramaniam et al., 2015). In particular, operating the HHP at a pressure of 200-400 MPa for 15-30 minutes increased the SDF% and improved the functional and technological properties of the fiber from lotus root residues (Gu et al., 2022), okra soybean (Mateos-Aparicio et al., 2010) purple flesh potato (Xie et al., 2017).

Ultrasound-assisted dispersion is a novel technique employed for processing IDFs. In particular, a comparative study between high intensity ultrasonication and high-pressure homogenization was conducted by Wu et al. (2020) with the aim of assessing the modifications induced by the processing of okara fibers and the isolation of nanocellulose. The ultrasound processes were conducted at different energy levels (400 W-15 min, 400 W-30 min, 600 W -15 min and 600 W-30 min) and using a power density of 0.33 W/ml while the high-pressure homogenization was conducted at different pressures and 3 cycles. For both processes coarse suspension (4% w/w) was previously prepared using HSH (10000 rpm, 5 min). Commercial citrus, apple, oat pea fibers were used to stabilize (by Pickering effects) emulsions produced by using high-intensity ultrasound (amplitude: 116 μm, time: 150 s, energy density: 225 kJ/l and power: 325 W) (Kalla-Bertholdt et al., 2021); this highlights that this technique is also suitable for biphasic system preparation.

A method based on cavitation jet processing was developed for the processing and modification of IDFs based food systems (Wu et al., 2020). In particular, suspensions with a fiber/water ratio of 1:8 were successfully produced at 25°C and 0.01 MPa at different processing times (3, 5, 8, 10, 12, and 15 min), highlighting the ability of this technique to produce systems with small fiber particles.

Recent works reported the ability of steam explosion process to improve the quality of IDFs from different sources (Tian et al., 2024; Yan et al., 2024). In particular, some physicochemical and functional properties of rice bran dietary fiber can be enhanced by steam explosion treatment by changing steam pressure (0.4, 0.8, 1.2, 1.6, and 2.0 MPa) and crushing degree (60, 80, and 100 mesh) (Tian et al., 2024). In another comparative work, the soluble fraction of coconut dietary fiber was increased (115%) and the overall quality improved by steam explosion process, however the authors reported and highlighted better results for fibers treated by extrusion-cooking (Yan et al., 2024).

7. Conclusions and future perspectives

This study underscores the critical role of insoluble dietary fibers (IDFs) in promoting sustainability and innovation in the food industry. Sourced from food by-products or waste such as citrus peels, apple pomace, and wheat bran, IDFs provide a dual function by offering both nutritional enhancements and technological improvements in food formulations. From the analysis of the papers cited in this works, it seems that in the past the study concerning IDFs were basically centered on their extraction and characterization, whereas, in the last

few years, the attention is much more focused on the applications of IDFs in enhancing the rheological properties and stability of food products in various formulations (dairy, bakery, and sauces) and on the design of such properties. In particular, currently, attention is paid to the study of their thickening and structuring ability, and rheological and microstructural analyses are largely employed to investigate such properties in different types of systems. In general, thickening and structuring properties of IDFs depend on several factors, such as the row material from which they are extracted, their particle size, concentration, pH, and processing. Rheological measurements and modelling represent a successful method for the characterization and design of IDF-based food systems, spacing from simple water-based systems, such as suspensions of hydrogel, to more complex formulation, such as bigels and dairy products like yogurts. Among all the techniques for modification of IDF and its incorporation into foods, high-speed homogenization, high-pressure homogenization, microfluidization, and extrusion are the most effective and studied processing techniques. Generally speaking, processing methods and conditions profoundly affect IDFs properties and their performances as thickening and structuring agents in food products. Hence, their study and optimization can provide improvements in their functionality and technological properties. Furthermore, with the aim of enhancing the properties of IDFs and IDF-based foods and to confer them tailored properties, the adoption of multistep processing methods, for example coupling a preliminary particle size reduction operation before the homogenization process, results to be widely used because it yields several advantages. It is worth noting that quite often the preliminary size reduction of fibers also limits and mitigates some intrinsic drawbacks that affect even the most effective techniques, for instance allowing the blockage of the processing systems (such as high-pressure homogenization and microfluidization). Finally, it is worth noting that more and more attention is given to technique able to process IDF into very small particles to incorporate them in complex biphasic systems and to enhance their chemical profile (increasing of soluble fraction) without incurring in problems typical of conventional methods, such as the Maillard reaction sometimes found in extrusion-cooking. In contrast to homogenization techniques and extrusion-cooking, the new processing methods like ultrasound-assisted dispersion, cavitation, steam explosion are still in early development, but promising results are continuously obtained.

Overall, the findings of this study suggest that ongoing research into processing techniques and fiber applications will further enhance the viability and scalability of IDF-based food production. This, in turn, will contribute to the development of food products that are both

nutritionally superior and environmentally sustainable, supporting the growing shift toward cleaner, more natural food ingredients.

Authors contributions

Domenico Mammolenti: Conceptualization and design; Formal analysis, Investigation; Methodology; Writing – original draft. **Francesca R. Lupi:** Investigation; interpretation of the data; Supervision; Writing – Review and Editing; Final approval of the version to be published. **Noemi Baldino:** Methodology; Software; Validation; Critical revision for intellectual content. **Domenico Gabriele**: Funding acquisition; Investigation; Project administration; Resources; Interpretation of the data; Writing – Review and Editing.

Acknowledgments

The authors are also grateful to project "Tech4You- Technologies for climate change adaptation and quality of life improvement", codice identificativo ECS 00000009, CUP H23C22000370006, Piano Nazionale di Ripresa e Resilienza, Missione 4, Componente 2, Investimento 1.5". Thanks are also due to the Italian Project PON "Ricerca e Innovazione" 2014–2020, Azione IV.5 "Dottorati su tematiche green" for funding the PhD position of one of the authors.

Disclosure statement

No potential conflict of interest was reported by the author(s).

References

21 CFR Part 172 .Food Additives Permitted for Direct Addition to Food for Human Consumption, 2024. , Title 21—Food and Drugs. Chapter I—Food and Drug Administration, Department of Health and Human Services Subchapter B—Food for Human Consumption.

Ağar, B., Gençcelep, H., Saricaoğlu, F.T., Turhan, S., 2016. Effect of sugar beet fiber concentrations on rheological properties of meat emulsions and their correlation with texture profile analysis. Food Bioprod. Process. 100, 118–131. https://doi.org/10.1016/j.fbp.2016.06.015

Ajila, C.M., Prasada Rao, U.J.S., 2013. Mango peel dietary fibre: Composition and associated bound phenolics. J. Funct. Foods 5, 444–450. https://doi.org/10.1016/j.jff.2012.11.017

Alexandri, M., Kachrimanidou, V., Papapostolou, H., Papadaki, A., Kopsahelis, N., 2022. Sustainable Food Systems: The Case of Functional Compounds towards the Development of Clean Label Food Products. Foods 11. https://doi.org/10.3390/foods11182796

Balasubramaniam, V.M.B., Martínez-Monteagudo, S.I., Gupta, R., 2015. Principles and application of high pressure-based technologies in the food industry. Annu. Rev. Food Sci. Technol. 6, 435–462. https://doi.org/10.1146/annurev-food-022814-015539

Barnes, H.A., Hutton, J.F., Walters F.R.S., K., 1989. An Introduction to Rheology, First, thi. ed. Elsevier Science B.V., Amsterdam, The Netherlands. https://doi.org/10.1016/b978-0-444-87469-6.50001-9

Bayod, E., Bolmstedt, U., Innings, F., Tornberg, E., 2005. Rheological characterization of fiber suspensions prepared from vegetable pulp and dried fiber: A comparative study. Annu. Trans. Nord. Rheol. Soc. 13, 249–253.

Bengtsson, H., Tornberg, E., 2011. Physicochemical characterization of fruit and vegetable fiber suspensions. I: Effect of homogenization. J. Texture Stud. 42, 268–280. https://doi.org/10.1111/j.1745-4603.2010.00275.x

Betoret, E., Betoret, N., Rocculi, P., Dalla Rosa, M., 2015. Strategies to improve food functionality: Structure-property relationships on high pressures homogenization, vacuum impregnation and drying technologies. Trends Food Sci. Technol. 46, 1–12. https://doi.org/10.1016/j.tifs.2015.07.006

Board of Directors of the American Association of Cereal Chemists, 2001. The definition of dietary fiber, Cereal Foods World.

Bruno, E., Lupi, F.R., Mammolenti, D., Baldino, N., Gabriele, D., 2024. Development and rheological modeling of dietary fiber and policosanol plant-based bigels for potential food applications. Food Hydrocoll. 150, 109733. https://doi.org/10.1016/j.foodhyd.2024.109733

Bruno, E., Lupi, F.R., Mammolenti, D., Mileti, O., Baldino, N., Gabriele, D., 2022. Emulgels Structured with Dietary Fiber for Food Uses : A Rheological Model. Foods 11.

Bruno, E., Lupi, F.R., Martin-Piñero, M.J., Girimonte, R., Baldino, N., Muñoz, J., Gabriele, D., 2021. Influence of different dispersing systems on rheological and microstructural properties of citrus fiber suspensions. Lwt 152. https://doi.org/10.1016/j.lwt.2021.112270

Castro, A., Céspedes, G., Carballo, S., Bergenståhl, B., Tornberg, E., 2013. Dietary fiber, fructooligosaccharides, and physicochemical properties of homogenized aqueous suspensions of yacon (Smallanthus sonchifolius). Food Res. Int. 50, 392–400. https://doi.org/10.1016/j.foodres.2012.10.048

Cepeda, E., Collado, I., 2014. Rheology of tomato and wheat dietary fibers in water and in suspensions of pimento purée. J. Food Eng. 134, 67–73. https://doi.org/10.1016/j.jfoodeng.2014.03.007

Chen, B., Zhao, X., Cai, Y., Jing, X., Zhao, M., Zhao, Q., Van der Meeren, P., 2023. Incorporation of modified okara-derived insoluble soybean fiber into set-type yogurt: Structural architecture, rheological properties and moisture stability. Food Hydrocoll. 137, 108413.

https://doi.org/https://doi.org/10.1016/j.foodhyd.2022.108413

Chen, J., Gao, D., Yang, L., Gao, Y., 2013. Effect of microfluidization process on the functional properties of insoluble dietary fiber. Food Res. Int. 54, 1821–1827. https://doi.org/10.1016/j.foodres.2013.09.025

Codex Alimentarius, . Guidelines on Nutrition Labelling, CXG 2-1985, 2021. , Codex Alimentarius, International food Standards. Food and Agriculture Organization of the United Nations (FAO); World Health Organizzation (WHO).

Colletti, A.C., Delgado, J.F., Cabezas, D.M., Wagner, J.R., Porfiri, M.C., 2020. Soybean Hull Insoluble Polysaccharides: Improvements of Its Physicochemical Properties Through High Pressure Homogenization. Food Biophys. 15, 173–187. https://doi.org/10.1007/s11483-019-09613-y

Cui, J., Lian, Y., Zhao, C., Du, H., Han, Y., Gao, W., Xiao, H., Zheng, J., 2019. Dietary Fibers from Fruits and Vegetables and Their Health Benefits via Modulation of Gut Microbiota. Compr. Rev. Food Sci. Food Saf. 18, 1514–1532. https://doi.org/10.1111/1541-4337.12489

Daou, C., Zhang, H., 2014. Functional and physiological properties of total, soluble, and insoluble dietary fibres derived from defatted rice bran. J. Food Sci. Technol. 51, 3878–3885. https://doi.org/10.1007/s13197-013-0925-y

de Moraes Crizel, T., Jablonski, A., de Oliveira Rios, A., Rech, R., Flôres, S.H., 2013. Dietary fiber from orange byproducts as a potential fat replacer. Lwt 53, 9–14. https://doi.org/10.1016/j.lwt.2013.02.002

Dickinson, E., 2013. Stabilising emulsion-based colloidal structures with mixed food ingredients. J. Sci. Food Agric. 93, 710–721. https://doi.org/10.1002/jsfa.6013

Du, H., Wang, X., Yang, H., Zhu, F., Cheng, J., Peng, X., Lin, Y., Liu, X., 2023. Effects of mulberry pomace polysaccharide addition before fermentation on quality characteristics of yogurt. Food Control 153, 109900. https://doi.org/https://doi.org/10.1016/j.foodcont.2023.109900

EFSA Panel on Dietetic Products, Nutrition, and A. (NDA), 2016. Scientific Opinion on Dietary Reference Values for carbohydrates and dietary fibre. EFSA J. 8, 1–77. https://doi.org/10.2903/j.efsa.2010.1462

European Parliament and Council, 2011. Commission Regulation (EU) Nº 1129/2011 of 11 November 2011 amending Annex II to Regulation (EC) Nº 1333/2008 of the European Parliament and of the Council by establishing a Union list of food additives. Off. J. Eur. Union L295, 1–177. https://doi.org/10.3000/19770677.L_2011.295.eng

Fernández-Fernández, A.M., Dellacassa, E., Medrano-Fernandez, A., Castillo, M.D., 2020. Citrus Waste Recovery for Sustainable Nutrition and Health, in: Rocio Campos-Vega, B. Dave Oomah, and H.A.V.-C. (Ed.), Food Wastes and By-products: Nutraceutical and Health Potential. John Wiley & Sons Ltd., pp. 193–222. https://doi.org/10.1002/9781119534167.ch7

Figuerola, F., Hurtado, M.L., Estévez, A.M., Chiffelle, I., Asenjo, F., 2005. Fibre concentrates from apple pomace and citrus peel as potential fibre sources for food enrichment. Food Chem. 91, 395–401. https://doi.org/10.1016/j.foodchem.2004.04.036

Gabriele, D., de Cindio, B., D'Antona, P., 2001. A weak gel model for foods. Rheol. Acta 40, 120–127. https://doi.org/10.1007/s003970000139

Gan, J., Xie, L., Peng, G., Xie, J., Chen, Y., Yu, Q., 2021. Systematic review on modification methods of dietary fiber. Food Hydrocoll. 119, 106872. https://doi.org/10.1016/j.foodhyd.2021.106872

Gao, K., Liu, T., Cao, L., Liu, Y., Zhang, Q., Ruan, R., Feng, S., Wu, X., 2022. Feasibility of pomelo peel dietary fiber as natural functional emulsifier for preparation of Pickering-type emulsion. J. Sci. Food Agric. 102, 4491–4499. https://doi.org/10.1002/jsfa.11804

Garcia-Amezquita, L.E., Tejada-Ortigoza, V., Pérez-Carrillo, E., Serna-Saldívar, S.O., Campanella, O.H., Welti-Chanes, J., 2019. Functional and compositional changes of orange peel fiber thermally-treated in a twin extruder. Lwt 111, 673–681. https://doi.org/10.1016/j.lwt.2019.05.082

Gidley, M.J., Yakubov, G.E., 2019. Functional categorisation of dietary fibre in foods: Beyond 'soluble' vs 'insoluble.' Trends Food Sci. Technol. 86, 563–568. https://doi.org/10.1016/j.tifs.2018.12.006

Grigelmo-Miguel, N., Martín-Belloso, O., 1998. Characterization of dietary fiber from orange juice extraction. Food Res. Int. 31, 355–361. https://doi.org/10.1016/S0963-9969(98)00087-8

Gu, Y., Niu, L., Song, J., Liu, Chunju, Zhang, Z., Liu, Chunquan, Li, D., Xiao, L., 2022. Effect of Pretreatment and High Hydrostatic Pressure on Soluble Dietary Fiber in Lotus Root Residues. J. Food Qual. 2022. https://doi.org/10.1155/2022/5565538

Guo, X., Chen, M., Li, Y., Dai, T., Shuai, X., Chen, J., Liu, C., 2020. Modification of food macromolecules using dynamic high pressure microfluidization: A review. Trends Food Sci. Technol. 100, 223–234. https://doi.org/10.1016/j.tifs.2020.04.004

Guo, X., McClements, D.J., Chen, J., He, X., Liu, W., Dai, T., Liu, C., 2021. The nutritional and physicochemical properties of whole corn slurry prepared by a novel industry-scale microfluidizer system. Lwt 144, 111096. https://doi.org/10.1016/j.lwt.2021.111096

Håkansson, A., 2018. Rotor-stator mixers: From batch to continuous mode of operation-A review. Processes 6, 1–17. https://doi.org/10.3390/pr6040032

He, K., Li, Q., Li, Y., Li, B., Liu, S., 2020a. Water-insoluble dietary fibers from bamboo shoot used as plant food particles for the stabilization of O/W Pickering emulsion. Food Chem. 310. https://doi.org/10.1016/j.foodchem.2019.125925

He, K., Zhang, X., Li, Y., Li, B., Liu, S., 2020b. Water-insoluble dietary-fibers from Flammulina velutiper used as edible stabilizers for oil-in-water Pickering emulsions. Food Hydrocoll. 101,

105519. https://doi.org/https://doi.org/10.1016/j.foodhyd.2019.105519

He, X., Dai, T., Sun, J., Liang, R., Liu, W., Chen, M., Chen, J., Liu, C., 2022. Disintegrating the Structure and Improving the Functionalities of Pea Fiber by Industry-Scale Microfluidizer System. Foods 11, 1–14. https://doi.org/10.3390/foods11030418

He, Y., Wang, B., Wen, L., Wang, F., Yu, H., Chen, D., Su, X., Zhang, C., 2022. Effects of dietary fiber on human health. Food Sci. Hum. Wellness 11, 1–10. https://doi.org/10.1016/j.fshw.2021.07.001

Hipsley, E.H., 1953. Dietary "Fibre" and Pregnancy Toxaemia. Br. Med. J. 2, 420 LP – 422. https://doi.org/10.1136/bmj.2.4833.420

Huang, X., Liu, Q., Yang, Y., He, W.Q., 2020. Effect of high pressure homogenization on sugar beet pulp: Rheological and microstructural properties. Lwt 125. https://doi.org/10.1016/j.lwt.2020.109245

Issar, K., Sharma, P.C., Gupta, A., 2017. Utilization of Apple Pomace in the Preparation of Fiber-Enriched Acidophilus Yoghurt. J. Food Process. Preserv. 41, 1–6. https://doi.org/10.1111/jfpp.13098

Jiang, Z., Mu, S., Ma, C., Liu, Y., Ma, Y., Zhang, M., Li, H., Liu, X., Hou, J., Tian, B., 2022. Consequences of ball milling combined with high-pressure homogenization on structure, physicochemical and rheological properties of citrus fiber. Food Hydrocoll. 127, 107515. https://doi.org/10.1016/j.foodhyd.2022.107515

Jiménez-Aguilar, D.M., López-Martínez, J.M., Hernández-Brenes, C., Gutiérrez-Uribe, J.A., Welti-Chanes, J., 2015. Dietary fiber, phytochemical composition and antioxidant activity of Mexican commercial varieties of cactus pear. J. Food Compos. Anal. 41, 66–73. https://doi.org/10.1016/j.jfca.2015.01.017

Jurić, S., Ferrari, G., Velikov, K.P., Donsì, F., 2019. High-pressure homogenization treatment to recover bioactive compounds from tomato peels. J. Food Eng. 262, 170–180. https://doi.org/10.1016/j.jfoodeng.2019.06.011

Kalla-Bertholdt, A.-M., Nguyen, P.-V., Baier, A.K., Rauh, C., 2021. Influence of dietary fiber on in-vitro lipid digestion of emulsions prepared with high-intensity ultrasound. Innov. Food Sci. Emerg. Technol. 73, 102799. https://doi.org/https://doi.org/10.1016/j.ifset.2021.102799

Kamble, M.G., Singh, A., Prabhakar, P.K., Meghwal, M., Singh, S. V., Chinchkar, V.A., 2022. Effect of high shear homogenization on quality characteristics of bael fruit pulp. Food Qual. Saf. 6, 1–43.

Keskin, S.O., Ali, T.M., Ahmed, J., Shaikh, M., Siddiq, M., Uebersax, M.A., 2022. Physico-chemical and functional properties of legume protein, starch, and dietary fiber—A review. Legum. Sci. 4, 1–15. https://doi.org/10.1002/leg3.117

Liu, J., Wang, R., Wang, X., Yang, L., Shan, Y., Zhang, Q., Ding, S., 2019. Effects of High-Pressure

Homogenization on the Structural, Physical, and Rheological Properties of Lily Pulp. Foods.

Liu, Y., Yi, S., Ye, T., Leng, Y., Alomgir Hossen, M., Sameen, D.E., Dai, J., Li, S., Qin, W., 2021. Effects of ultrasonic treatment and homogenization on physicochemical properties of okara dietary fibers for 3D printing cookies. Ultrason. Sonochem. 77, 105693. https://doi.org/10.1016/j.ultsonch.2021.105693

Lupi, F.R., Puoci, F., Bruno, E., Baldino, N., Marino, R., Gabriele, D., 2020. The effects of process conditions on rheological properties of functional citrus fibre suspensions. Food Bioprod. Process. 121, 54–64. https://doi.org/10.1016/j.fbp.2020.01.018

Lupton, J.R., 2010. Codex definition of dietary fibre and issues requiring resolution. Wageningen Academic, Leiden, The Netherlands, pp. 13–24. https://doi.org/https://doi.org/10.3920/978-90-8686-692-2_002

Martínez, R., Torres, P., Meneses, M.A., Figueroa, J.G., Pérez-Álvarez, J.A., Viuda-Martos, M., 2012. Chemical, technological and in vitro antioxidant properties of mango, guava, pineapple and passion fruit dietary fibre concentrate. Food Chem. 135, 1520–1526. https://doi.org/10.1016/j.foodchem.2012.05.057

Mateos-Aparicio, I., Mateos-Peinado, C., Rupérez, P., 2010. High hydrostatic pressure improves the functionality of dietary fibre in okara by-product from soybean. Innov. Food Sci. Emerg. Technol. 11, 445–450. https://doi.org/10.1016/j.ifset.2010.02.003

McCleary, B. V., 2003. Dietary fibre analysis. Proc. Nutr. Soc. 62, 3–9. https://doi.org/10.1079/pns2002204

McClements, D.J., 2016. Food Emulsions-Principles, Practices, and Techniques, Third Edit. ed. CRC Press Taylor & Francis Group.

Moelants, K.R.N., Cardinaels, R., Jolie, R.P., Verrijssen, T.A.J., Van Buggenhout, S., Zumalacarregui, L.M., Van Loey, A.M., Moldenaers, P., Hendrickx, M.E., 2013. Relation Between Particle Properties and Rheological Characteristics of Carrot-derived Suspensions. Food Bioprocess Technol. 6, 1127–1143. https://doi.org/10.1007/s11947-011-0718-0

Moelants, K.R.N., Cardinaels, R., Van Buggenhout, S., Van Loey, A.M., Moldenaers, P., Hendrickx, M.E., 2014. A Review on the Relationships between Processing, Food Structure, and Rheological Properties of Plant-Tissue-Based Food Suspensions. Compr. Rev. Food Sci. Food Saf. 13, 241–260. https://doi.org/10.1111/1541-4337.12059

Morales-Medina, R., Dong, D., Schalow, S., Drusch, S., 2020. Impact of microfluidization on the microstructure and functional properties of pea hull fibre. Food Hydrocoll. 103, 105660. https://doi.org/https://doi.org/10.1016/j.foodhyd.2020.105660

Navarro-González, I., García-Valverde, V., García-Alonso, J., Periago, M.J., 2011. Chemical profile, functional and antioxidant properties of tomato peel fiber. Food Res. Int. 44, 1528–1535. https://doi.org/10.1016/j.foodres.2011.04.005

O'Shea, N., Arendt, E.K., Gallagher, E., 2012. Dietary fibre and phytochemical characteristics of fruit and vegetable by-products and their recent applications as novel ingredients in food products. Innov. Food Sci. Emerg. Technol. 16, 1–10. https://doi.org/10.1016/j.ifset.2012.06.002

Oladiran, D.A., Emmambux, N.M., 2018. Nutritional and Functional Properties of Extruded Cassava-Soy Composite with Grape Pomace. Starch/Staerke 70, 1–11. https://doi.org/10.1002/star.201700298

Pathania, S., Kaur, N., 2022. Utilization of fruits and vegetable by-products for isolation of dietary fibres and its potential application as functional ingredients. Bioact. Carbohydrates Diet. Fibre 27, 100295. https://doi.org/10.1016/j.bcdf.2021.100295

Payling, L., Fraser, K., Loveday, S.M., Sims, I., Roy, N., McNabb, W., 2020. The effects of carbohydrate structure on the composition and functionality of the human gut microbiota. Trends Food Sci. Technol. 97, 233–248. https://doi.org/10.1016/j.tifs.2020.01.009

Qi, J., Song, L., Zeng, W., Liao, J., 2021. Citrus fiber for the stabilization of O/W emulsion through combination of Pickering effect and fiber-based network. Food Chem. 343, 128523. https://doi.org/https://doi.org/10.1016/j.foodchem.2020.128523

Quin, W., Sun, L., Miao, M., Zhang, G., 2021. Plant-sourced intrinsic dietary fiber: Physical structure and health function. Trends Food Sci. Technol. 118, 341–355. https://doi.org/10.1016/j.tifs.2021.09.022

Redgwell, R.J., Curti, D., Robin, F., Donato, L., Pineau, N., 2011. Extrusion-induced changes to the chemical profile and viscosity generating properties of citrus fiber. J. Agric. Food Chem. 59, 8272–8279. https://doi.org/10.1021/jf201845b

Rosa-Sibakov, N., Carvalho, M.J. de O., Lille, M., Nordlund, E., 2022. Impact of Enzymatic Hydrolysis and Microfluidization on the Techno-Functionality of Oat Bran in Suspension and Acid Milk Gel Models. Foods 11. https://doi.org/10.3390/foods11020228

Schmid, V., Steck, J., Mayer-Miebach, E., Behsnilian, D., Bunzel, M., Karbstein, H.P., Emin, M.A., 2021. Extrusion processing of pure chokeberry (Aronia melanocarpa) pomace: impact on dietary fiber profile and bioactive compounds. Foods 10, 1–19. https://doi.org/10.3390/foods10030518

Serial, M.R., Velichko, E., Nikolaeva, T., den Adel, R., Terenzi, C., Bouwman, W.G., van Duynhoven, J.P.M., 2021. High-pressure homogenized citrus fiber cellulose dispersions: Structural characterization and flow behavior. Food Struct. 30, 100237. https://doi.org/10.1016/j.foostr.2021.100237

Su, D., Zhu, X., Adhikari, B., Li, D., Wang, L., 2020a. Effect of high-pressure homogenization on the rheology, microstructure and fractal dimension of citrus fiber-oil dispersions. J. Food Eng. 277, 109899. https://doi.org/10.1016/j.jfoodeng.2019.109899

Su, D., Zhu, X., Wang, Y., Li, D., Wang, L., 2020b. Effect of high-pressure homogenization on rheological properties of citrus fiber. Lwt 127, 109366. https://doi.org/10.1016/j.lwt.2020.109366

Su, D., Zhu, X., Wang, Y., Li, D., Wang, L., 2019. Effects of high-pressure homogenization on physical and thermal properties of citrus fiber. Lwt 116. https://doi.org/10.1016/j.lwt.2019.108573

Szafrańska, J.O., Sołowiej, B.G., 2020. Effect of different fibres on texture, rheological and sensory properties of acid casein processed cheese sauces. Int. J. Food Sci. Technol. 55, 1971–1979. https://doi.org/10.1111/ijfs.14485

Tabibloghmany, F.S., Mazaheri Tehrani, M., Koocheki, A., 2020. Optimization of the extrusion process through response surface methodology for improvement in functional and nutritional properties of soybean hull. J. Food Sci. Technol. 57, 4054–4064. https://doi.org/10.1007/s13197-020-04439-w

Tang, D., Marangoni, A.G., 2006. Microstructure and fractal analysis of fat crystal networks. JAOCS, J. Am. Oil Chem. Soc. 83, 377–388. https://doi.org/10.1007/s11746-006-1216-9

Tejada-Ortigoza, V., Garcia-Amezquita, L.E., Campanella, O.H., Hamaker, B.R., Welti-Chanes, J., 2022. Extrusion effect on in vitro fecal fermentation of fruit peels used as dietary fiber sources. Lwt 153. https://doi.org/10.1016/j.lwt.2021.112569

Tejada-Ortigoza, V., Garcia-Amezquita, L.E., Serna-Saldívar, S.O., Welti-Chanes, J., 2016. Advances in the Functional Characterization and Extraction Processes of Dietary Fiber. Food Eng. Rev. 8, 251–271. https://doi.org/10.1007/s12393-015-9134-y

Tian, X.-Y., Liu, J.-F., Cheng, Z., Wu, N.-N., Tan, B., 2024. Structure, thermal stability, physicochemical and functional characteristics of insoluble dietary fiber obtained from rice bran with steam explosion treatment: Effect of different steam pressure and particle size of rice bran. Food Res. Int. 187, 114310. https://doi.org/https://doi.org/10.1016/j.foodres.2024.114310

Ubando-Rivera, J., Navarro-Ocaña, A., Valdivia-López, M.A., 2005. Mexican lime peel: Comparative study on contents of dietary fibre and associated antioxidant activity. Food Chem. 89, 57–61. https://doi.org/10.1016/j.foodchem.2004.01.076

Van Audenhove, J., Bernaerts, T., Putri, N.I., Van Rooy, L., Van Loey, A.M., Hendrickx, M.E., 2022. The role of mechanical collapse by cryogenic ball milling on the effect of high-pressure homogenization on the microstructural and texturizing properties of partially pectin-depleted tomato cell wall material. Food Res. Int. 155, 111033. https://doi.org/10.1016/j.foodres.2022.111033

Van Buggenhout, S., Wallecan, J., Christiaens, S., Debon, S.J.J., Desmet, C., Van Loey, A., Hendrickx, M., Mazoyer, J., 2015. Influence of high-pressure homogenization on functional properties of orange pulp. Innov. Food Sci. Emerg. Technol. 30, 51–60.

https://doi.org/10.1016/j.ifset.2015.05.004

Vitaglione, P., Napolitano, A., Fogliano, V., 2008. Cereal dietary fibre: a natural functional ingredient to deliver phenolic compounds into the gut. Trends Food Sci. Technol. 19, 451–463. https://doi.org/10.1016/j.tifs.2008.02.005

Wang, H., Wang, P., Kasapis, S., Truong, T., 2024. Pomelo (Citrus grandis L.) peels as effective sorbents for diverse gel matrices: The influence of particle size and powder concentration. J. Food Eng. 370, 111966. https://doi.org/10.1016/j.jfoodeng.2024.111966

Wang, L., Wu, J., Luo, X., Li, Yongfu, Wang, R., Li, Yanan, Li, J., Chen, Z., 2018. Dynamic High-Pressure Microfluidization Treatment of Rice Bran: Effect on Pb(II) Ions Adsorption In Vitro. J. Food Sci. 83, 1980–1989. https://doi.org/10.1111/1750-3841.14201

Wang, Y., Sun, P., Li, H., Adhikari, B.P., Li, D., 2018. Rheological Behavior of Tomato Fiber Suspensions Produced by High Shear and High Pressure Homogenization and Their Application in Tomato Products. Int. J. Anal. Chem. 2018, 1–12. https://doi.org/10.1155/2018/5081938

Willemsen, K.L.D.D., Panozzo, A., Moelants, K., Cardinaels, R., Wallecan, J., Moldenaers, P., Hendrickx, M., 2018. Effect of pH and salts on microstructure and viscoelastic properties of lemon peel acid insoluble fiber suspensions upon high pressure homogenization. Food Hydrocoll. 82, 144–154. https://doi.org/10.1016/j.foodhyd.2018.04.005

Willemsen, K.L.D.D., Panozzo, A., Moelants, K., Debon, S.J.J., Desmet, C., Cardinaels, R., Moldenaers, P., Wallecan, J., Hendrickx, M.E.G., 2017. Physico-chemical and viscoelastic properties of high pressure homogenized lemon peel fiber fraction suspensions obtained after sequential pectin extraction. Food Hydrocoll. 72, 358–371. https://doi.org/10.1016/j.foodhyd.2017.06.020

Wolf, B., 2010. Polysaccharide functionality through extrusion processing. Curr. Opin. Colloid Interface Sci. 15, 50–54. https://doi.org/10.1016/j.cocis.2009.11.011

Wu, C., Teng, F., McClements, D.J., Zhang, S., Li, Y., Wang, Z., 2020. Effect of cavitation jet processing on the physicochemical properties and structural characteristics of okara dietary fiber. Food Res. Int. 134. https://doi.org/10.1016/j.foodres.2020.109251

Wu, Q., Wu, J., Ren, M., Zhang, X., Wang, L., 2021. Modification of insoluble dietary fiber from rice bran with dynamic high pressure microfluidization: Cd(II) adsorption capacity and behavior. Innov. Food Sci. Emerg. Technol. 73, 102765. https://doi.org/10.1016/j.ifset.2021.102765

Xie, F., Li, M., Lan, X., Zhang, W., Gong, S., Wu, J., Wang, Z., 2017. Modification of dietary fibers from purple-fleshed potatoes (Heimeiren) with high hydrostatic pressure and high pressure homogenization processing: A comparative study. Innov. Food Sci. Emerg. Technol. 42, 157–164. https://doi.org/10.1016/j.ifset.2017.05.012

Yadav, M.P., Kale, M.S., Hicks, K.B., Hanah, K., 2017. Isolation, characterization and the functional properties of cellulosic arabinoxylan fiber isolated from agricultural processing by-products, agricultural residues and energy crops. Food Hydrocoll. 63, 545–551. https://doi.org/10.1016/j.foodhyd.2016.09.022

Yan, J., Li, Y., Bai, S., Zheng, J., Hassan, N.A., Lu, B., Hu, A., 2024. Comparison of structural, physicochemical and functional properties of dried coconut dietary fiber by steam explosion and extrusion modification. Ind. Crops Prod. 218, 118916. https://doi.org/https://doi.org/10.1016/j.indcrop.2024.118916

Yang, X., Li, A., Li, X., Sun, L., Guo, Y., 2020. An overview of classifications, properties of food polysaccharides and their links to applications in improving food textures. Trends Food Sci. Technol. 102, 1–15. https://doi.org/10.1016/j.tifs.2020.05.020

Yildiz, E., Ozcan, T., 2019. Functional and textural properties of vegetable-fibre enriched yoghurt. Int. J. Dairy Technol. 72, 199–207. https://doi.org/10.1111/1471-0307.12566

Yin, Z., Wang, Z., He, Z., Zeng, M., Qin, F., Chen, J., 2021. Effect of particle size and microstructure on the physical properties of soybean insoluble dietary fiber in aqueous solution. Food Biosci. 41, 100898. https://doi.org/10.1016/j.fbio.2021.100898

Zhu, X., Lundberg, B., Cheng, Y., Shan, L., Xing, J., Peng, P., Chen, P., Huang, X., Li, D., Ruan, R., 2018. Effect of high-pressure homogenization on the flow properties of citrus peel fibers. J. Food Process Eng. 41. https://doi.org/10.1111/jfpe.12659

CHAPTER 2

Impact of solutes and temperature on rheological and microscopic properties of particle gels from insoluble citrus-derived dietary fiber

Impact of solutes and temperature on rheological and microscopic properties of particle gels from insoluble citrus-derived dietary fiber

Domenico Mammolenti[a], Francesca Romana Lupi*[a], Elisabetta Bruno[a], Antonio D'Agostino[b], Olga Mileti[a], Noemi Baldino[a], Domenico Gabriele[a]

[a]Department of Information, Modeling, Electronics and Systems, (D.I.M.E.S.) University of Calabria, Via P. Bucci, Cubo 39C, I-87036 Rende (CS), Italy

[b]JRS Silvateam Ingredients s.r.l., Via Marco Polo 72/74, I-87036, Rende (CS), Italy

domenico.mammolenti@unical.it; o.mileti@dimes.unical.it;
francesca.lupi@unical.it; noemi.baldino@unical.it;
elisabetta.bruno@unical.it; domenico.gabriele@unical.it;
adagostino@silvateam.com;

Corresponding author

Francesca Romana Lupi

Department of Information, Modeling, Electronics and System Engineering (D.I.M.E.S.)

Via P. Bucci – Cubo 39C

I-87036 Rende (CS), Italy

Email: francesca.lupi@unical.it

Tel. (+39) 0984 494009

Abstract

The presence of different solutes, i.e., salts and sweeteners, and the adopted thermal condition during processing affects significantly rheological behavior and microstructure of foods based on dietary fibers.

In this work, the interactions between water and insoluble dietary fiber (IDF) from citrus and different solutes, such as sodium chloride (NaCl) calcium chloride ($CaCl_2$), sucrose and low-calories sweeteners (erythritol, sorbitol) were investigated. A study on fiber hydration properties, such as water holding capacity (WHC) and water swelling capacity (WSC), was performed using the different aqueous systems and temperature. Then, rheological properties of particle gels were studied. Microstructure was investigated with FTIR, Cryo-SEM and ζ-potential, aiming at understanding better the effects of solutes and their influence on macroscopic properties.

Salt addition, owing to the shielding effects of cations on negative charges of fiber particles, yields the formation of larger and more compact clusters with a reduction in gel strength. As a consequence, at large salt concentrations, instability phenomena and phase separation occurred.

The addition of sweeteners, on the other hand, affects hydrogen bonding by reducing the fiber hydration and, therefore, the gel strength yielding a less compact structure. This effect seems dependent on the molecular weight and on OH functional group.

Keywords

Dietary fiber; gelled suspension; solutes;

1. Introduction

In recent years, the interest in using dietary fiber to develop novel foods is growing, owing to both its potential positive effects on human health [1–4] and its technological properties, related to the ability of structuring water phases [5]. Its inclusion in food allows to reduce other less-healthy additives and ingredients and, at the same time, to keep the desired texture and physical stability of the final product, improving the nutritional content [6]. Indeed, it is well known that a correct daily intake is associated with several physiological benefits such as the reduction and the prevention of the risks of obesity and diabetes and the improvement of the intestinal health by increasing fecal bulk density [2]. Dietary fiber consists of carbohydrate polymers (with 10 or more monomers) not hydrolyzed by the enzymes in the human intestine [7]. It is often classified as soluble, SDF, (e.g., pectin, gums, galactomannans, mucilage, etc.) and insoluble dietary fiber, IDF, (e.g., cellulose, hemicellulose, lignin) depending on its attitude to be dissolved in water and its fermentability in colon (being IDF typically non-fermentable or least-fermentable than SDF) [8,9]. These differences affect both the physiological effects and the mechanism of water structuring. Soluble polymers, e.g., pectin or galactomannans, in suitable conditions (depending on pH, temperature, co-solute presence, etc.) interact with each other building a three-dimensional network, where flexible polymer chains are the building blocks, entrapping the liquid phase ("polymer gels"); on the other hand, insoluble particles are able to adsorb water, swelling and interacting with each other transforming a liquid suspension to a "particle gel" [10,11]. The main fiber components are constituents of plant cell walls [12], therefore, nowadays, agricultural wastes, like peels, pomace, hulls, seeds, etc. are very interesting sources of fiber particularly rich in the insoluble fraction [8].

About technological perspective, different aspects, concerning fiber, were investigated and reported in literature, like the effects of extraction [13–15], processing [11,16,17], and recently their use to structure the water phase in food emulgel and bigel [18,19]. However, to date, the interactions between fibers and other food components have not received due attention. With the aim of exploiting their structuring properties in real systems (both for salty and sweet foods), the influence of other water-soluble components plays a very important role because they can change both the molecular and surface interactions, can bind water in a different way [20] and, as a consequence, can modify the network strength [6]. Hence, a fundamental study of water medium composition and temperature, on rheological properties and stability of dietary fiber-based systems, represents a crucial step to design new healthy foods. Investigations concerning the effect of ionic strength and pH on rheology

and microstructure of cellulose nanofibrils suspensions [21] and the effect of ionic strength on hydrogels properties are available in literature [22]. From these studies, carried out on systems similar to IDF particle hydrogel, it emerged that ion type, ion concentration and fiber volume fraction play a key role in determining the microstructure and rheological behavior, which can also undergo changes, passing from dilute to semi dilute regime of fiber fraction, for instance. The influence of pH on the extraction of lemon peel acid insoluble fiber and on the consistency and microstructure of its suspensions was deeply investigated by Willemsen et al. [17,23]. The authors found that for pH above 3.5 the surface of fiber is negatively charged and between pH 4.5-7 the suspensions showed improved viscoelasticity. However, carrying out tests at constant electrical conductivity and controlled pH, they also observed that the effect of pH is strictly related to ionic concentration, finding that concentration and type of ions play a crucial role in affecting rheology, microstructure and stability of suspensions [23]. Even though few information is available on the interactions between fiber and ions (neutrals or acid/basic), the interaction of fibers with other basic ingredients in food preparations, like sweeteners, and their effect on rheology, microstructure and stability are still unexplored.

In addition, only functional properties of potato fibers were investigated as a function of temperature [24] whereas, to the best of our knowledge, no studies are present in the literature focusing on the effect of temperature on rheological properties of suspensions and gels containing dietary fibers.

In this work, a systematic investigation about the effects of temperature, salts and sweeteners on particle gels produced with a commercial citrus dietary fiber, was undertaken. Two salts commonly used in food processing and with different ionic strengths (i.e., sodium and calcium chloride) were investigated in a wide range of concentrations, ranging between 0.001 M and 1 M. Moreover, the effects of common sucrose were studied and compared to those of two low-calories natural sweeteners, widely used in food industry, increasing their concentration up to 50% w/w (or up to the solubility limit if lower than 50% w/w). Two polyalcohols, erythritol and sorbitol, were chosen for their sweetening power close to that of sucrose (0.6-0.7 with respect to sucrose) and a low caloric content (0.2 kcal/g for erythritol and 2.5 kcal/g for sorbitol) [25] and for these reasons are commonly used in foods.

The effect of solutes addition was investigated through the determination of both hydration properties, such as water holding capacity and water swelling capacity, and rheological parameters in small amplitude oscillations sweep tests at different temperatures. Aiming at relating the macroscopic effects to microstructural modifications, ζ-potential and FTIR

spectroscopy were used to analyze the surface and molecular interactions, respectively, whereas electron microscopy was used to highlight morphological changes.

2. Materials and methods

2.1.Materials

Citrus fiber (trade name Vitacel CF 312 ®), provided by JRS Silvateam Ingredients (Italy), was used to prepare particle gel. The Insoluble (mass) fraction of Vitacel CF 312 is between 70% and 80%, and the soluble fraction between 4% and 8%.

Investigated solutes were sodium chloride (NaCl) from Sigma-Aldrich (USA), calcium chloride ($CaCl_2$) and sucrose ($C_{12}H_{22}O_{11}$, MW=342.3 Da) from VWR Chemicals (USA), erythritol ($C_4H_{10}O_4$, MW=122.12 Da) from NKD Living (UK), sorbitol ($C_6H_{14}O_6$, MW=182.17 Da) from Carlo Erba (Italy). Distilled water was used to prepare all samples.

With the aim of investigating the effects of potential solutes, different aqueous solutions were prepared using either salts or sweeteners commonly adopted in food processing. In particular, solutions containing either a monovalent cation (i.e., NaCl) or a divalent cation (i.e., $CaCl_2$) were prepared at a concentration of 0.001, 0.01, 0.1 and 1 M. Solutions containing sweeteners, i.e., sucrose, erythritol and sorbitol were prepared at a concentration of 10, 20, 30 and 50% w/w (the latter only for sucrose and sorbitol). Owing to solubility limits close to 40% w/w at 25°C [26], in the case of erythritol it was not possible to prepare sample at 50% w/w. The proper amount of either salt or sweetener was dissolved in distilled water and the solutions were stirred (AREX Heating Magnetic Stirrer, Velp Scientific, Italy) at 300 rpm. Solutions with low concentration were prepared at 25°C by mixing for 2 h, whereas for more concentrated solutions, to make the solute dissolution faster, the systems were slightly heated at 40°C and longer times were used, depending on solute type and concentration.

2.2.Physical characterizations of citrus fiber

As a preliminary step, a characterization of citrus fiber was performed. Bulk density was determined following a literature procedure with some modifications [27]. A 50 ml graduate cylinder was completely filled with dietary fiber and gently tapped against a plain surface several times, until no further change in volume was observed. The volume occupied by dietary fiber was recorded as well as the mass of fiber. Bulk density (g/mL) was calculated as ratio of mass by volume. The moisture was determined with HB43 moisture analyzer

(Mettler Toledo, USA) set at 160°C for 5-6 min and by recording the finale moisture (on wet basis) when the mean weight loss per unit of time drops below 1 mg per 50 s, whereas the water activity was measured using the AwTherm (Rotronic, Switzerland). Particle size distribution of citrus fiber was determined with Mastersizer 3000 (Malvern Panalytical, UK) equipped with the dry accessory Aero S. Color measurement was carried out with a colorimeter Croma Meter CR-400 (Konica Minolta, Japan), and data were recorded in the CieLab space. The color sampling was performed twice, using the white standard plate as background.

2.3. Hydration properties

The hydration properties were estimated following the procedures proposed in literature [28,29] with slight modifications. Briefly, for Water Holding Capacity (WHC), 1 g of fiber was manually mixed with 40 g of distilled water and left for 24 h at room temperature (25°C). The mixture was then centrifuged at 4000 rpm (relative centrifugal force 3220 x g) for 20 minutes (5810, Eppendorf, Germany). The supernatant was removed, and the solid residue was weighted. The WHC value was calculated following Eq.1.

$$WHC = \frac{m_w - m_d}{m_d} \quad (1)$$

where m_w and m_d are the mass (in g) of wet and dry fiber respectively. For Water Swelling Capacity (WSC), 0.5 g of fiber were manually mixed with distilled water in a graduate cylinder adding water up to a final volume of 50 ml. The system was left at 25°C for 24 h after which the hydrated bed volume was recorded. The WSC value was calculated following Eq. 2.

$$WSC = \frac{V_h - V_d}{m_d} \quad (2)$$

where V_h and V_d are the volume (in ml) of hydrated and dry fiber respectively whereas m_d is the mass (in g) of the dry fiber. In addition, WHC e WSC were also assessed placing samples, properly sealed, in static oven (Model ED 400, Binder, Germany) at 45, 65, and 85°C and in fridge at 5°C for the 24 h of equilibration. WHC and WSC were evaluated for samples prepared using both distilled water and solutions containing either salts or sweeteners at different concentrations. All tests were carried out in duplicate, and the results averaged. For the results deriving from these tests, fiber was simply indicated as "F" and, when a solute was present, a code referring to it (N for NaCl, C for $CaCl_2$, Su for sucrose, Er for erythritol, So for sorbitol) was added to the sample ID.

2.4. Preparation of particle gel

Particle gels with different concentrations of citrus fiber (1%, 1.5%, 2%, 2.5% and 3% w/w) were prepared dispersing the fiber in either distilled water or specific solutions with a Ultraturrax T50 (IKA-Warke, Germany) at 8000 rpm for 5 min following a procedure elsewhere described [16]. Aiming at keeping the temperature constant during the homogenization, the vessel containing the sample was immersed in water at 25°C. After the dispersion, the samples were stored for 24 h at 4°C and then characterized.

Aiming at better comparing the effects of salts having different ionic charges, the salt concentration was given in terms of ionic strength, I (mol/l) [30]:

$$I = \frac{1}{2} \sum_{i=1}^{n} c_i \, {z_i}^2 \tag{4}$$

where c_i and z_i are the molar concentration and the charge concentration of ion i, respectively.

In a similar way, to make easier the comparison of the effects of sweeteners with a different number of OH groups and different molecular weights, the OH equivalent concentration, OH_{eq}, (eq/l), i.e., the concentration of OH groups in solution, was defined as (eq. 5):

$$OH_{eq} = \frac{\rho \, w \, N_{OH}}{MW} \tag{5}$$

where w is the mass fraction (g/g), N_{OH} the number of OH groups per mol, ρ the solution density (g/l) and MW is the molecular weight of the sweeteners (Da). Literature data were used to evaluate density values of sucrose, sorbitol and erythritol solutions at different concentration [31–33]. Particle gels with different fiber content were named following the format "xF" where x is the fiber weight percentage used in the sample, for example 1F stands for sample with 1% w/w of fiber. When a solute was present, a code referring to it (N for NaCl, C for $CaCl_2$, Su for sucrose, Er for erythritol, So for sorbitol) was added to the sample ID; when necessary the solute code was followed by the solute concentration (in mass fraction or molar concentration depending on the solute). For instance, 1F_So refers to samples with 1% of fiber content in a sorbitol solution whereas 1F_So10 refers to samples with 1% of fiber content in solution containing 10% w/w of sorbitol. Sample ID and compositions are reported in Tab. 1 (samples in distilled water), Tab. 2 (samples in salt solution) and Tab. 3 (samples in sweetener solution).

Sample group ID	Fiber content (% w/w)	Fractal dimension (-)
xF	1	2.40±0.01[a]
	1.5	2.390±0.004[a]
	2	2.392±0.001[a]
	2.5	2.397±0.005[a]
	3	2.395±0.003[a]

Tab. 1. Composition and fractal dimension of particle gels in distilled water. Different letters, for the same parameter, refer to significantly different values.

Sample group ID and used salt	Fiber content (% w/w)	Salt concentration (M)	Ionic strength (M)	Fractal dimension (-)
xF_N NaCl	1	0.001	0.001	2.399±0.005[a]
		0.01	0.01	2.433±0.003[b]
		0.1	0.1	2.446±0.003[c]
		1	1	n.a.
	2	0.001	0.001	2.401±0.004[a]
		0.01	0.01	2.424±0.001[b]
		0.1	0.1	2.432±0.006[bc]
		1	1	2.437±0.008[c]
	3	0.001	0.001	2.422±0.005[a]
		0.01	0.01	2.437±0.002[b]
		0.1	0.1	2.428±0.012[ab]
		1	1	2.435±0.001[ab]
xF_C $CaCl_2$	1	0.001	0.003	2.440±0.002[a]
		0.01	0.03	2.449±0.005[b]
		0.1	0.3	n.a.
		1	3	n.a.
	2	0.001	0.003	2.434±0.002[a]
		0.01	0.03	2.440±0.001[b]
		0.1	0.3	n.a.
		1	3	n.a.
	3	0.001	0.003	2.436±0.002[a]
		0.01	0.03	2.4414±0.0003[b]
		0.1	0.3	2.440±0.001[bc]
		1	3	2.437±0.002[ac]

Tab. 2. Composition, ionic strength and fractal dimension of particle gel in salt solutions. Different letters (superscript), for the same parameter, refer to significantly different values. Statistical analysis was performed within sample groups with the same type of solute and the same fiber concentration. For a few samples the data are not available (n.a.) owing to phase separation phenomena.

Sample group ID and adopted sweetener	Fiber content (% w/w)	Sweetener concentration (% w/w)	OH_{eq} (eq/l)	Fractal dimension (-)
xF_Su Sucrose	1	10	2.4	2.385±0.003[a]
		20	5.1	2.394±0.009[a]
		30	7.9	2.386±0.001[a]
		50	14.4	2.392±0.009[a]
	2	10	2.4	2.377±0.002[a]
		20	5.1	2.373±0.005[ab]
		30	7.9	2.363±0.001[bc]
		50	14.4	2.360±0.007[c]
	3	10	2.4	2.385±0.001[a]
		20	5.1	2.375±0.002[b]
		30	7.9	2.3610±0.0002[c]
		50	14.4	2.352±0.003[d]
xF_Er Erythritol	1	10	3.3	2.393±0.007[a]
		20	6.6	2.372±0.004[b]
		30	9.8	2.384±0.002[a]
	2	10	3.3	2.375±0.001[a]
		20	6.6	2.369±0.003[a]
		30	9.8	2.360±0.006[b]
	3	10	3.3	2.387±0.006[a]
		20	6.6	2.373±0.004[b]
		30	9.8	2.3634±0.0004[c]
xF_So Sorbitol	1	10	3.4	2.389±0.004[a]
		20	7.0	2.387±0.005[ab]
		30	10.8	2.381±0.001[b]
		50	19.0	2.391±0.005[a]
	2	10	3.4	2.385±0.004[a]
		20	7.0	2.379±0.001[a]
		30	10.8	2.360±0.007[b]
		50	19.0	2.303±0.012[c]
	3	10	3.4	2.385±0.004[a]
		20	7.0	2.379±0.001[a]
		30	10.8	2.360±0.007[b]
		50	19.0	2.303±0.012[c]

Tab. 3. Composition, OH_{eq} and fractal dimension of particle gels in sweeteners solutions. Different letters, for the same parameter, refer to significantly different values. Statistical analysis was performed within sample groups with the same type of solute and the same fiber concentration.

2.5.Rheological characterization and analysis

Particle gels were characterized with a controlled stress rheometer, MCR 702e (Anton Paar, Austria), equipped with parallel plates geometry with a diameter of 25 or 50 mm (according to sample consistency) using a gap of 1.8±0.1 mm, and a Peltier system for temperature control. Frequency sweep tests at 25°C were performed between 0.1 and 10 Hz, in linear viscoelastic conditions previously determined through amplitude sweep test (data not shown). This frequency range was assumed to be sufficient to investigate the rheological properties of the samples studied, in agreement with previous work on similar systems [11,18,19]. In addition, temperature dependence of selected samples (with fiber concentration 1%, 2%, 3% w/w) was investigated with dynamic temperature ramp tests at 1 Hz in linear conditions (determined with amplitude sweep tests performed at different temperatures) increasing the temperature from 25°C up to 95°C with a ramp rate of 2 °C/min. All measurements were repeated three times, the results are shown in terms of mean value and standard deviation. To avoid the evaporation of water from the sample during the tests, silicon oils (20 cSt for tests at 25°C and 120 cSt for tests at higher temperature) were used to cover the sample rim.

The rheological data were analyzed in terms of complex modulus (G^*) and phase angle (δ) at 1 Hz. According to the literature [11,18,19] the viscoelastic behavior of particle gels, following a weak gel behavior, can be described from a microrheological point of view using a fractal model [19,34] (Eq. 6):

$$G' = \lambda\, \phi^{\frac{1}{3-D}} \tag{6}$$

where G' is the complex modulus (Pa), λ is the interaction parameter (Pa), ϕ is the volume fraction of fibers (dimensionless) and D is the fractal dimension (dimensionless). Considering the mass fraction of dietary fiber instead of its volume fraction the relation between the complex modulus and the fractal parameters can be rewritten as (Eq. 7):

$$G' = \lambda'\, x_f^{\frac{1}{3-D}} \tag{7}$$

where x_f is the fiber mass fraction (dimensionless) and λ' is a modified interaction parameter (Pa). Eq. 7 was used to describe the fiber concentration dependence of the rheological data. The fractal dimension can be determined from the slope of the storage modulus as a function of frequency, following the approach already adopted for similar systems [11,18,19]. The relation between the storage modulus, the frequency and the fractal dimension, is summarized in Eq. 8 and Eq. 9:

$$G' = k\, \omega^n \tag{8}$$

$$n = \frac{3\,(5 - 2D)}{2(5 - d)} \tag{9}$$

where k is the preexponential factor ($Pa^{1/n}$), n is the exponent of the power law (dimensionless) and D is the fractal dimension (dimensionless) and d is the Euclidean dimension of the system (d = 3).

It is worth noticing that for these systems G′ is almost one order of magnitude greater than G″ and approximately equal to G*, therefore Eq. 8 was used to fit complex modulus data and to determine the fractal dimension (Eq. 9); then the interaction parameter was determined using Eq. 7 to fit complex modulus at 1 Hz as a function of fiber concentration, according to the approach already used for similar systems [19]. The fractal dimension was used to describe the relation microstructure-properties as function of both I and OH_{eq}.

2.6. FTIR spectroscopy

IR spectra of citrus fibers powder, of sweeteners and of selected particle gel samples were acquired at room temperature with a Nicolet iS-10 FTIR spectrometer (Thermo Fisher Scientific, USA) equipped with a Smart iTX ATR sampling accessory. Specifically, particle gel samples with 1% w/w, 2% w/w and 3% w/w of fiber were characterized with the aim of investigating the effect of concentration; samples at 3% w/w of fiber and different concentrations of NaCl (0.001M, 0.1 M), $CaCl_2$ (0.01 M and 1 M), sucrose (20% w/w, 50% w/w), erythritol (30% w/w), sorbitol (50% w/w), were investigated to assess the effects of solutes on particle gel properties. The spectra were acquired with a number of scans of 32, in a wavenumber (W.N.) interval ranging from 500 to 4000 cm^{-1}. For the spectra detection a resolution of 2 cm^{-1} was used. Spectra analysis was carried out with the software Origin Pro (Version 2021b; OriginLab Corporation, USA). Each spectrum was acquired twice, and the signals were averaged.

2.7. ζ-potential

The ζ-potential (ζ) of citrus fiber in the gelled suspensions was determined with Litesizer 700 (Anton Paar, Austria). ζ measurements were carried out, at 25°C, on particle gels with different fiber concentrations (1% w/w, 2% w/w and 3% w/w) and, at 3% w/w fiber fraction, with different concentration of either salts or sweeteners. The samples were diluted 1 to 100 (w/w) with distilled water and left under mixing for 2 h before the test. For each sample, the

data of ζ were acquired in triplicate, and each measure was in turn the computation of three repetitions.

2.8. SEM and Cryo-SEM

The sample morphology was investigated using scanning electron microscopy (FlexSem 1000 II, Hitachi, Japan). The micrographs of powder were acquired at 200X with an accelerating voltage of 5 kV in low vacuum condition (50 Pa). The morphology of selected particle gels was investigated in cryoscopy conditions. Specifically, particle gels with 1% w/w and 3% w/w of fiber, samples with 3% w/w of fiber and 0.1 M of NaCl, sample with 1% w/w of fiber and 10% w/w of sucrose were observed. The micrographs in cryo-mode were acquired at 100X and 500X using an accelerating voltage of 15 kV and a pressure of 50 Pa (low vacuum). Samples in the specimen holder were frozen at -35 °C using a Peltier cooling stage (Coolstage, Deben UK) and kept to this temperature during the scanning. All the images were obtained from the backscattered electron (BSE) signal, and no metallization of the samples surface was applied for the observation.

2.9. Statistical analysis

Data fitting and statistical analysis were performed with the software Origin Pro (Version 2021b; OriginLab Corporation, USA). A one-way ANOVA test was used to compare the value of rheological parameters and ζ; differences were considered significant for $p < 0.05$, Fisher test was used to compare the means.

3. Results and discussion

3.1. Physical, structural and hydration properties of citrus fiber

Physical and hydration properties of citrus fiber are reported in Tab.4. Particle size distribution is quite large: fine fraction (i.e., particles smaller than 30 μm) is less than 10% of the total, whereas almost all particles (i.e., 90% of the total) are smaller than 318 μm. Water holding capacity and water swelling capacity are 16.1 ± 0.6 g/g and 16.2 ± 0.4 ml/g, respectively, and are in agreement with literature data [28,29]. SEM images (Fig. 1a) highlight a heterogeneous distribution of dimensions and shapes in which both globular and fibrillar particles are present. Fig. 1b shows the FTIR spectrum of dietary fiber. The peak at 3328 cm^{-1} is related to stretching vibration of OH functional group whereas the C=O stretching of the hemicellulose and lignin fraction can be located through the peak at 1733

cm^{-1} [35]. According to the literature, the absorption band at 1636 cm^{-1} is connected to both adsorbed water and to the stretching of carboxyl group [35,36] whereas the two peaks observed at 1505 cm^{-1} and 1540 cm^{-1} are connected to aromatic skeleton of lignin [29,37]. The peaks at 1242 cm^{-1} and 1020 cm^{-1} can be ascribed to the stretching vibration of C-O bonds, whereas that at 1157 cm^{-1} is generated by the asymmetrical stretching of the bridge C-O-C [29,36]. Finally, the peak at 895 cm^{-1} is representative of the β-1,4 glycosidic bonds of cellulose and hemicellulose [29,36].

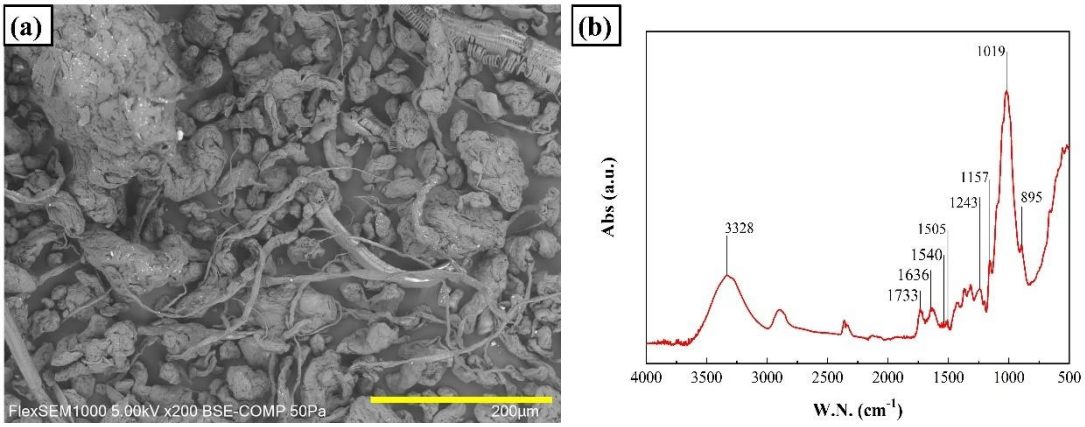

Fig. 1. Surface morphology and molecular features of citrus fiber: (a) SEM micrograph at 200X (bar indicates 200 µm) and (b) FTIR spectrum.

Properties	Value
Humidity (%)	8.3 ± 0.1
Bulk density (g/ml)	0.51 ± 0.03
Water activity (-)	0.38 ± 0.2
Particle size D_{10} (µm) D_{50} (µm) D_{90} (µm)	 35.5 124 318
Color parameters L* a* b*	 84.1 ± 0.3 0.3 ± 0.1 19.1 ± 0.4
Water Holding Capacity – WHC (g/g)	16.1 ± 0.6
Water Swelling Capacity – WSC (ml/g)	16.2 ± 0.4

Tab.4. Physical, structural, and functional properties of citrus fiber.

3.2.Effect of fiber concentration and temperature on particle gel properties

Rheological results were interpreted in terms of G^* and δ at 1 Hz and reported in Fig. 2a. For all samples, dynamic moduli exhibit a linear trend as frequency function in a log-log plot; data of selected samples, at different fibers and solute concentrations, are shown, as an example, in Fig. S1 of the Supplementary Materials (SM) in terms of complex modulus (G^*) and phase angle (δ). From Fig. 2a, it can be seen that G^*increases, in a nonlinear way, with the increase of the fiber concentration, whereas δ is almost constant (close to 10°). The G^* data, as frequency function, were fitted (Eq. 8) to estimate the fractal dimension (Eq. 9) at different concentrations (fitting parameters are reported in Tab. 1); no statistical differences among obtained values were observed and, therefore, an average fractal dimension D equal to 2.396 ± 0.007 was computed and used to fit G^* with the fractal model (Eq. 7) estimating the interaction parameter $\lambda' = 2.3 \pm 0.7\ 10^6$ Pa.

ζ values of fiber in particle gels with a concentration of 1% w/w, 2% w/w and 3% w/w were found to be -37 ± 2 mV, -39 ± 3 mV, -38 ± 4 mV; therefore, as reasonably expected, the values do not depend on fiber concentration and an average value of -38 ± 3 mV was assumed for particle gels in distilled water and, according to the literature [38] it indicates a good physical stability of these systems.

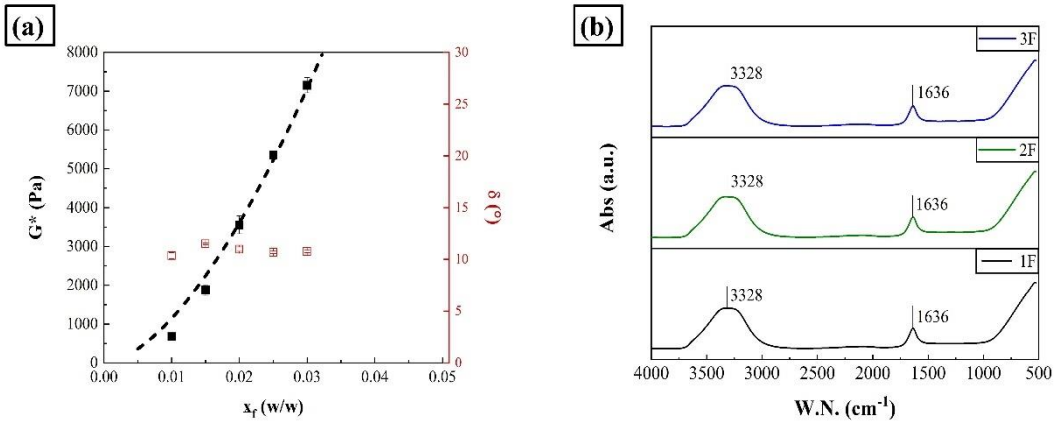

Fig. 2. Rheology and macromolecular interactions of particle gels with different fiber concentrations: (a) complex modulus and phase angle and (b) FTIR spectra. Dashed line refers to data fitting (Eq. 7).

From the FTIR spectra of samples at different fiber concentrations (Fig. 2b) only the peak connected to OH stretching vibration and to the banding vibration of the adsorbed water can be clearly observed. The first is located at 3328 cm^{-1} whereas the second at 1636 cm^{-1}. A

variation of fiber concentration in samples did not correspond to a change of the spectra, since these two peaks were found at the same W.N. values and with the same intensity for all the samples.

Temperature ramp test highlighted that G^* increases with the temperature (Fig. 3a), starting approximately from 45°C, whereas δ slightly decreases (Fig. 3b), indicating an increase in both "consistency" (related to the complex modulus) and structuration degree of the fiber network (described by the phase angle trend).

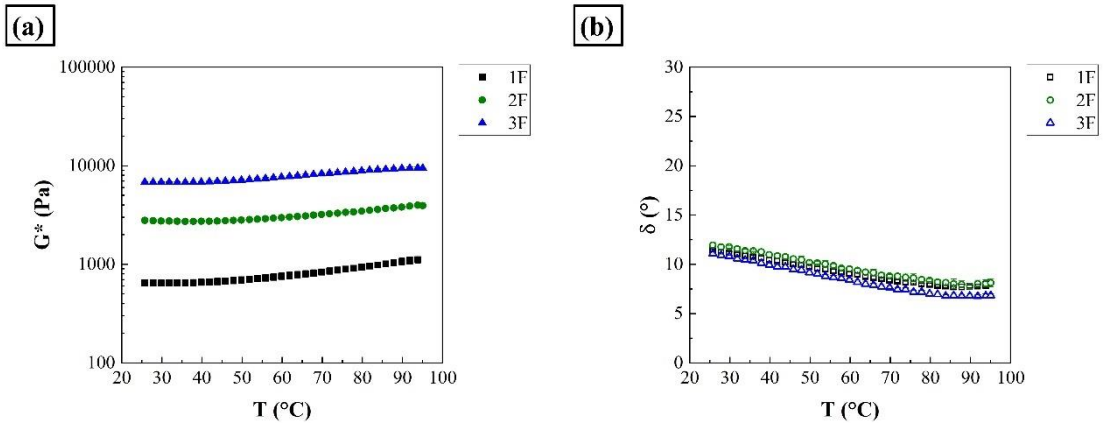

Fig. 3. Rheology of particle gels with increasing fiber content at different temperatures: (a) complex modulus (b) phase angle.

Aiming at better understanding the observed behavior, the effects of temperature on fiber-water interactions were investigated through the determination of ζ, WHC and WSC at different temperatures. The results reported in Fig.4a show no significant variation of ζ from 5°C up to 45°C whereas, at 65°C, a slight decrease is observed. WHC (Fig. 4b) increases from 5 °C up to 25 °C and then an apparent plateau seems present with values almost independent of temperature and ranging, approximately, between 15 g/g and 16 g/g. On the other hand, a continuous increase in WSC (from approximately 15 ml/g up to 19 ml/g) is observed, suggesting a progressive swelling of particles with temperature, in agreement with literature results for dietary fiber from potato [24]. Therefore, it could be speculated that the increase in particles swelling, and hydration enhances particle-particle interactions and yields a more homogenous microstructure with stronger elements, having a larger "effective" volume, responsible for network formation. As a consequence, an increase in complex modulus with temperature and a decrease in phase angle, are observed during the temperature ramp test.

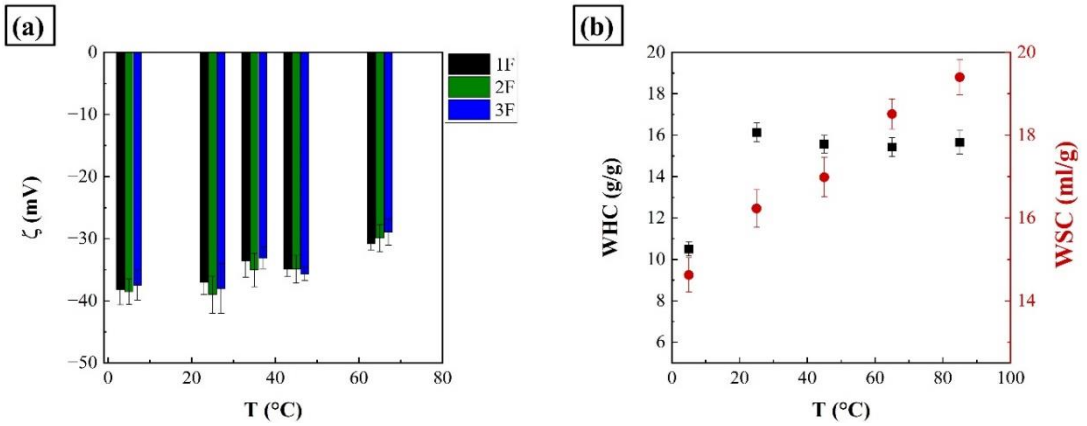

Fig. 4. (a) ζ of particle gels and (b) WHC (black square) and WSC (red circle) of citrus fiber as function of temperature.

3.3.Effect of salt on particle gel properties

The results of the frequency sweep tests of samples at different ionic strength were interpreted in terms of relative complex modulus, G_r^*, and phase angle, δ, and are summarized in Fig. 5. Particle gel with 1% w/w of fiber and 1 M of NaCl, and with concentration of fiber lower than 3% w/w and $CaCl_2$ equal to 0.1 and 1 M, undergo phase separation during the 24 h of storage, as shown in Fig. S3. From Fig. 5a, independently of the salt type, a non-linear and sharp decrease of the complex modulus with increasing I (up to 0.1 M) can be observed for particle gel samples prepared at all fiber concentrations. As shown, the loss in consistency also depends on the fiber concentration (more relevant effects are observed when using lower fiber content) and then on the ratio between the ion and fiber concentrations [21,22]. In particular, for samples with 3% w/w of fiber, both ions seem to induce a similar effect on G^* whereas decreasing the fiber content the loss of consistency became more and more significant, suggesting among other things a nonlinear dependency from fiber content, and a greater influence of the $CaCl_2$ on consistency and stability can be appreciated, in agreement with literature results [23]. The phase angle plot in Fig. 5b shows that all samples follow a common microstructural trend. In particular, the decrease of phase angle suggests an increase in the structuring degree of the samples as the ionic strength increases. Furthermore, some sort of limit condition in phase angle trend can be identified close to 0.03 M where an asymptotic trend arises ($\delta \sim 6°$). Indeed, above this concentration value, no marked differences are detectable.

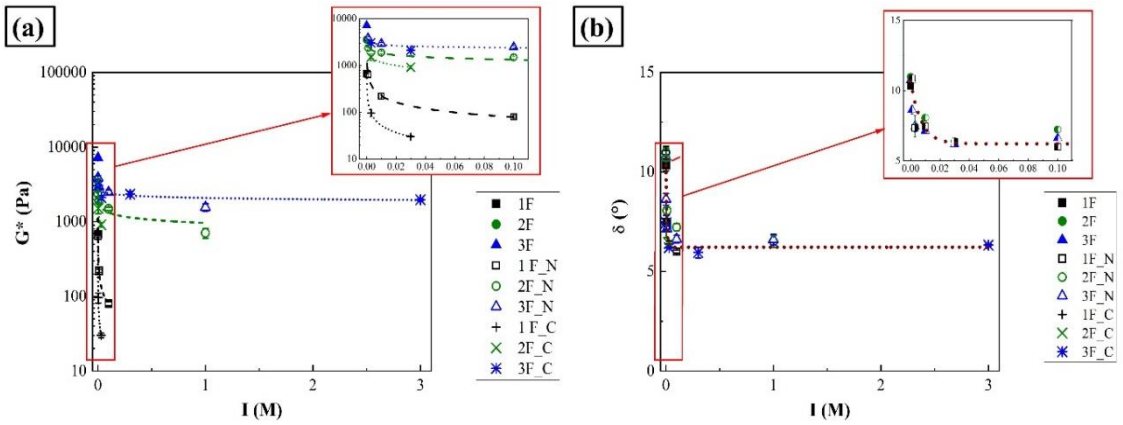

Fig. 5. Rheology of particle gel at different ionic strength: (a) complex modulus, (b) phase angle. Lines provide a guide to highlight the trends.

Looking at the results of the ANOVA analysis of fractal dimension in Tab. 2 it is possible to see that the ionic strength tendentially yields an increase in the fractal dimension D, reaching, for some set of samples, an almost constant trend (samples with no significant difference). Aiming at better understanding the effects of salt addition and the potential changes in microstructure, determinations of ζ were performed on different particle gel samples (Fig. 6a). As previously discussed, fiber particles exhibit a negative surface charge and an average value of -38 ± 3 mV is observed for the neat particle hydrogel, independently of the concentration. When salts are added, a decrease of the absolute value of ζ, with increasing ionic strength is found, suggesting that added cations shield the negative charges on particle surface and reduce the repulsive forces, in agreement with literature works on similar systems [21–23]. Because of this charge shielding, particle-particle interactions are promoted, and aggregation can occur, resulting in the formation of larger cluster as highlighted by higher values of fractal dimension, and lower values of δ with increasing ionic strength; as a consequence, a weakening of the gel is observed and confirmed by the reduction of complex modulus. No significant effect associated with fiber concentration was observed on ζ at different ionic strength. It is worth noting that for samples with 1% w/w of fiber at ionic strength of 0.3 M and 3 M, phase separation phenomena occurred except for sample at 3% w/w of fiber which exhibited, at 3 M, a value of ζ equal to -6.5 ± 1.2 mV. Then, this value could be assumed as a rough estimate of a stability threshold. For smaller absolute values, the shielding effects of cations on (negative) surface charges are so effective to cause the collapse of the fiber network and the fiber aggregation.

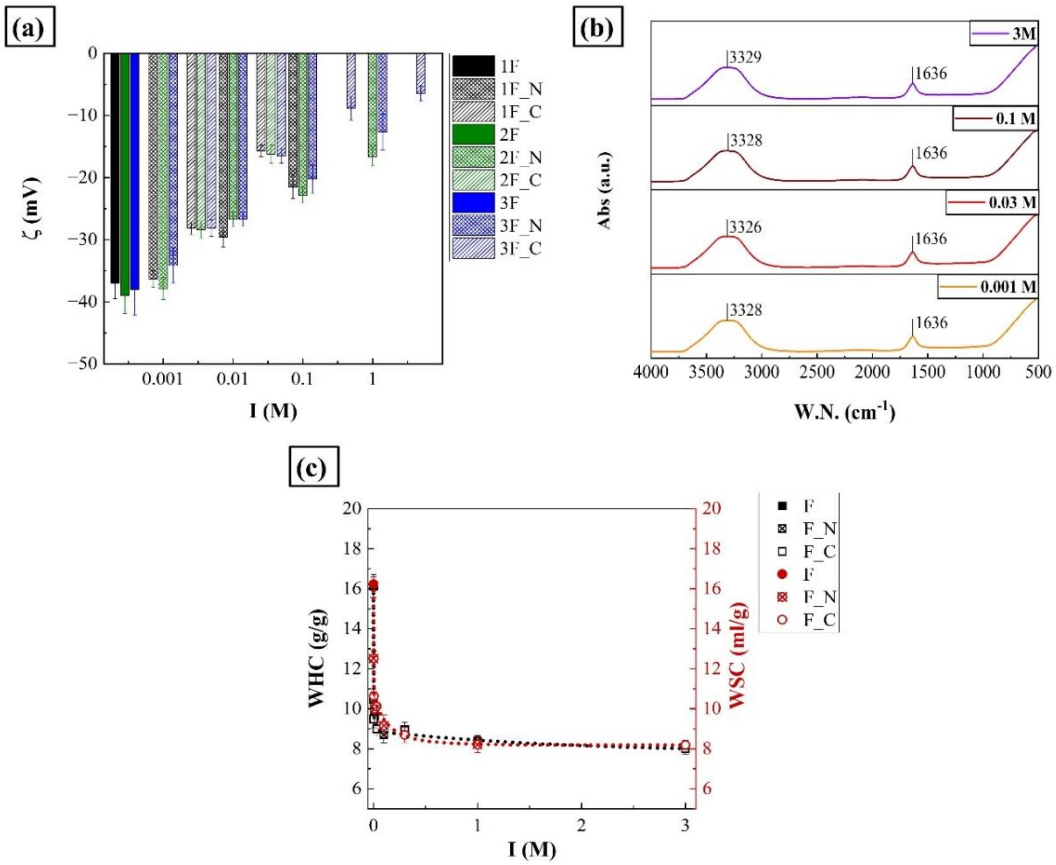

Fig. 6. (a) ζ of particle gels, (b) FTIR spectra at different salt concentrations for samples with 3% w/w of fiber and (c) WHC and WSC for fiber as a function of ionic strength. Lines are guides to highlight the trends.

FT-IR spectra of samples with different salt concentrations and 3% w/w of fiber (Fig. 6b) do not highlight any appreciable differences; the peak related to OH group vibration is located at around 3328 cm^{-1} for all samples, whereas the peak related to the absorbed water remains unchanged at 1636 cm^{-1}. Furthermore, for both peaks, signal intensity is not affected by the ionic strength. In particular, relative intensity of absorption at 1636 cm^{-1} and at 3326-3329 cm^{-1}, calculated, at each W.N, as the ratio between peak height of samples with solute (salts) and peak height of neat sample remains within 2% for both the bands at 1636 cm^{-1} and at 3326-3329 cm^{-1} by increasing ionic strength from 0 M to 3 M. These results suggest that the addition of salt does not affect the hydrogen bonds of the particle gel network. The effect of ion strength and ion type on the hydration properties of citrus fiber is reported in Fig. 6c. In agreement with results derived from rheological characterization, the hydration properties decrease nonlinearly by increasing the ionic strength. Specifically, WHC and WSC decrease from approximately 16 g/g and 16 ml/g to 8 g/g and 8 ml/g, respectively, by increasing I from 0 M to 3 M. This confirms that the formation of aggregates, due to the change in

electrostatic repulsion, reduces the ability of the fiber to adsorb water and swell decreasing the strength of the three-dimensional structure and the ability to entrap water.

3.4.Effect of OH_{eq} group and sweeteners on particle gel properties

Experimental data at 1 Hz (Fig. S3 of SM), obtained from frequency sweep tests, shows that the addition of sweeteners yields a relevant reduction in relative complex modulus and a common linear trend, almost independent of the type of sweetener, arises in a semi-log plot. Starting from this common trend, data were rearranged in terms of relative complex modulus (G_r^*), defined as the ratio between the complex modulus of the sweeteners-added sample and the complex modulus of the neat gel at the same fiber concentration. The results derived from frequency sweep tests of all samples, in terms of G_r^* and δ at 1 Hz, are reported in Fig. 7. From Fig.7a, it can be observed that G_r^* values of samples at all fiber concentrations follow a common decreasing linear trend as OH_{eq} increases, in semi-log scale. The data of G_r^* were related to OH_{eq} by fitting them to the empirical relation reported in Eq.10

$$G_r^* = A * \exp\left[B * \left(OH_{eq}\right)\right] \quad (10)$$

where $A = 0.87 \pm 0.04$ (-) and $B = -0.041 \pm 0.005 \left(OH_{eq}\right)^{-1}$.

The trend of δ, reported in Fig.7b, suggests a slight reduction in structure with the increase of OH_{eq} that can be due to a reduction of the number of interactions among the fiber particles of the gel network.

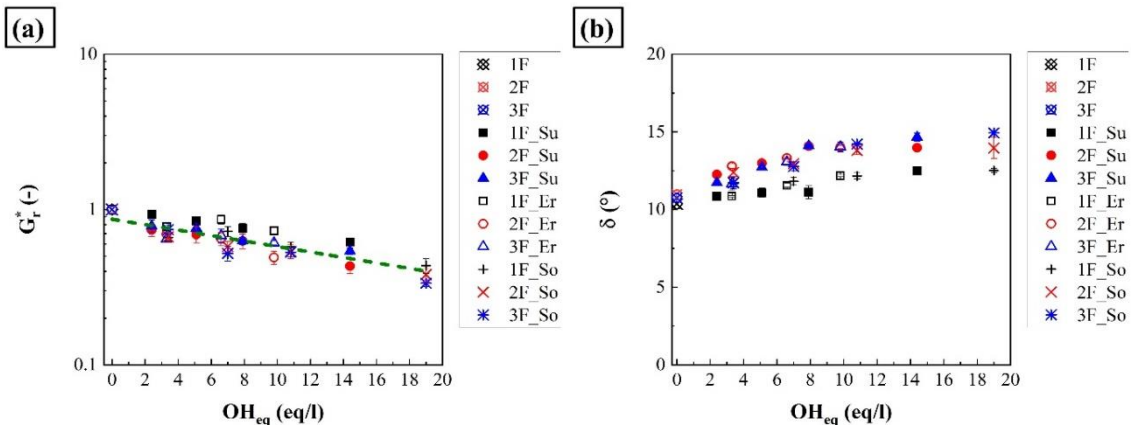

Fig. 7. Rheology of particle gel at different OHeq: (a) relative complex modulus, (b) phase angle. Dashed line refers to data fitting (Eq. 10).

Fig.8a reports ζ as a function of OH_{eq}. Only the data of samples produced with 3% w/w of fiber were determined and reported, since no differences given by fiber concentration were found in the case of neat and salt-added particle gels samples. Regardless of the sweeteners type and concentration, no sample shows particular ζ trends, and the values are distributed around to -35 mV indicating, as expected, the addition of low molecular weight carbohydrates does not exert any effects on surface charge of citrus fiber particles.

From Fig.8b it is possible to observe that particle gels with sweeteners exhibit different FTIR spectra by increasing OH_{eq}. In particular, the wavelength of the peak of -OH vibration ranges between approximately 3328 cm^{-1} and 3256 cm^{-1}, without a specific trend. This peak is affected by the type of sweetener used, as can be deducted by the comparison of spectra with those of pure sweeteners in Fig.S4, and it cannot be used as an indicator of the hydrogen bonds changes in the gel matrix as reported in literature in similar cases [39,40]. It is worth noting that the peak related to the adsorbed water/carboxyl group undergoes a slight shift from 1636 cm^{-1} to 1640 cm^{-1} and a tendential decrease of the intensity with the increasing of OH_{eq} added to the particle gel. Considering that this peak is not present in sweeteners spectra (Fig.S4) but only in the spectra of particle gel samples, and considering that, for citrus fiber and coconut fiber powders, the decrease in intensity of peak at 1635-50 cm^{-1} was already associated to a breakage of hydrogen bonds [35,41], it is reasonable to assume that also for particle hydrogels its decrease of intensity indicates H-bond breakage and their reduction in number [35,41], whereas its shift towards higher W.N. can be associated to a weakening of the hydrogen bond in terms of energy. Consequently, the shift found for the peak of samples with the increasing of OH_{eq} can be interpreted as a confirmation of hydrogen bond and, consequently, network weakening (resulting in the decrease of G_r^*). On the other hand, the decrease of intensity can be related to a slight reduction in the number of hydrogen bonds that, in turn, could cause the reduction of structuring degree highlighted by the increasing trend in δ. In particular, relative intensity of absorption at 1636-1640 cm^{-1}, calculated as the ratio between peak height of samples with solute (sweeteners) and peak height of neat sample decreased from 1 to 0.76 (-24%) by increasing the OH_{eq} from 0 eq/l to 19 eq/l. In contrast, the relative intensity of the peak related to -OH vibration remains almost constant, within 6%, despite the influence of the different types of sweeteners, confirming that for such systems, it cannot be used as an indicator of the changes in hydrogel bonds.

The WHC and WSC (Fig.8c) decrease from around 16 g/g and 16 ml/g to 10 g/g and 12 ml/g, respectively, indicating a greater effect on WHC. A further increase of sweeteners

concentration does not affect the hydration properties, indicating a sort of minimum hydration condition (in both WHC and WSC) in presence of sweeteners. The observed reduction of hydration properties of fibers further supports the formation of a less structured and consistent gel network discussed above.

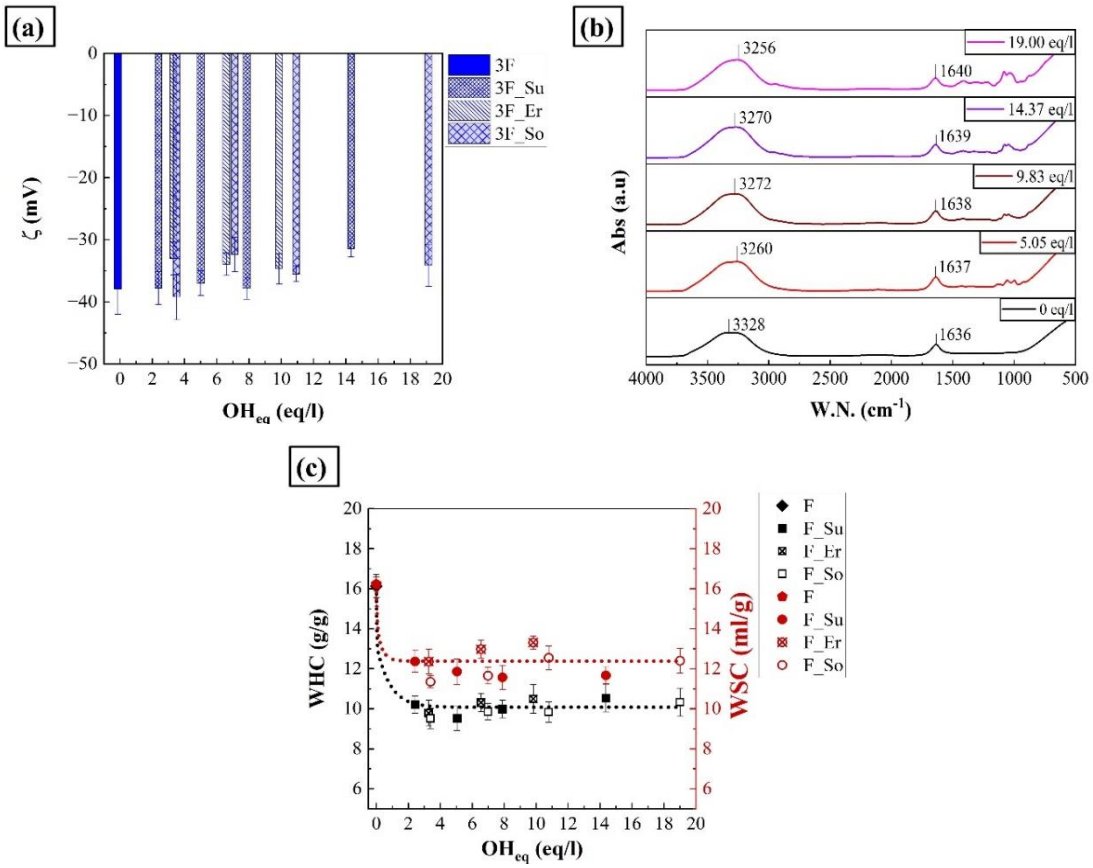

Fig. 8. (a) ζ of particle gels, (b) FTIR spectra at different salt concentrations for samples with 3% w/w of fiber and (c) WHC and WSC for fiber as function of OHeq. Lines are guides to highlight the trends.

3.5.Effects of temperature on particle gels with solute addition

Temperature ramp tests were also carried out on samples containing salts and sweeteners with the aim of investigating the combined effect of temperature and solute; some data are provided as an example in Fig. S5a-b of the SM. It can be seen that solute addition does not modify the typical trend already described for neat gels, the complex modulus slightly increases with temperature and only a vertical shift of the curves, due to the already discussed effects of the solutes, is observed (Fig.S5a). On the other hand, different trends are observed for phase angles (Fig.S5b); samples containing sugars are characterized by the decreasing

trend already observed for neat samples, even if the values are larger than those observed without sweeteners at the same fiber concentration and they depend on sweetener concentration, in agreement with results discussed at 25°C. Samples containing salts are characterized by low values of phase angle, almost independent of temperature. This is probably due to the reduction in swelling capacity, owing to the salts, that it is not modified by the increase in temperature.

3.6.Morphology of particle gels

The electron microscopy can be helpful in highlighting the change in microstructure caused by the solute addition. The comparison between Fig. 9a (neat sample) and Fig. 9b (NaCl 0.1 M) evidences the formation of less swollen and more aggregated particles when the salt is present with larger voids among them.

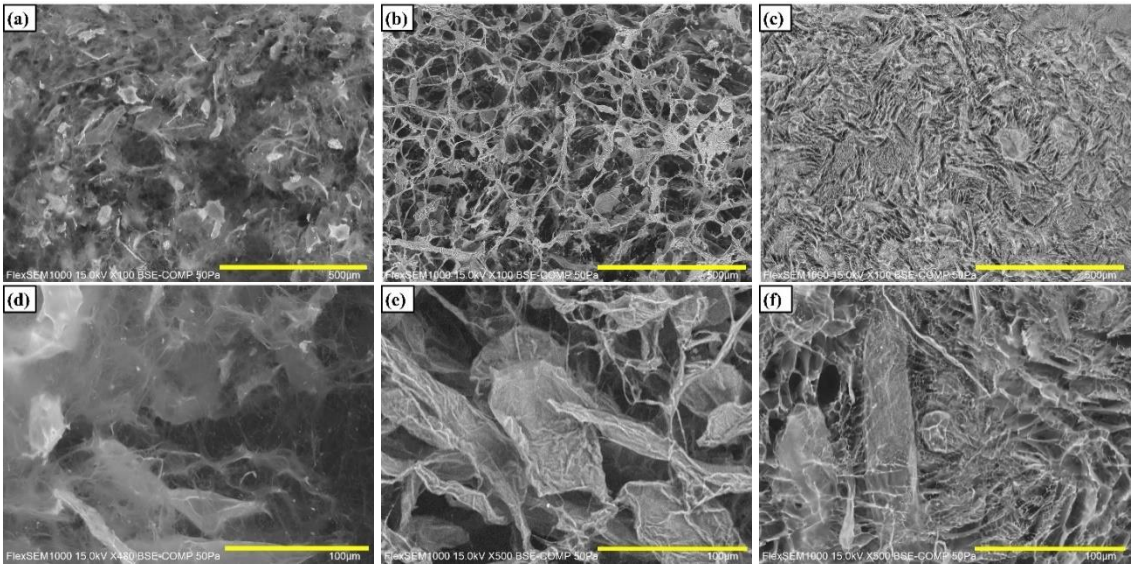

Fig. 9. Morphology of particle gels with 3% w/w of fiber: (a) neat sample at 100X, (b) sample with 0.1M of NaCl at 100X, (c) sample with 10% w/w of sucrose at 100X, (d) neat sample at 500X, (e) sample with 0.1M of NaCl at 500X, (f) sample with 10% w/w of sucrose at 500X. For images at 100X the bar indicates 500 µm whereas for those at 500X indicates 100 µm.

This is also more evident in Fig. 9d and Fig. 9e where particles are less hydrated is the sample containing NaCl. Fig. 9c shows the microstructure of a sample containing sucrose; it can be noticed that, even in this case, the fiber in the network appears less swollen and completely surrounded and wrapped by a sweetener matrix which hindered the swelling of particles and

the possibility to interact with each other. These effects are more evident in Fig.9f where less hydrated particles (with respect to neat sample, Fig. 9d) are present. In both cases a weaker structure is obtained, yielding, either at low fiber concentration or at large solute fraction, a phase separation, Fig.S2.

4. Conclusions

The effect of temperature and solutes (salts and sweeteners) on rheological behavior and microstructure of dietary fiber-in-water systems was investigated, aiming at better understanding the potential behavior of fibers as structuring agents in practical applications. In the range of investigated concentrations, fiber suspensions behave as gels and their behavior is described by the fractal model.

Temperature ramp tests highlighted a slight increase in complex modulus and a decrease in phase angle, suggesting that the gel network becomes stronger and more structured owing to the increase in swelling effects, evidenced by the increase in Water Swelling Capacity, caused by the temperature.

The addition of solutes significantly affects gel behavior. When salts (both NaCl and $CaCl_2$) are added, cations shield negative charges on fiber particles (as highlighted by the reduction of absolute value of ζ) hindering fiber separation. This yields a reduction in particles hydration and the formation of larger and more compact aggregates with reduced interactions among fibers (and therefore a reduction in gel strength). The effects seem more relevant when $CaCl_2$ is used and, at high salt content or low fiber concentration, these shielding effects yield phase separation phenomena. When increasing temperature, an almost constant phase angle is observed suggesting that the reduction in swelling ability, caused by the ions effect, is not modified by the temperature.

Sweeteners (erythritol, sorbitol and sucrose) do not modify the electrostatic interactions whereas they act on hydrogen bonding, reducing as a final effect, also in this case, the particle hydration and, therefore, the gel strength (lower G*) with a less compact structure (lower fractal dimension). It is worth noticing that the effects seem strongly related to the number of OH groups and when experimental data, in terms of complex modulus and phase angle, are plotted as a function of the "equivalent number" of OH groups, they follow a common linear trend in a semilogarithmic plot.

The results obtained evidence that investigated dietary fibers exhibit very interesting structuring properties, slightly enhanced by an increase in temperature; these results further

confirm their potential use, as structuring agent, even in high temperature applications (such as baking products). On the other hand, the presence of solutes commonly adopted in foods, such as salts and sweeteners, reduces their structuring ability and fiber fractions, larger than expected, can be necessary to obtain the desired structuring effects.

Acknowledgements

The authors are grateful to project "Tech4You- Technologies for climate change adaptation and quality of life improvement", code ECS 00000009, CUP H23C22000370006, Next Generation EU, Piano Nazionale di Ripresa e Resilienza, Missione 4, Componente 2, Investimento 1.5".

The authors are also grateful to PON "Ricerca e Innovazione" 2014-2020, Azione IV.5 "Dottorati su tematiche green" for founding the PhD position of one of the authors.

References

[1] T.M. Barber, S. Kabisch, A.F.H. Pfei, M.O. Weickert, The Health Benefits of Dietary Fibre, Nutrients 12 (2020) 1–17.

[2] Y. He, B. Wang, L. Wen, F. Wang, H. Yu, D. Chen, X. Su, C. Zhang, Effects of dietary fiber on human health, Food Science and Human Wellness 11 (2022) 1–10. https://doi.org/10.1016/j.fshw.2021.07.001.

[3] R. Tan, Q. Tang, B. Xia, C. Fu, L. Wang, Organic acid treatments on citrus insoluble dietary fibers and the corresponding effects on starch in vitro digestion, Int J Biol Macromol 275 (2024) 134082. https://doi.org/https://doi.org/10.1016/j.ijbiomac.2024.134082.

[4] J. Zheng, T. Huang, F. Fan, X. Jiang, P. Li, J. Ding, X. Sun, Z. Li, Y. Fang, Potentials of dietary fiber and polyphenols in whole grain wheat flour to release the liver function and intestinal tract injury in lead-induced mice, Int J Biol Macromol 278 (2024) 134180. https://doi.org/https://doi.org/10.1016/j.ijbiomac.2024.134180.

[5] X. Li, L. Wang, B. Tan, R. Li, Effect of structural characteristics on the physicochemical properties and functional activities of dietary fiber: A review of structure-activity relationship, Int J Biol Macromol 269 (2024) 132214. https://doi.org/https://doi.org/10.1016/j.ijbiomac.2024.132214.

[6] H. Kunzek, S. Müller, S. Vetter, R. Godeck, The significance of physico chemical properties of plant cell wall materials for the development of innovative food products, European Food Research and Technology 214 (2002) 361–376. https://doi.org/10.1007/s00217-002-0487-0.

[7] W. Quin, L. Sun, M. Miao, G. Zhang, Plant-sourced intrinsic dietary fiber: Physical structure and health function, Trends Food Sci Technol 118 (2021) 341–355. https://doi.org/10.1016/j.tifs.2021.09.022.

[8] S. Pathania, N. Kaur, Utilization of fruits and vegetable by-products for isolation of dietary fibres and its potential application as functional ingredients, Bioactive Carbohydrates and Dietary Fibre 27 (2022) 100295. https://doi.org/10.1016/j.bcdf.2021.100295.

[9] D. Dhingra, M. Michael, H. Rajput, R.T. Patil, Dietary fibre in foods: A review, J Food Sci Technol 49 (2012) 255–266. https://doi.org/10.1007/s13197-011-0365-5.

[10] V. Buckin, E. Kudryashov, Ultrasonic shear wave rheology of weak particle gels, Adv Colloid Interface Sci 89–90 (2001) 401–422. https://doi.org/10.1016/S0001-8686(00)00060-9.

[11] F.R. Lupi, F. Puoci, E. Bruno, N. Baldino, R. Marino, D. Gabriele, The effects of process conditions on rheological properties of functional citrus fibre suspensions, Food and Bioproducts Processing 121 (2020) 54–64. https://doi.org/10.1016/j.fbp.2020.01.018.

[12] A. Sharoba, M. Farrag, A. Abd El-Salam, Utilization of Some Fruits and Vegetables Wastes As a Source of Dietary Fibers in Cake Making, Journal of Food and Dairy Sciences 4 (2013) 433–453. https://doi.org/10.21608/jfds.2013.72084.

[13] Q. Gu, X. Gao, Q. Zhou, Y. Li, G. Li, P. Li, Characterization of soluble dietary fiber from citrus peels (Citrus unshiu), and its antioxidant capacity and beneficial regulating effect on gut microbiota, Int J Biol Macromol 246 (2023) 125715. https://doi.org/10.1016/j.ijbiomac.2023.125715.

[14] K. Wang, M. Li, Y. Wang, Z. Liu, Y. Ni, Effects of extraction methods on the structural characteristics and functional properties of dietary fiber extracted from kiwifruit (Actinidia deliciosa), Food Hydrocoll 110 (2021). https://doi.org/10.1016/j.foodhyd.2020.106162.

[15] F. Xu, S. Zhang, T. Zhou, G.I.N. Waterhouse, Y. Du, D. Sun-Waterhouse, P. Wu, Green approaches for dietary fibre-rich polysaccharide production from the cooking liquid of Adzuki beans: Enzymatic extraction combined with ultrasonic or high-pressure homogenisation, Food Hydrocoll 130 (2022) 107679. https://doi.org/10.1016/j.foodhyd.2022.107679.

[16] E. Bruno, F.R. Lupi, M.J. Martin-Piñero, R. Girimonte, N. Baldino, J. Muñoz, D. Gabriele, Influence of different dispersing systems on rheological and microstructural properties of citrus fiber suspensions, Lwt 152 (2021). https://doi.org/10.1016/j.lwt.2021.112270.

[17] K.L.D.D. Willemsen, A. Panozzo, K. Moelants, S.J.J. Debon, C. Desmet, R. Cardinaels, P. Moldenaers, J. Wallecan, M.E.G. Hendrickx, Physico-chemical and viscoelastic properties of high pressure homogenized lemon peel fiber fraction suspensions obtained after sequential pectin extraction, Food Hydrocoll 72 (2017) 358–371. https://doi.org/10.1016/j.foodhyd.2017.06.020.

[18] E. Bruno, F.R. Lupi, D. Mammolenti, O. Mileti, N. Baldino, D. Gabriele, Emulgels Structured with Dietary Fiber for Food Uses : A Rheological Model, Foods 11 (2022).

[19] E. Bruno, F.R. Lupi, D. Mammolenti, N. Baldino, D. Gabriele, Development and rheological modeling of dietary fiber and policosanol plant-based bigels for potential food applications, Food Hydrocoll 150 (2024) 109733. https://doi.org/https://doi.org/10.1016/j.foodhyd.2024.109733.

[20] M. Migliori, D. Gabriele, R. Di Sanzo, B. De Cindio, S. Correra, Viscosity of multicomponent solutions of simple and complex sugars in water, J Chem Eng Data 52 (2007) 1347–1353. https://doi.org/10.1021/je700062x.

[21] L. Jowkarderis, T.G.M. van de Ven, Intrinsic viscosity of aqueous suspensions of cellulose nanofibrils, Cellulose 21 (2014) 2511–2517. https://doi.org/10.1007/s10570-014-0292-5.

[22] F. Fneich, J. Ville, B. Seantier, T. Aubry, Structure and rheology of aqueous suspensions and hydrogels of cellulose nanofibrils: Effect of volume fraction and ionic strength, Carbohydr Polym 211 (2019) 315–321. https://doi.org/10.1016/j.carbpol.2019.01.099.

[23] K.L.D.D. Willemsen, A. Panozzo, K. Moelants, R. Cardinaels, J. Wallecan, P. Moldenaers, M. Hendrickx, Effect of pH and salts on microstructure and viscoelastic properties of lemon peel acid insoluble fiber suspensions upon high pressure homogenization, Food Hydrocoll 82 (2018) 144–154. https://doi.org/10.1016/j.foodhyd.2018.04.005.

[24] M.H. Waliullah, T. Mu, M. Ma, Recovery of total, soluble, and insoluble dietary fiber from potato (Solanum tuberosum) residues and comparative evaluation of their structural, physicochemical, and functional properties, J Food Process Preserv 45 (2021) 1–12. https://doi.org/10.1111/jfpp.15650.

[25] M. Carocho, P. Morales, I.C.F.R. Ferreira, Sweeteners as food additives in the XXI century: A review of what is known, and what is to come, Food and Chemical Toxicology 107 (2017) 302–317. https://doi.org/10.1016/j.fct.2017.06.046.

[26] S. Ohmori, Y. Ohno, T. Makino, T. Kashihara, Characteristics of erythritol and formulation of a novel coating with erythritol termed thin-layer sugarless coating, Int J Pharm 278 (2004) 447–457. https://doi.org/10.1016/j.ijpharm.2004.04.004.

[27] Z. ul Islam, N.A. Mir, A. Gani, Effect of controlled enzymatic treatment on the physicochemical, structural and functional properties of high-intensity ultrasound treated album (Chenopodium album) protein, Food Hydrocoll 144 (2023) 108940. https://doi.org/10.1016/j.foodhyd.2023.108940.

[28] Y. Zhang, J. Qi, W. Zeng, Y. Huang, X. Yang, Properties of dietary fiber from citrus obtained through alkaline hydrogen peroxide treatment and homogenization treatment, Food Chem 311 (2020) 125873. https://doi.org/10.1016/j.foodchem.2019.125873.

[29] B. Chen, Y. Cai, T. Liu, L. Huang, X. Deng, Q. Zhao, M. Zhao, Improvements in physicochemical and emulsifying properties of insoluble soybean fiber by physical-chemical treatments, Food Hydrocoll 93 (2019) 167–175. https://doi.org/10.1016/j.foodhyd.2019.01.058.

[30] A. Sarkar, H. Kamaruddin, A. Bentley, S. Wang, Emulsion stabilization by tomato seed protein isolate: Influence of pH, ionic strength and thermal treatment, Food Hydrocoll 57 (2016) 160–168. https://doi.org/10.1016/j.foodhyd.2016.01.014.

[31] Y.F. Hu, Z.X. Zhang, Y.H. Zhang, S.S. Fan, D.Q. Liang, Viscosity and density of the nonelectrolyte system mannitol + sorbitol + sucrose + H2O and its binary and ternary subsystems at 298.15 K, J Chem Eng Data 51 (2006) 438–442. https://doi.org/10.1021/je0503608.

[32] X. Jiang, C. Zhu, Y. Ma, Density and viscosity of sorbitol/maltitol in l-ascorbic acid aqueous solutions at T = (293.15 to 323.15) K, J Mol Liq 188 (2013) 67–73. https://doi.org/10.1016/j.molliq.2013.09.023.

[33] X. Jiang, C. Zhu, Y. Ma, Densities and viscosities of erythritol, xylitol, and mannitol in l -ascorbic acid aqueous solutions at T = (293.15 to 323.15) K, J Chem Eng Data 58 (2013) 2970–2978. https://doi.org/10.1021/je400395u.

[34] D. Tang, A.G. Marangoni, Microstructure and fractal analysis of fat crystal networks, JAOCS, Journal of the American Oil Chemists' Society 83 (2006) 377–388. https://doi.org/10.1007/s11746-006-1216-9.

[35] J. yi Huang, J. song Liao, J. ru Qi, W. xin Jiang, X. quan Yang, Structural and physicochemical properties of pectin-rich dietary fiber prepared from citrus peel, Food Hydrocoll 110 (2021) 106140. https://doi.org/10.1016/j.foodhyd.2020.106140.

[36] N. Abidi, L. Cabrales, C.H. Haigler, Changes in the cell wall and cellulose content of developing cotton fibers investigated by FTIR spectroscopy, Carbohydr Polym 100 (2014) 9–16. https://doi.org/10.1016/j.carbpol.2013.01.074.

[37] O. Derkacheva, D. Sukhov, Investigation of lignins by FTIR spectroscopy, Macromol Symp 265 (2008) 61–68. https://doi.org/10.1002/masy.200850507.

[38] C. Cano-Sarmiento, D.I. Téllez-Medina, R. Viveros-Contreras, M. Cornejo-Mazón, C.Y. Figueroa-Hernández, E. García-Armenta, L. Alamilla-Beltrán, H.S. García, G.F. Gutiérrez-López, Zeta Potential of Food Matrices, Food Engineering Reviews 10 (2018) 113–138. https://doi.org/10.1007/s12393-018-9176-z.

[39] M.G. De Paola, D. Mammolenti, F.R. Lupi, M.P. De Santo, D. Gabriele, V. Calabrò, Formulation and process investigation of glycerol/starch suspensions for edible films production by tape casting, Chemical Papers 76 (2022) 1525–1538. https://doi.org/10.1007/s11696-021-01956-6.

[40] O. Mileti, D. Mammolenti, N. Baldino, F.R. Lupi, D. Gabriele, Starch films loaded with tannin: the study of rheological and physical properties, Int J Biol Macromol 254 (2024) 127973. https://doi.org/10.1016/j.ijbiomac.2023.127973.

[41] Y. Zheng, Y. Li, Physicochemical and functional properties of coconut (Cocos nucifera L) cake dietary fibres: Effects of cellulase hydrolysis, acid treatment and particle size distribution, Food Chem 257 (2018) 135–142. https://doi.org/10.1016/j.foodchem.2018.03.012.

Supplementary Material

Impact of solutes and temperature on rheological and microscopic properties of particle gels from insoluble citrus-derived dietary fiber

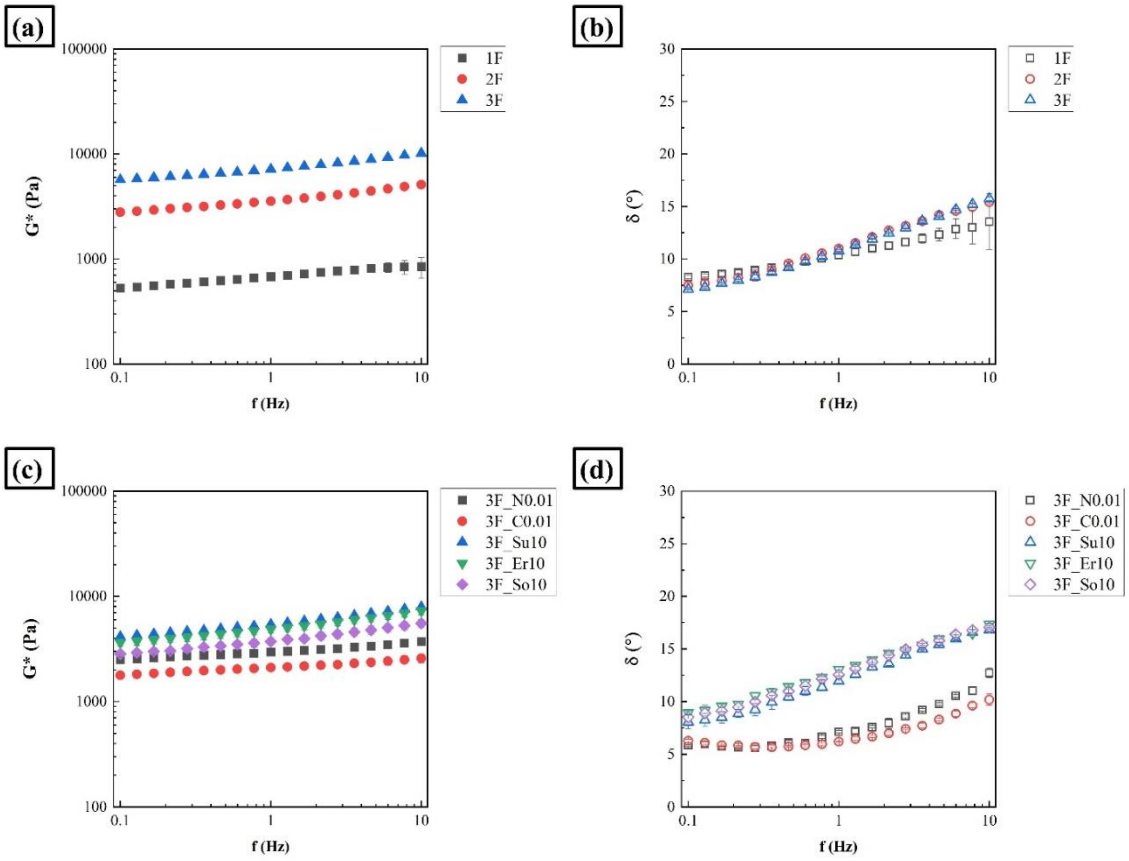

Fig. S1. Frequency sweep test: (a) complex modulus of samples with 1, 2 and 3% w/w of fiber, (b) phase angle of samples with 1, 2 and 3% w/w of fiber, (c) complex modulus of samples with 3% of fiber different type of solute (0.01 M NaCl, 0.01 M $CaCl_2$, 20% w/w sucrose, 20% w/w erythritol, 20% w/w sorbitol and 20% w/w sorbitol) and (d) phase angle of samples with 3% of fiber different type of solute (0.01 M NaCl, 0.01 M $CaCl_2$, 10% w/w sucrose, 10% w/w erythritol, 10% w/w sorbitol and 10% w/w sorbitol).

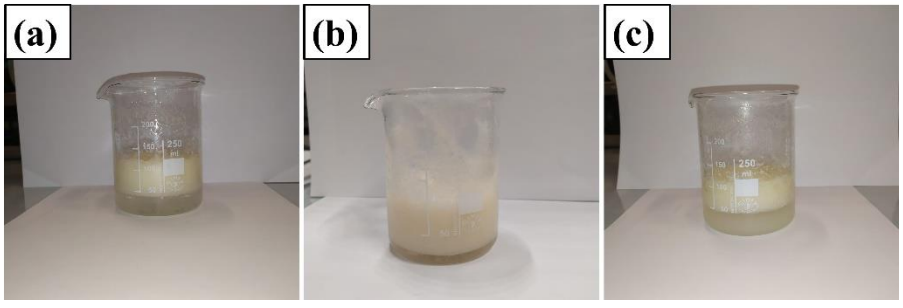

Fig. S2. Picture of unstable samples: (a) 1% w/w of fiber and 0.1 M $CaCl_2$, (b) 2% w/w of fiber and 0.1 M $CaCl_2$ and (c) 1% of fiber and 1 M NaCl.

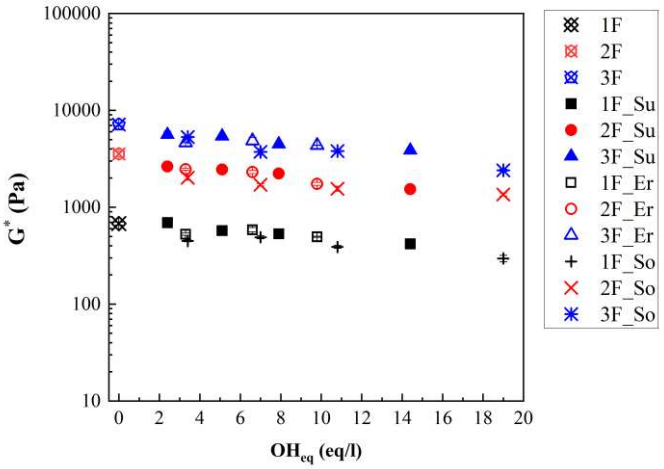

Fig. S3. Complex modulus of samples with different OH equivalents.

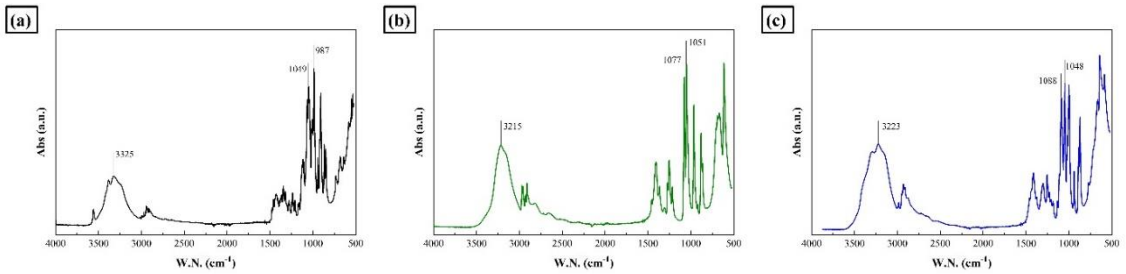

Fig. S4. FTIR spectra of sweeteners: (a) sucrose, (b) erythritol and (c) sorbitol.

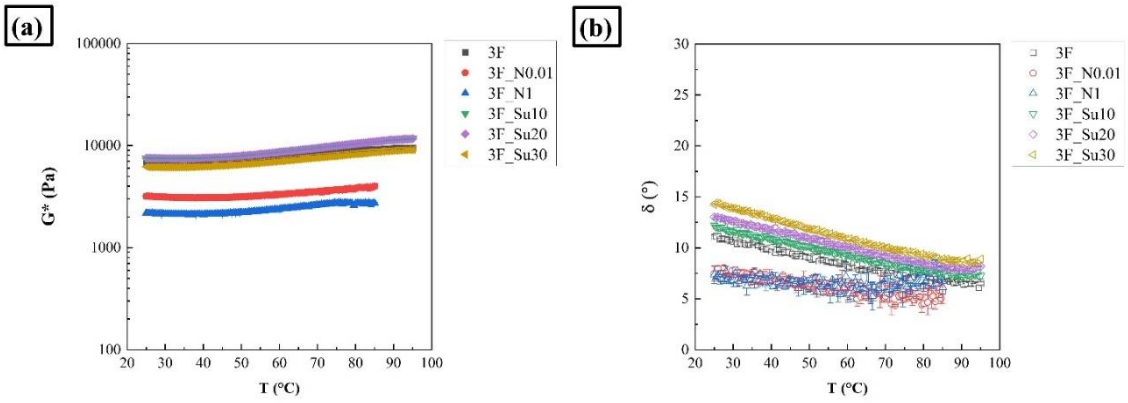

Fig. S5. Time cure test: (a) complex modulus of samples with 3% of fiber and different type and concentration of solute (no solute, 0.01 M NaCl, 1 M NaCl, 10% w/w, 20% w/w, 30% w/w of sucrose) and (b) phase angle of samples with 3% of fiber and different type and concentration of solute (no solute, 0.01 M NaCl, 1 M NaCl, 10% w/w, 20% w/w, 30% w/w of sucrose).

CHAPTER 3

The rheological modeling of food emulgels: application and insights on the interfacial contribution and estimation of droplets radius

The rheological modeling of food emulgels: application and insights on the interfacial contribution and estimation of droplets radius

Abstract

The rheological modelling of food emulsion is an emerging topic in the fields of food science and technology because of its potentiality in designing foods with desired consistency. To date, several approaches, theoretical, semi-empirical and empirical, have been proposed. In the present research work the comparison and the application of semi-empirical models based on Palierne theory of composite gels is proposed. The approach used considered the interfacial rheological properties and the effect of composition on microstructure. Modelled samples contained citrus fiber as structuring agent of the water phase and soy lecithin as emulsifier. Hydrogels with different fiber content (1% – 4% w/w) and emulgels with different fiber content (1% – 4% w/w) and different oil phase fraction (5% – 50% w/w) were produced by microfluidization. The linear viscoelastic behavior was investigated with frequency sweep test and data for modelling were expressed in terms of relative complex modulus (G_r^*), defined as the ratio of the complex modulus of the emulgel and the complex modulus of the continuous phase, and related to the oil phase volume fraction (φ). Furthermore, interfacial rheological measurements were also carried out aiming at determining specific properties, such as interfacial tension (γ), interfacial dilatational modulus (E_i) and interfacial shear modulus (G_i). Particle/droplets size distribution analysis was also carried out and considered in the modelling by empirical equations. Optical and confocal microscopy successfully monitored the morphology of samples providing solid support to rheological description and revealing even a phase transition from O/W emulgel to bi-continuous microemulsion.

Key words

Dietary fibers, composite gel, food structure, emulsion microscopy, interface engineering, texture

1. Introduction

Emulgels or emulsion gels are O/W or W/O multiphasic systems in which one of the two phases is structured [1–4]. In general, emulgel can be seen as a subcategory of composite gel in which only one of the two phases exhibited gel behavior whereas the other is a viscous liquid [2,3,5]. The emulgels have several applications which range from the pharmaceutical to food field [2–4,6]. Most of emulgels in food industry consist in O/W multiphasic systems in which the water phase is structured by a gelling agent such as proteins, pectins, dietary fibers, gums, gelatin [1,3,7–10] and often emulsifiers, like lecithin, Tween 80 and Span 20, can be also present [8–10]. The utilization of emulgels in foods is typically related to fat replacement and reduction and/or to transport of active compounds [2–5,10].

In addition to the investigation into new ingredients and new technology for emulgel, the research aimed at investigating the rheological modelling of such systems to design foods with expected consistency. Very recently, advancements in the rheological modeling of multiphase food systems like emulgels and bigels have been proposed by several authors [7,10–13]. The rheological behavior of composite gel, from a theoretical point of view, was developed for ideal systems in dilute condition in the works of Fröhlich and Stack [14] and Kerner [15]. Real systems like viscoelastic-type foods are very complex and far from ideal theoretical systems, this makes hard the physical modeling and the consequent application of equations for food design. A lot of factors have been considered in the development of equations for non-ideal systems. Starting from ideal composite gels, Lewis and Nielsen [16] studied the effect of concentration limit due to inclusion packing and proposed a correction parameter. Palierne [17] developed, theoretically, the equations for the description of incompressible composite gels taking into account interfacial tension and moduli for polydisperse composite systems. Afterwards, Pal [18] validated a simplified form of Palierne equation taking into account only the interfacial tension. For food systems, recently, van Aken et al. [5], starting from Palierne approach, simplifying it by considering monodisperse systems, and Lewis and Nielsen correction, developed an additional equation targeted to quantify the effects of particles/droplets aggregation. The same authors in a subsequent works validate this approach by modelling food systems containing porcine skin gelatin, whey protein and beef/milk fat [7]. For consistent systems, with two immiscible structured networks, like bigels, a novel semiempirical equation was recently developed by modifying the Palierne equation [11,12]. Particularly, the author introduced in the equation a coefficient dependent from the ratio between the elastic moduli of the dispersed phase and the continuous phase and modified the deviation from dilution condition proposed by Lewis and

Nielsen [11,12]. The modelled systems consisted in bigels in which the oil phase, Extra Virgin Olive (EVO) oil was structured with policosanol or glyceryl monostearate, whereas the continuous phase was structured with low methoxyl pectin or citrus fiber.

The analysis of the literature, dealing with these biphasic materials, highlights that the interface plays a relevant role for systems in which dispersed phase (typically the oil phase) is much less consistent than the continuous phase (typically the water phase) like emulgel systems.

Recently, Bruno and coauthors [10] proposed a modified form of Palierne model introducing an empirical correction and taking into account the interfacial contribution by interfacial tension, similarly, to Pal [18] and by assuming a constant value for the droplets diameter. This model, in which an empirical fitting parameter was introduced, has been developed for emulgels structured with citrus fiber and containing sunflower oil and soy lecithin.

In this context, the present research work proposes a semi-empirical approach to model emulgels with the water phase structured by citrus fiber and the oil phase, EVO oil, containing soy lecithin. As well known, all the ingredients used in the formulations, i.e., citrus fiber, EVO oil and lecithin show interesting physiological benefits and are suitable for healthy food preparations and meet the criteria for attractive nutritional claims like vegan, plant-based, source of fiber and so on [19–23]. Hydrogel and emulgels samples were prepared by using an advanced homogenization technique, the dynamic high pressure microfluidization, or more simply microfluidization which is a very attractive dispersion/emulsification process for food industry [8,9,24].

Bulk rheology in linear viscoelastic conditions was used for the determination of the complex modulus of single phase and emulgels; microstructural and morphological investigation were carried out to provide microstructural data, also suitable to relate the droplets radius to the sample composition.

Concerning the interfacial contribution analysis, different types of measurements were carried out aiming at obtaining all the parameters required for the application of the generalized Palierne equation (interfacial tension, interfacial dilatational modulus and interfacial shear modulus). Different models were investigated and compared aiming at identifying a potential tool suitable to describe different types of emulgels and, possibly, enough simple to be used in potential practical applications.

2. Material and methods

2.1.Materials

Citrus fiber (trade name Vitacel CF 312 ®) was kindly provided by JRS Silvateam Ingredients S.r.l. (Italy). Organic soy lecithin was purchased from IVOVITAL GmbH (Germany). Distilled water and extra virgin olive oil, EVO oil, (De Santis, Italy) were used for the preparation of the aqueous and oil phases respectively.

Heinz light mayonnaise (Kraft-Heinz, USA), with 26% w/w of fats (named B1), and Philadelphia light (Mondelēz International, USA), with 12% of fats (named B2), were bought in a local supermarket and used as commercial benchmarks for model validation.

All chemicals were used as received without any purification.

2.2.Samples preparation

Particle hydrogels at different fiber fractions in water phase (x_f, in w/w) and emulgels with different fiber fraction in water phase (x_f, in w/w) and oil fraction (ϕ, in w/w or φ, in v/v) were prepared using a two-step protocol based on high-speed homogenization (HSH) and dynamic high pressure microfluidizer (DHPM).

For all the preparations a batch of 200 g of samples was pre-homogenized using Ultraturrax T50 (IKA-Werke, Germany) equipped with the G45F tool at 4000 rpm for 1 min. Coarse system was treated with Microfluidizer M110P (Microfluidics Int. Corp., USA) at 25000 psi (1724 bar) using a series of two Z-type interactions chambers (H30Z and G10Z) with channel diameters of 200 μm and 87 μm, respectively. The outlet of the homogenizer was thermally controlled through a thermostatic ice bath, and the sample temperature was approximately 17-20 °C. Samples were stored at 4°C for 24 hours before the characterizations.

The sample ID, composition and some rheological parameters of hydrogel samples at different fiber fractions are reported in Tab.1.

For the emulgel preparation the oil phase was added to the water phase with a slow flow rate (approximately 11 - 14 g/min) while pre-homogenizing the sample with Ultraturrax at 500 rpm; after oil addition, further pre-homogenization was prolonged for 1 min at 4000 rpm. Oil phase containing 15% w/w of soy lecithin was prepared according to the literature [10] dissolving powdered lecithin in extra virgin olive (EVO) oil at 70 °C for 30 minutes using a magnetic stirrer at 300 rpm (AREX Heating Magnetic Stirrer, Velp Scientifica, Italy). The

oil phase was then cooled down to 25 °C by immersion in thermostatic water bath under stirring at 300 rpm.

The sample ID, composition and some rheological parameters of emulgels samples with fixed fiber fraction different oil phases are reported in in Tab.2 whereas those of emulgels with different fiber and different oil fraction are reported in Tab. 3.

Some pictures of hydrogel and emulgel samples are reported in Fig.S1a and Fig.S1b, respectively, of the Supplementary Material (SM).

Sample ID	x_f **(w/w)**	G_C^* **(Pa)**	δ (°)
H1	0.010	2200 ± 40	6.5 ± 0.2
H1.5	0.015	4600 ± 200	7.1 ± 0.1
H2	0.020	8200 ± 600	7.64 ± 0.08
H2.5	0.025	13700 ± 800	7.9 ± 0.1
H3	0.030	19800 ± 900	8.1 ± 0.1
H3.5	0.035	23100 ± 700	8.3 ± 0.1
H4	0.040	27600 ± 400	8.6 ± 0.2

Tab. 1. Sample ID, composition, complex modulus (G_C^*), phase angle (δ) of hydrogels with different fiber fractions.

Sample ID	x_f **(w/w)**	ϕ **(w/w)**	φ **(v/v)**	G_E^* **(Pa)**	δ (°)
E1/5	0.01	0.05	0.54	1680 ± 40	6.7 ± 0.1
E1/10	0.01	0.10	0.11	1300 ± 50	6.78 ± 0.03
E1/15	0.01	0.15	0.16	970 ± 50	7.0 ± 0.2
E1/20	0.01	0.20	0.21	590 ± 20	7.4 ± 0.298
E1/25	0.01	0.25	0.26	430 ± 20	9.1 ± 0.4
E1/30	0.01	0.30	0.31	334 ± 6	9.9 ± 0.4
E1/35	0.01	0.35	0.37	280 ± 20	10.9 ± 0.4
E1/40	0.01	0.40	0.42	311 ± 7	11.6 ± 0.1
E1/45	0.01	0.45	0.47	330 ± 5	11.8 ± 0.2
E1/50	0.01	0.50	0.52	501 ± 6	10.12 ± 0.08

Tab. 2 Sample ID, composition, complex modulus (G_E^*) and phase angle (δ) of emulgels with different oil fractions.

Sample ID	x_f (w/w)	ϕ (w/w)	φ (v/v)	G_E^* (Pa)	δ (°)
E2/10	0.02	0.10	0.11	3900 ± 200	7.5 ± 0.1
E2/15	0.02	0.15	0.16	2600 ± 100	7.60 ± 0.08
E2/20	0.02	0.20	0.21	1700 ± 100	8.05 ± 0.08
E2/30	0.02	0.30	0.31	1300 ± 60	8.4 ± 0.1
E2/40	0.02	0.40	0.42	1010 ± 70	9.2 ± 0.2
E3/10	0.03	0.10	0.11	8340 ± 90	7.92 ± 0.08
E3/15	0.03	0.15	0.16	4800 ± 200	7.79 ± 0.05
E3/20	0.03	0.20	0.21	3500 ± 200	8.01 ± 0.06
E3/30	0.03	0.30	0.31	3100 ± 100	8.6 ± 0.2
E3/40	0.03	0.40	0.42	2080 ± 20	8.34 ± 0.06
E4/10	0.04	0.10	0.11	11400 ± 300	8.2 ±0.1
E4/15	0.04	0.15	0.16	7554 ± 6	8.2 ± 0.1
E4/20	0.04	0.20	0.21	4900 ± 200	8.21 ± 0.02
E4/30	0.04	0.30	0.31	4300 ± 200	8.27 ± 0.04
E4/40	0.04	0.40	0.42	3400 ± 100	8.39 ± 0.08

Tab.3. Sample ID, composition, complex modulus (G_E^*) and phase angle (δ) of emulgels with different fiber fractions and oil fractions.

2.3.Rheological modelling of emulgel

Relative complex modulus was defined for emulgels, (Eq.1) as the ratio between the complex modulus of the emulgel (G_E^*, in Pa) and the complex modulus of the continuous phase (G_C^*, in Pa) evaluated both at 1 Hz and it was used for system description and modelling.

$$G_r^* = \frac{G_E^*}{G_C^*} \tag{1}$$

Starting from the Fröhlich and Sack theory [14] and following the mathematical developments proposed by other authors [15,25,26] the mechanical behavior of composite gels in terms of the relative modulus (G_r^*) can be linked to the volume fraction of dispersed phase (φ) and to the Poisson ratio (ν_m), through the Kerner equation (Eq.2).

$$G_r^* = \frac{15(1-\nu_m)(M-1)\varphi}{M(8-10\nu_m)+7-5\nu_m-(8-10\nu_m)(M-1)\varphi} + 1 \tag{2}$$

where M is the ratio between the complex modulus of dispersed phase (G_D^*, in Pa) and the complex modulus of the continuous phase (G_C^*, in Pa), Eq.3.

$$M = \frac{G_D^*}{G_C^*} \tag{3}$$

For incompressible materials $\nu_m = 0.5$ and Eq.2 becomes:

$$G_r^* = \frac{1 + \frac{3}{2}H\varphi}{1 - H\varphi} \tag{4}$$

the so-called Kerner equation for incompressible material (named simply Kerner equation or Kerner model throughout the text). The Kerner equation or Kerner model is the starting point for modelling composite deformable materials. The parameter H (dimensionless) can be considered as a sort of "deformability coefficient" which, in its simplest form takes into account only the mutual action of both the viscoelasticity of dispersed phase (G_D^*) and continuous phase (G_C^*) through the moduli ratio M, according to Eq.5.

$$H = \frac{2(M-1)}{2M+3} \tag{5}$$

For non-deformable droplets, $M \to \infty$ and $H = 1$, while for completely deformable droplets $M \to 0$ and $H = -2/3$, which is the lowest limit if the interfacial rheology is not considered. Looking at Eq.4 it is easy to note that negative values of H leads to a decreasing function of G_r^* with φ, which means that the dispersed phase gives a negative contribution to the consistency of the system (weakening action). On the contrary, positive values of H leads to an increasing function of G_r^* with φ, i.e., the dispersed phase gives a positive contribution to the consistency of the composite (strengthening action) while for $H = 0$, G_r^* is independent from φ. In general, H is also related to interfacial rheological properties of the composite systems as reported by Palierne [17]. According to the simplified Palierne approach adopted by Pal et al. [18] and modified by Bruno et al. [10] for food emulgels, the parameter H can be replaced by H', Eq.6-7, which represents a deformability coefficient function of moduli ratio (M), interfacial tension (γ, in N/m), complex modulus of the continuous phase (G_C^*, in Pa) and droplets radius (R, in m). In Eq.6-7 the composite system is assumed to be made by monodisperse droplets.

$$H = H' \tag{6}$$

$$H' = \frac{2(M-1)(19M-16) + \left(\frac{8\gamma}{G_C^* R}\right)(5M+2)}{(2M+3)(19M+16) + \left(\frac{40\gamma}{G_C^* R}\right)(M+1)} \tag{7}$$

Considering the most general equation for composite gel, i.e., the extended Palierne equation [17], in addition to moduli ratio, interfacial tension, continuous phase modulus and droplet radius, also the interfacial dilatational modulus (E_i, in N/m) and the interfacial shear modulus (G_i, in N/m) give a contribution to the deformability coefficient of composite gel. In this

generalized approach, H is replaced by H'' and, for monodisperse composite materials, it can be calculated according to Eq.8-10.

$$H = H'' = \frac{E}{D} \tag{8}$$

$$E = 2(M-1)(19M+16) + \frac{48E_i\gamma}{G_C^{*2}R^2} + \frac{32G_i\,(\gamma+E_i)}{G_C^{*2}R^2} + \frac{8\gamma}{G_C^*R}\,(5M+2) + \frac{2E_i}{G_C^*R}(23M-16) + \frac{4G_i}{G_C^*R}(13M+8) \tag{9}$$

$$D = (2M+3)(19M+16) + \frac{48E_i\gamma}{G_C^{*2}R^2} + \frac{32G_i\,(\gamma+E_i)}{G_C^{*2}R^2} + \frac{40\gamma}{G_C^*R}\,(M+1) + \frac{2E_i}{G_C^*R}\,(23M+32) + \frac{4G_i}{G_C^*R}(13M+12) \tag{10}$$

The composite gel equation, Eq.4, was developed for ideal systems (monodisperse and perfectly spherical particles/droplets, no aggregation).

The expression of Eq.4 and Eq.8 derives from Palierne equation in its original form [17], i.e., for polydisperse systems reported in Eq.11.

$$G_r^* = \frac{1 + \frac{3}{2}\sum_I \varphi_I \frac{E_I}{D_I}}{1 - \sum_I \varphi_I \frac{E_I}{D_I}} \tag{11}$$

In Eq.11, the rheological contribution of each inclusion (droplets) of type I is considered and properly weighted.

To take into account the concentration effect and the limit in the amount of dispersed phase Lewis and Nielsen [16] proposed a correction by introducing the crowding factor (ψ, dimensionless), which is related to the maximum packing volume fraction of dispersed phase. Particularly, according to Lewis and Nielsen, Eq.4 can be rewritten by introducing ψ in the denominator, Eq.12, or even in both numerator and denominator, Eq.13.

$$G_r^* = \frac{1 + \frac{3}{2}H\varphi}{1 - \psi H\varphi} \tag{12}$$

$$G_r^* = \frac{1 + \frac{3}{2}\psi H\varphi}{1 - \psi H\varphi} \tag{13}$$

In addition to the crowding factor, other issues, like droplets size distribution, droplets shape, aggregation phenomena, morphological changes, make the systems description more complex and Eq.12-13 results unsuitable for modelling real systems. Indeed, as reported by

Bruno et al [10] by applying Eq.11 to real emulgels the crowding factor, ψ, lose its physical meaning becoming a simple empirical fitting parameter.

Starting with these considerations, in the present work an equation similar to Eq.12 is proposed, even if ψ is replaced by a parameter A which has the meaning of a corrective empirical parameter grouping all the non-ideality factors (Eq.14).

$$G_r^* = \frac{1 + \frac{3}{2}H\varphi}{1 - AH\varphi} \tag{14}$$

The adopted modelling strategy involves the computation of Eq.14 by calculating H using the previously described equations. Specifically, three different cases are studied: the first, Eq.13 in which the deformability coefficient (H) is estimated according to Eq. 5 representing a modified form of Kerner model (mK); the second case, Eq.14 in which the deformability coefficient (H') is estimated according to Eq. 6-7 representing a modified form of the simplified Palierne model (msP) and the third, Eq.14 in which the deformability coefficient (H'') is estimated according to Eq. 8-10 representing a modified form of the extended Palierne model (meP).

In the cases of the calculation of H' and of H'', although the interfacial rheological properties can be identified univocally it is worth noticing that the identification of the droplets radius (R), which is assumed equal for all droplets (monodisperse systems), represents an interesting challenge. Indeed, this highlights the difficulties of defining a "mean" diameter of the experimental droplet size distribution, to be used in the model, among different potential definitions [27,28].

2.4.Rheological modelling of hydrogel

Aiming at relating the consistency of the emulgel to the fiber fraction in the water phase (the continuous phase), in the contest of food design, the Eq.1 have to be coupled to a relation between the complex modulus (G_C^*) and the fiber fraction in the water phase (x_f). In particular, in order to keep a practical approach, the complex modulus of particle gels was related to fiber fraction, by simple power law relations, reported in Eq.15-16.

$$G_C^*(\omega) = k\ \omega^n \tag{15}$$

$$G_C^* = A\ {x_f}^B \tag{16}$$

where G_C^* is the complex modulus (Pa) of the water (continuous) phase, i.e., of the hydrogel, k and n are fitting parameters, ω is the oscillation frequency (s^{-1}), x_f is the fiber fraction (w/w), A and B are fitting parameters.

2.5.Rheological characterization

Rheological characterization was carried out using the stress-controlled rotational rheometer Haake MARS 40 (Thermo Fisher Scientific, USA) equipped with parallel sandblasted plates (diameter 35 mm gap 1.6 ± 0.2 mm) for hydrogel, emulgel and benchmarks characterization, whereas for oil phase smooth parallel plates (diameter 50 mm, gap 1.0 ± 0.2 mm) were used. Stress sweep tests were carried out to identify the linear viscoelastic region. Frequency sweep tests were carried out between 0.1 and 10 Hz using the stress values in the linear viscoelastic conditions. In order to limit the evaporation of water from the sample during the measurements a cover cell was used. All the measurements were carried out at 25°C and repeated three times. The results are shown in terms of average value and standard deviation.

2.6. Interfacial rheological analysis and characterization

The determination of the interfacial properties to be used for the extended modelling of the systems (Eq.7, Eq.9-10), i.e., interfacial tension (γ), interfacial dilatational modulus (E_i) and interfacial shear modulus (G_i), was carried out using different types of interfacial rheological methods. With the assumption that both lecithin and fibers can absorb at the O/W interface until the formation a monolayer which divides the water phase from the oil phase and that, exceeding such concentrations, commonly indicated as saturation condition of the interface, the interfacial rheological properties do not change, all the interfacial properties were determined in saturation condition of the O/W interface, in agreement with the procedure already used in a previous work on similar systems [10].

In particular, the equilibrium interfacial tension (γ_{eq}), defined according to literature [29], was determined by static interfacial tension measurements. The saturation condition was determined by measuring the equilibrium interfacial tension (γ_{eq}) in different condition of fiber fraction in water phase (x_f) and lecithin fraction in oil phase (x_l), i.e., by the interfacial adsorption isotherm. The interfacial tension (γ) used for the rheological modelling was assumed to be equal to the γ_{eq}in saturation condition., i.e., the condition of x_f and x_l at which a monolayer of fiber and lecithin is formed at the O/W interface.

Preliminary interfacial dynamic tests in dilatational kinematic evidenced experimental difficulties related to optical interferences yielding high error bars and poor reproducibility. For this reason, the interfacial dilatational modulus was determined by interfacial dilatational relaxation tests in saturation condition of the interface. Specifically, the interfacial

dilatational modulus (E_i) in Eq.9-10 was associated to the effective surface modulus ($E_{d,eff}$) defined according to literature [29] by Eq.17.

$$E_{d,eff} = \frac{\Delta\gamma}{\frac{\Delta A}{A}} \tag{17}$$

where A is the area of the drop, ΔA is the difference of area between the final value of expansion/compression and the equilibrium value and $\Delta\gamma$ is the difference of interfacial tension associated to expansion/compression.

Static interfacial tension measurements and relaxation tests were carried out with FTA 200 tensiometer (First ten angstrom, USA) based on axisymmetric drop shape analysis (ADSA) and equipped with fta32 v2.0 software. For all measurements, a glass Hamilton syringe (1710TLL) equipped with a stainless-steel needle (d = 20 gauge) was used. Tests were performed at room temperature (22 ± 2°C).

The interfacial shear modulus (G_i) was associated to the interfacial complex shear modulus (G_i^*) determined from frequency sweep test in shear kinematics, in saturation condition of the interface, using the Interfacial Shear Rheometer ISR400 (KSV Instruments, Finland), equipped with a magnetic needle (weight = 0.0081 g, length = 31 mm). The frequency sweep test was performed in the frequency range of 0.5 – 2.0 Hz.

2.7.Laser diffraction and microstructural analysis

Particles/droplets size distribution (P/DSD) of samples was determined by the laser diffraction technique with a Mastersizer 2000 (Malvern. UK), using Hydro2000G accessory for wet dispersion. Samples were diluted and gently dispersed in distilled water before the analysis. Every P/DSD acquisition was the result of computations of three signals and for each sample three independent acquisitions were collected and the results averaged. As microstructural parameters connected to particle size of hydrogel and droplet size of emulgel both the surface diameter ($D_{3,2}$) and the volume diameter ($D_{4,3}$), expressed according to Eq.18 and Eq.19, respectively, were used as quantitative parameters.

$$D_{3,2} = \frac{\sum_{i=1}^{N} n_i {d_i}^3}{\sum_{i=1}^{N} n_i {d_i}^2} \tag{18}$$

$$D_{4,3} = \frac{\sum_{i=1}^{N} n_i {d_i}^4}{\sum_{i=1}^{N} n_i {d_i}^3} \tag{19}$$

where d_i is the diameter (in μm) of the i-th class of particles and n_i is the number of particles in the i-th class, i.e., with a diameter equal to d_i.

For the choice of the most suitable estimation of droplets radius (R) used for calculation of H' and H'' (Eq.6-7, Eq.8-10), i.e., the radius which "takes into account" the interfacial contributions, in the rheological modeling of composite gel containing uniform droplets, both definitions reported in Eq.18 and Eq.19 were used. Therefore, the droplets radius of the models was defined according to two cases, one as the half of surface mean diameter, $R = D_{3,2}/2$, and the other as the half of volume mean diameter, $R = D_{4,3}/2$. From a physical perspective, in the first case, greater importance is given to small-diameter droplets, whereas in the second case, it is assumed that the rheological behavior is more affected by large-sized droplets.

It is worth noticing that it was assumed that for the emulgel the obtained size distribution is more related to the oil droplets than to the fiber particles in water phase and therefore can be used to have a mean radius representing the oil phase. To take into account the change in microstructure, and consequently in the droplets size, due to composition, empirical correlations, based on best fitting, were adopted, to relate both $D_{3,2}$ and $D_{4,3}$ to the composition, in terms of oil phase volume fraction (φ) and fiber fraction in water phase (x_f). The obtained expressions were used for the estimation of the droplet radius (R).

2.8.Contrast phase optical microscopy (CPOM)

Optical microscopy investigations were carried out on emulgel samples using Axio Scope A1 (Carl Zeiss, Germany) in contrast phase mode with a magnification of 100X and the immersion objective with Immersol® 518N (Zeiss, Germany) was used.

2.9.Confocal laser scanning microscopy (CLSM)

Confocal laser scanning microscopy (CLSM) investigations were carried out on emulgels samples by using Stellaris 8 (Leica microsystem, Germany) microscope equipped with 63X immersion object (1.4 oil). Micrographs were taken according to sample autofluorescence without any staining. Both reflectance and emission signal were used in morphological investigation. For reflectance analysis the excitation wavelength was 631 nm and the spectral position 619 – 647 nm, for water phase morphology the excitation was at 405 nm and the spectral position of emission at 410 – 605 nm, while for oil phase the excitation was 638 nm and the spectral position of emission at 648 – 833 nm. Images were acquired with a scanning speed of 400 Hz, a resolution of 512 X 512 pixels and processed by LAS X software (Leica).

3. Results and discussion

3.1.Rheology of single phases

Complex modulus and phase angle at 1 Hz of particle hydrogel samples at different fiber concentrations (x_f) are reported in Fig. 1a. The modulus significantly increases with the increasing of the fiber concentration indicating an increase in consistency, in agreement with results already obtained in the literature on similar samples [10,11]. On the other hand, the phase angles slightly increase with the increasing of fiber fraction, indicating a decrease of the structuring degree with the increase of fiber fraction, in contrast to previous results on similar hydrogels [10], in which phase angle resulted independent on fiber fraction. However, this could be explained considering that citrus fiber structuring effect is related also to homogenization power as previously described [30,31] and in the present work the same power was used for samples with different fiber fraction (and consistency); as a consequence, a lower degree of activation, hydration, swelling and networking could be expected for more concentrated systems.

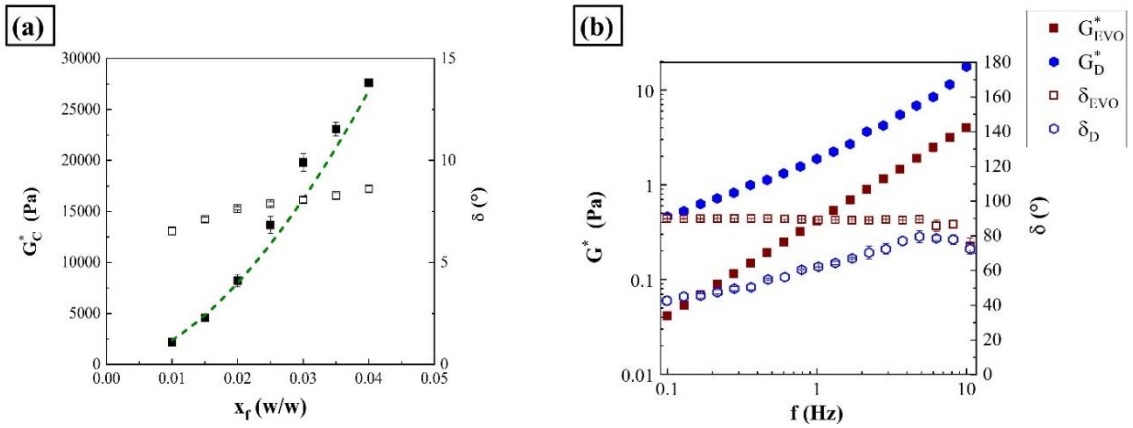

Fig.1. Rheology of single phases: (a) complex modulus, phase angle and fractal model of particle hydrogel samples and (b) Frequency sweep test of EVO oil and oil phase. Dashed line refers to data fitting (Eq. 15)

The complex modulus and the phase angle of both pure EVO oil and oil phase (i.e. EVO oil with 0.15 w/w of soy lecithin) are reported in Fig.1b. As can be seen, the addition of lecithin to EVO oil yields an increase of the complex modulus ($G_D^* > G_{EVO}^*$) and a decrease of the phase angle ($\delta_D < \delta_E$). However, the value of phase angle is higher than 45° in all the frequency range, indicating, as expected, that lecithin added EVO oil still behaves as a liquid-like material. Indeed, the lecithin alone is not able to form organogel or other

structured oily systems [32], then lecithin addition cannot introduce elastic component in the bulk rheology of the oil phase, unlike other oleogelators [11]. Furthermore, these results are in agreement with the results obtained on sunflower oil and a different soy lecithin in a previous study [10]. According to the experimental results, the value of complex modulus at 1 Hz of the disperse phase (G_D^*) used in models is equal to 1.87 ± 0.04 Pa.

3.2.Microstructure of samples

It is worth noticing that for hydrogel the laser diffraction, used to estimate size distribution, is due only to citrus fibers particles whereas for emulgels both citrus fiber particles and oil phase droplets generate diffraction. Consequently, the results of hydrogel analysis will be presented as Particle Size Distribution (PSD) whereas that of emulgels as Particle/Droplets Size Distribution (P/DSD).

The analysis of particle gel samples highlighted that particle size distribution does not depend on fiber concentration (x_f), in the range 0.01 - 0.04 w/w, and the following mean PSD parameters can be assumed for all systems: $D_{3,2}$ = 22.1 ± 0.1 μm and $D_{4,3}$ = 48.9 ± 2.1 μm. The P/DSD of emulgels with x_f = 0.01 w/w of fiber and different oil mass fraction (ϕ) is reported in Fig.2a. Looking at the figure it is possible to observe that increasing ϕ, the distribution moves toward lower value of size. The decrease of droplet size with increasing ϕ in emulgels is not unexpected, since the consistency of the oil phase is much lower than that of citrus fiber hydrogel matrix, then applying the same power to samples with different ϕ, smallest droplets will be produced in case of samples richer in (a less consistent) oil phase. For a low fraction of oil phase, a monomodal distribution was found whereas for ϕ > 0.25 w/w a bimodal distribution was observed. Furthermore, for ϕ > 0.40 w/w the distributions shift below 1 micron and the shape of the distribution curves notably changes, suggesting a potential change in microstructure.

The P/DSD of emulgel samples with different fiber concentration and ϕ = 0.1 w/w is reported in Fig.2b. For fiber content higher than 0.01 w/w a second peak in the distribution can be observed at larger size and, increasing the fiber content, the height and width of this peak increase. Considering this observation and the parameters of the PSD of hydrogel samples, it could be speculated that the peaks at larger size (~10–100 μm) could be attributed to fiber particle rather than to droplets.

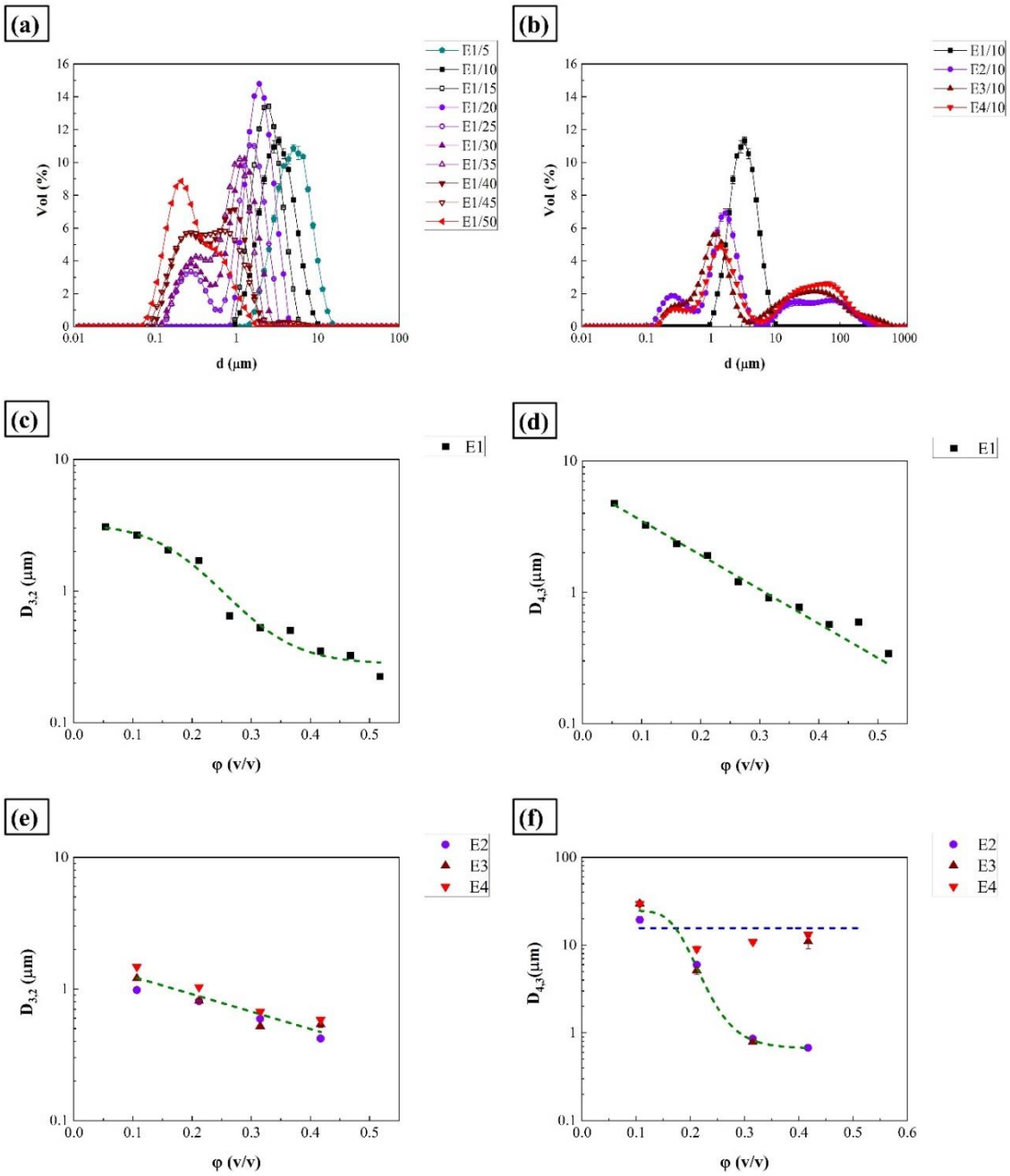

Fig.2. Droplets/particle size distribution of samples and droplets radius estimations: (a) emulgels E_1/x, (b) emulgels E_x/10, and (c) $D_{3,2}$ as a function of φ for set of samples E1 (d) $D_{4,3}$ as a function of φ for set of samples E1, (e) $D_{3,2}$ as a function of φ for samples E2, E3 and E4 and (c) $D_{4,3}$ as a function of φ for samples E2, E3 and E4. Dashed line reports the data fitting.

As reported in Fig.2c and Fig.2d, the data of surface diameter ($D_{3,2}$) and volume diameter ($D_{4,3}$) of set of samples E1, as a function of oil fraction, follows a different trend compared to that of E2, E3 and E4. On the contrary, by grouping the $D_{3,2}$ of set of samples E2, E3,

and E4 a common decreasing trend, as reported in Fig.2e was found. Concerning the $D_{4,3}$, no clear trend turns out by grouping E2, E3 and E4 as reported in Fig.2f, since some set of samples seems to have a $D_{4,3}$ which decrease with φ whereas others like E4 seem to have a constant value of $D_{4,3}$ with φ . $D_{3,2}$ data of set E1 was fitted using the sigmoidal-type law (Bolzman equation) reported in Eq.20 and Fig.2c.

$$D_{3,2} = \frac{A - B}{1 + e^{\frac{\varphi - C}{D}}} + B \tag{20}$$

with the following fitting parameters $A = 3.3 \pm 0.3$ (μm), $\mathrm{B} = 0.3 \pm 0.1$ (μm), $\mathrm{C} = 0.19 \pm 0.02\ (-)$ and $\mathrm{D} = 0.06 \pm 0.01\ (-)$. On the contrary, the mathematical relation used for the fitting of $D_{4,32}$data of set of samples E1 was the exponential-type law reported in Eq.21 and Fig.2d.

$$D_{4,3} = A\, e^{B\varphi} \tag{21}$$

with the following fitting parameters $A = 6.4 \pm 0.2$ (μm), $\mathrm{B} = -6.0 \pm 0.2\ (-)$. Similarly, the mathematical relation used to fit $D_{3,2}$ data of set samples E2, E3 and E4 was an exponential-type law, in Eq.22 and Fig.2e.

$$D_{3,2} = A\, e^{B\varphi} \tag{22}$$

with the following fitting parameters $A = 1.7 \pm 0.1$ (μm), $\mathrm{B} = -3.0 \pm 0.5\ (-)$.

For the set of samples E2 and E3 a sigmoidal-type law was adopted for the fitting of the $D_{4,3}$, data, as reported in Eq. 23 and Fig.2f (green dashed line). For the sake of simplicity, the point of set of samples E3 at φ = 0.42 (ϕ = 0.4) was excluded from the data fitting because resulted notably distant from the assumed trend (a further investigation on this will be necessary).

$$D_{4,3} = \frac{A - B}{1 + \left(\frac{\varphi}{C}\right)^{D}} + B \tag{23}$$

The following fitting parameters were obtained $A = 28 \pm 11$ (μm), $\mathrm{B} = 0.7 \pm 4.9$ (μm), $\mathrm{C} = 0.2 \pm 0.3(-)$ and $\mathrm{D} = 9 \pm 90\ (-)$. Finally, for set of samples E4 a common mean value of the $D_{4,3}$ equal to 15.6 ± 8.5 μm, see Fig.2f (blue dashed line), was used for a rough description of the samples.

This value with the Eq.20-22, with the respective fitting parameters, were rearranged as $R = D_{3,2}/2$ and $R = D_{4,3}/2$ and then inserted in Eq.6-7, and Eq.8-10 for the estimation of the deformability coefficients H' and H''.

3.3.Interfacial rheological behavior

Interfacial characterizations results are summarized in Fig.3a-c. The analysis of saturation condition was carried out in terms of equilibrium interfacial tension (γ_{eq}) [29] and it is reported in the Fig.2a. The adsorption isotherm of oil phase/water interface reports saturation condition at 0.005 w/w of lecithin (x_l) while looking at the γ_{eq} values of oil phase/hydrogel interface it is possible to conclude that also 0.005 w/w is the saturation condition in term of fiber fraction (x_f). The average value between the γ_{eq} at x_f = 0.005 w/w and γ_{eq} at x_f = 0.001 w/w (both in saturation condition) resulted to be 3.4 ± 0.2 · 10^{-3} N/m and was used as value of interfacial tension (γ) for models in computing Eq.7, Eq.9 and Eq.10.

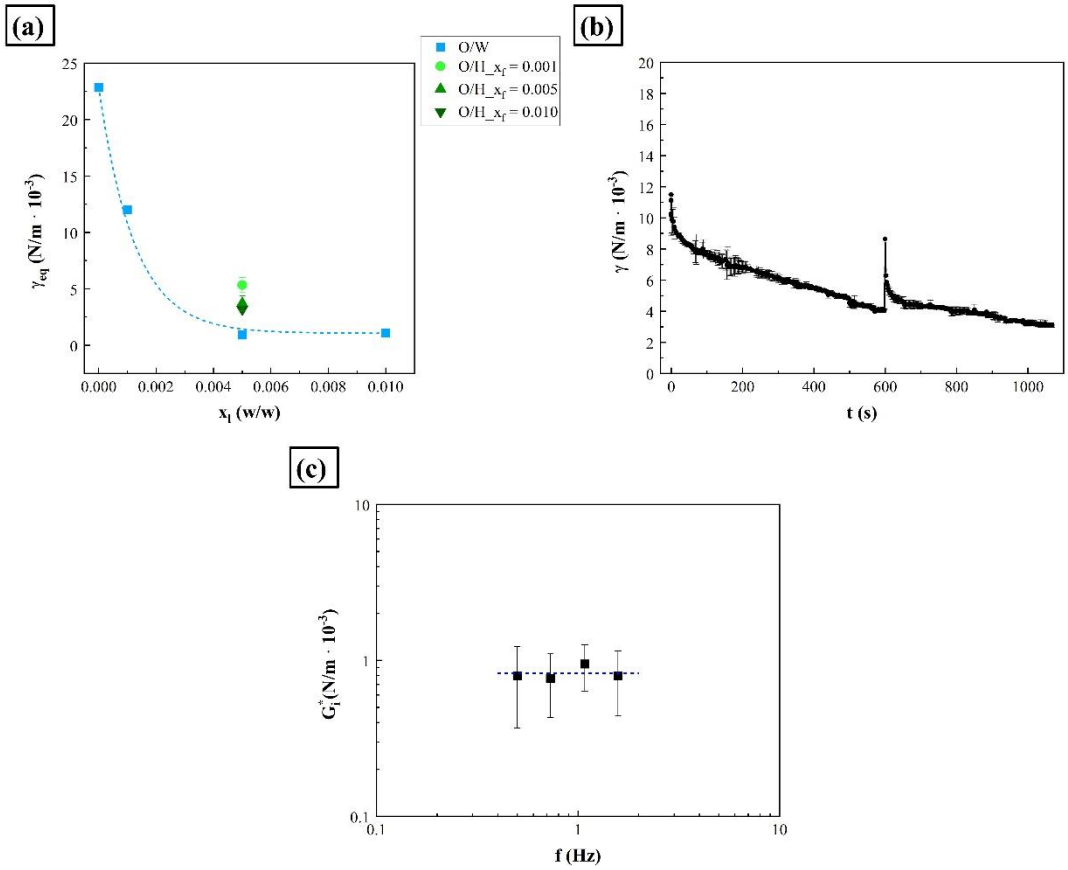

Fig.3. Interfacial rheological study: (a) static interfacial tension measure, (b) interfacial dilatation relaxation test and (c) interfacial shear frequency sweep test. Dashed line in (a) is a guide to highlight the isotherm, in (c) represents the mean value of complex shear interfacial modulus.

Carrying out relaxation test on sample in saturation condition the curve reported on Fig.2b was found and an effective interfacial modulus ($E_{d,eff}$) of 17.8 ± 0.7 · 10^{-3} N/m was

calculated. This value was used as elastic dilatational modulus (E_i) in computing Eq. 9 and Eq.10. From the figure, it is tis possible to appreciate the sharp variation of interfacial tension due to droplets dilatation around 600 s and the subsequent relaxation until the equilibrium value. It is worth noting that the data show a slightly large error bar, which can be attributed to the difficulties in carrying out interfacial tests on such types of samples. The complex shear interfacial modulus and phase angle are reported in Fig.2c. From the figure an apparent constant trend with frequency can be seen and also in this type of test the error bars are rather large. Since G_i^* resulted substantially constant in the frequency windows, as reasonable value at 1 Hz the mean of all the values can be considered. The mean values of G_i^* resulted 8.3 ± 0.2 · 10^{-4} N/m and it was used as G_i in computing Eq.9 and Eq.10.

3.4.Morphology of emulgels

The morphology of selected emulgel samples (E1/30, E1/50, E4/10, E4/30) is reported in the micrographs in Fig.4; a rather uniform spatial distribution of droplets can be observed, even if droplets with different sizes can be observed in agreement with the previous (quantitative) considerations on droplets size distribution of the emulgel samples. Looking at the CLMS micrographs these observations are confirmed and better highlighted by observation scale and colors (in blue the fiber network and in green the oil phase droplets) giving better morphological details. Looking at the red spots associated to the reflexing signal it is possible to observe some very small fragments of crystalline material, probably microcrystalline cellulose bonded to the oil droplets interface by Pickering effect [33,34]. However, this mechanism of stabilization is not predominant in such systems owing to the large size of the particles compared to that of droplets.

Finally, the microstructural change of emulgel with ϕ = 0.50 (φ = 0.52), E1/50, is visible from both optical and confocal micrographs. Specifically, for the highest oil phase volume fraction the droplets became extremely small, and they aggregate so much that they are no longer distinguishable and the formation of a bi-continuous microemulsion can be assumed. The formation of bi-continuous microemulsion for high oil phase volume fraction is not surprising since it contains lecithin which is an emulsifier particularly suitable for the formation of bi-continuous microemulsion, if it results to be predominant in O/W systems rich in oil phase fraction [35,36].

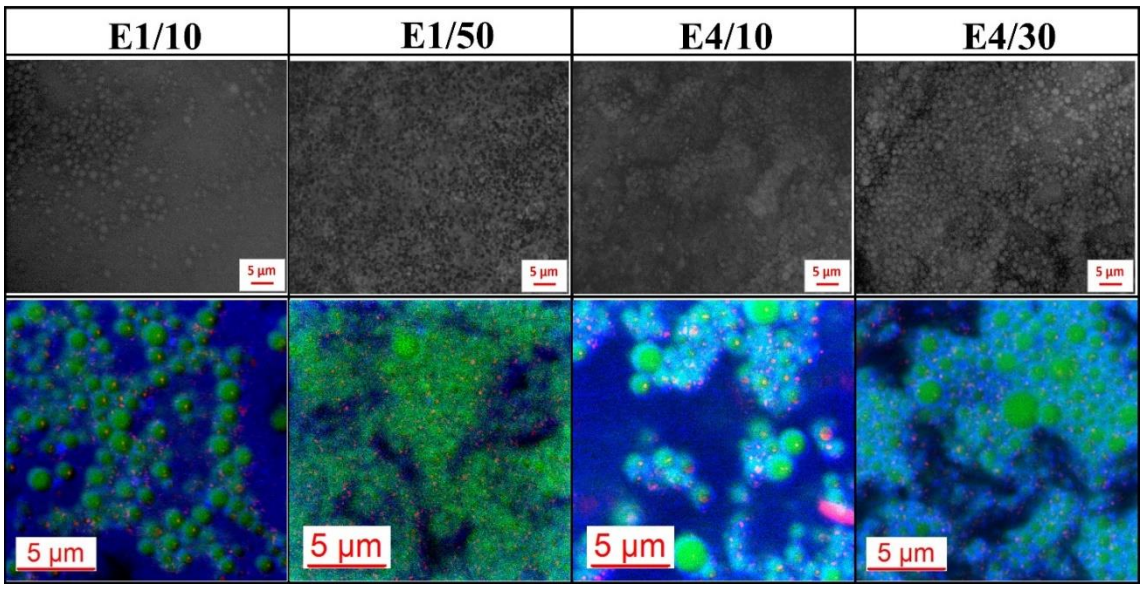

Fig.4. Optical and CLSM micrographs of emulgel samples

3.5.Rheological properties of emulgels

The rheological parameters of emulgel samples in terms of complex modulus (G^*), relative complex modulus (G_r^*) and phase angle (δ) evaluated at 1 Hz as function of oil phase volume fraction (φ) are reported in Fig.5a, Fig.5b and Fig.5c, respectively.

From Fig.5a, it is possible to observe that for samples E2, E3 and E4 G^* decreases with the increasing φ, whereas for sample E1 a non-monotonous trend, with a minimum at φ = 0.37 is observed. Comparing the different sets of samples, it is possible to say that the higher the fiber content the higher the values of G^*, however this increase became progressively smaller, indicating some sort of asymptotic condition in G^* increase due to fiber fraction.

Concerning the G_r^*, as it can be seen in Fig.5b, the trends with φ are the same of that reported for the G^*, and are in agreement with results described in the literature for similar systems [10]. It is worth noticing that, in contrast to G^*, G_r^* decreases with increasing fiber fraction, even if differences among different sets decreases with x_f and samples E3 and E4 almost overlap. Finally, for high φ, G_r^* seems to be independent of fiber fraction.

Interesting results were also obtained in terms of phase angle, δ, as reported in Fig.5c. Specifically, for set of samples E3 and E4 δ remains almost constant in the whole range of φ, , similarly to previous results [10], whereas samples E2 increases with the increase of oil fraction. Finally, for the set of samples E1 the phase angle increases with the increasing of φ in the emulgel formulation up to φ = 0.47 while for φ = 0.52 it sharply decreases. It is interesting to observe that sample E1/50 also exhibited a relevant difference in both shape

of DSD and morphology with respect to those of the other samples, indicating that the differences in δ could be due to a completely different microstructure.

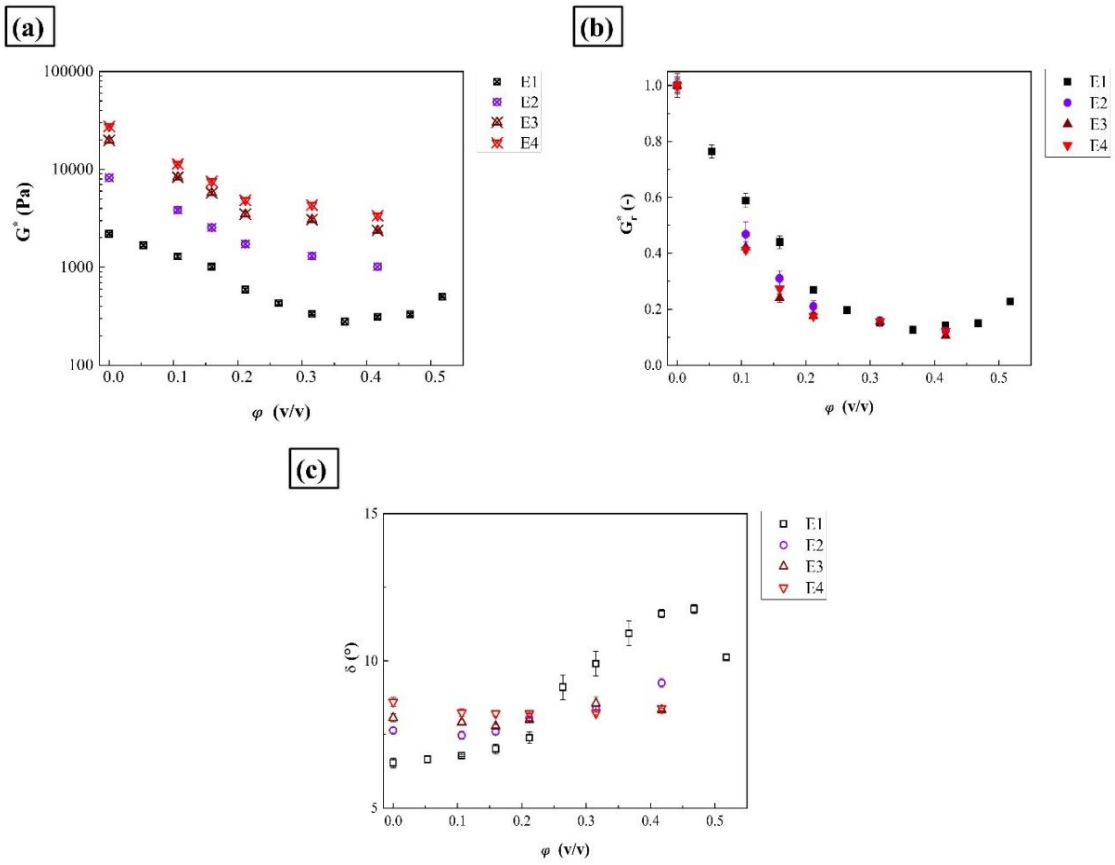

Fig.5. Rheology at 1 Hz of emulgel samples at different oil phase volume fraction: (a) complex modulus (b) relative complex modulus and (b) phase angle.

3.6.Rheological modeling: analysis of the interface-bulk contributions

The evaluation of the contribution of single interfacial parameters with respect to bulk rheological properties was carried out using three dimensionless rheological parameters. The approach used is similar to the definition of the moduli ratio M, but takes into account the interfacial parameters, the droplets radius and the complex modulus of the continuous phase. In particular, the following interface-bulk moduli ratio were defined according to Eq.24, Eq.25 and Eq.26, respectively: tension-bulk moduli ratio (M_γ), elongational-bulk moduli ratio (M_E) and shear-bulk moduli ratio (M_G). They were used to evaluate the interfacial contribution to system rheology.

$$M_\gamma = \frac{\gamma}{G_c^* R} \tag{24}$$

$$M_E = \frac{E_i}{G_c^* R} \tag{25}$$

$$M_G = \frac{G_i}{G_c^* R} \tag{26}$$

where G_c^* (in Pa) is the continuous phase complex modulus, R (in m) is the droplets radius, γ (in N/m) is the interfacial tension, E_i (N/m) and G_i (N/m) are the interfacial dilatational and shear modulus, respectively. Since for the present systems the interfacial properties are assumed to be composition independent, i.e., assuming that the interfacial tension, the dilatational modulus and the shear modulus do not exceed the values reached in the saturation condition of the interface, the factors which affect the interface-bulk moduli ratio because of composition are G_c^* and R. For different sets of samples, with a constant x_f (and, therefore, G_c^*), the interface-moduli ratio M_γ, M_E, $M_{\gamma G}$ at different φ are reported in the semi-log plots in Fig.6a, Fig.6b and Fig.6c, respectively. It is worth noting that the values reported in the figures are calculated by assuming $R = D_{3,2}/2$, whereas the same calculation by using $R = D_{4,3}/$ are under processing.

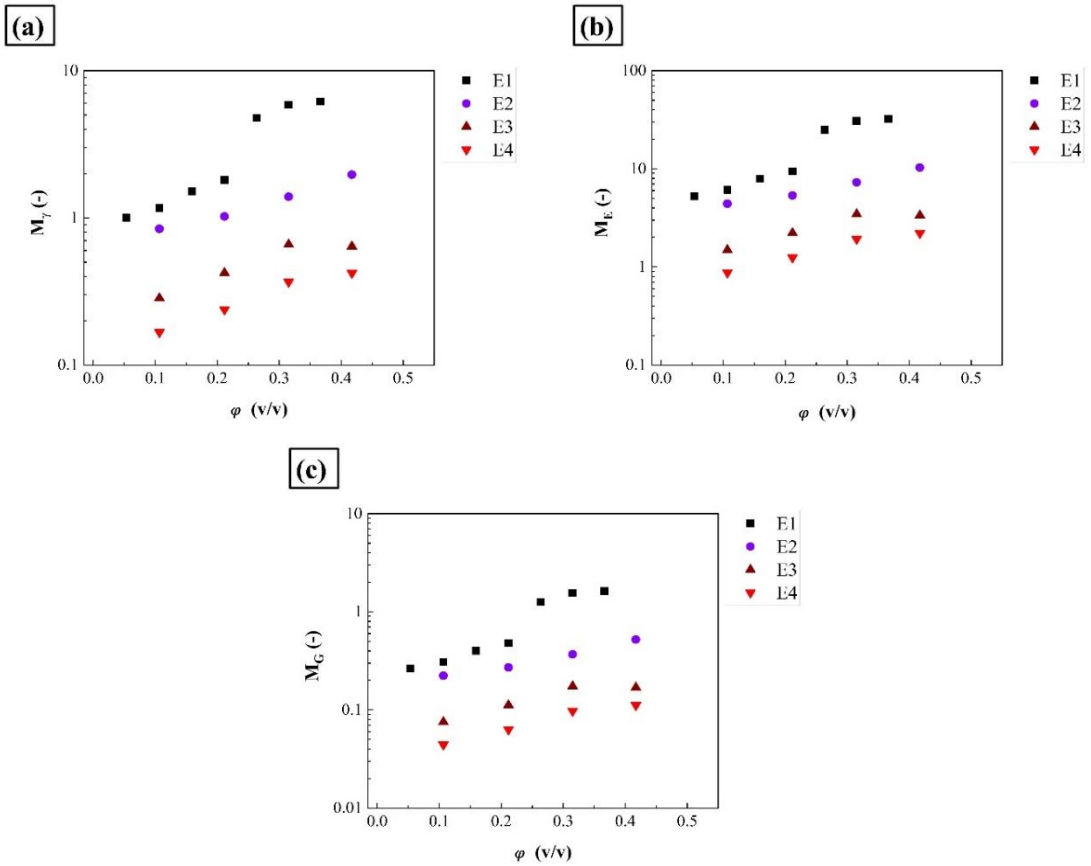

Fig.6. Interface-bulk moduli ratio: (a) tensional-bulk ratio, (b) elongational-bulk ratio and (c) shear-bulk ratio.

As expected, qualitatively for each set of samples all interface-bulk moduli ratios follow the same trend with φ and considering that $E_i > \gamma > G_c^*$ higher values for M_E with respect to M_γ and M_G were found. In particular, M_γ ranges from 0.17 to 6.2, M_E from 0.87 to 32 whereas M_G from 0.044 to 1.6. In addition, because of G_c^* increase with fiber fraction, according to Fig.1a and Eq.15., interface-bulk moduli ratios decrease with the increasing of fiber fraction, once again some sort of asymptotic trend with increasing of x_f is highlighted. Finally, because of the differences in the functionality of R with φ, the interface-bulk moduli of samples E1 exhibited a sharp increase around φ = 0.20-25, on the contrary, moduli ratio of other sets of samples increases more or less linearly in the semi-log plot. It is worth noticing that interface-bulk moduli ratios are significantly greater than zero, except some samples like E4/10 which showed for instance M_G = 0.044, consequently, interfacial rheological properties (γ, E_i, G_i) cannot be considered physically neglectable.

4. Rheological modeling: Influence of interfacial contribution and droplets radius estimation

As previously described, rheological properties of emulgels were modelled using three different approaches: modified Kerner model (mK), (Eq. 13), modified simplified Palierne model (msP) (Eq. 6-7,13) and modified extended Palierne model (meP) (Eq.8-10,13). For the last two cases the fitting of data was done by relating the droplets radius to both $D_{3,2}$ and $D_{4,3}$ ($R = D_{3,2}/2$ and $R = D_{4,3}/2$) according to the observations and considerations reported above. The data fitting of samples E1, E2, E3 and E4 using the modified Kerner model is reported in Fig.7 and it shows that mK fits rather well the experimental data, as reported also by the statistical parameters in Tab.4.

Sample ID	A	std. err (A)	%err (A)	R^2	χ^2	RSS
E1	10.3	1.3	12.6	0.9634	0.0037	0.0260
E2	15.2	1.1	7.2	0.9937	0.0007	0.0034
E3	19.2	1.7	8.9	0.9910	0.0010	0.0051
E4	18.4	1.4	7.6	0.9935	0.0007	0.0036

Tab.4. Results of the modified Kerner model (mK): A–fitting parameters, std. err (A)–standard error on the parameter, %err (A)–percentage error on parameter, R^2–correlation coefficient, χ^2–chi-square and RSS–residual sum of square

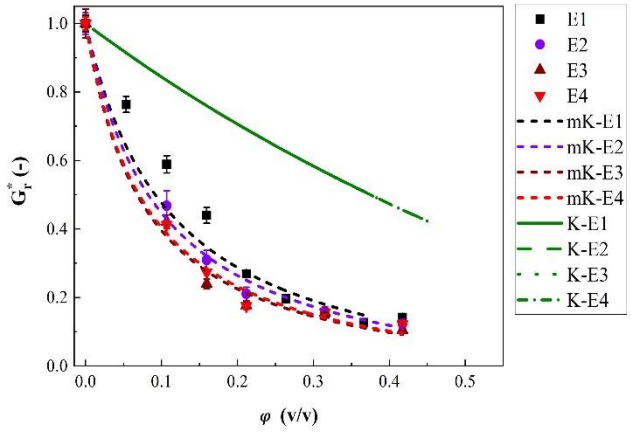

Fig.7. Rheological modelling of emulgel consistency: comparison of fitting with the Kerner equation and modified Kerner equation. Lines reports the data fitting.

On the other hand, the theoretical Kerner equation (K) overestimate the consistency, like simplified and extended Palierne models (Fig.S2a and Fig.S2b, respectively) and it provides results almost independent of fiber fractions (as expected, since H of different samples is almost the same, around – 2/3).

When the other two models are considered (Fig. 8) it can be seen that results obtained with msP and meP are strictly dependent on the relation used for the estimation of the droplets radius (R). For instance, for set of samples E1 the msP in the case of $R = D_{3,2}/2$ and in the case of $R = D_{4,3}/2$ is reported in Fig.8a. No model was found to be able to describe the experimental data. This result is rather in contrast with previous works on similar systems [10], in which, however, the droplets radius was assumed to be constant and expressed as the half of the averaged equivalent circular area diameter determined (d_s), determined by imaging method. On the contrary by using meP the samples description improves, as reported in Fig. 8b. In such case the estimation of $R = D_{3,2}/2$ gives the best results. Looking at the data fitting of samples E4 in Fig.8c it is possible to see that in such case msP fits well the data, in agreement with previous results on the rheological modeling of similar emulgels [10], even if the radius estimation resulted different. Specifically in the present case, model msP fits properly the data of the set of samples E4 with both types of radius estimations, although the relation $R = D_{4,3}/2$ provide slightly better results. However, as reported in Fig.8d, the meP describes well the data only if R is the estimated from $D_{4,3}$, in contrast to results obtained for set of samples E1. This suggests that equations used for the fitting are very sensitive to expression and magnitude of the radius of the droplets, i.e., if it is related

to small-sized rather than large-sized droplets in our case, and its correct estimation is necessary for a rational application of the modified simplified Palierne model and of the modified extended Palierne model. Furthermore, it deserves to be mentioned that the modeled emulgel are characterized by a rather polydisperse droplets size distribution and the assumption of monodisperse systems can limit the validity of the equations used. Indeed, as proposed by Palierne theory [17] the interfacial contribution linked to the droplets should by weighted according to their polydispersity. However, it must be highlighted that a rigorous estimation of droplets polydispersity in such systems requires due attention and accurate analysis, since the samples are made of both particle and droplets, consequently P/DSD data contain information on both of them.

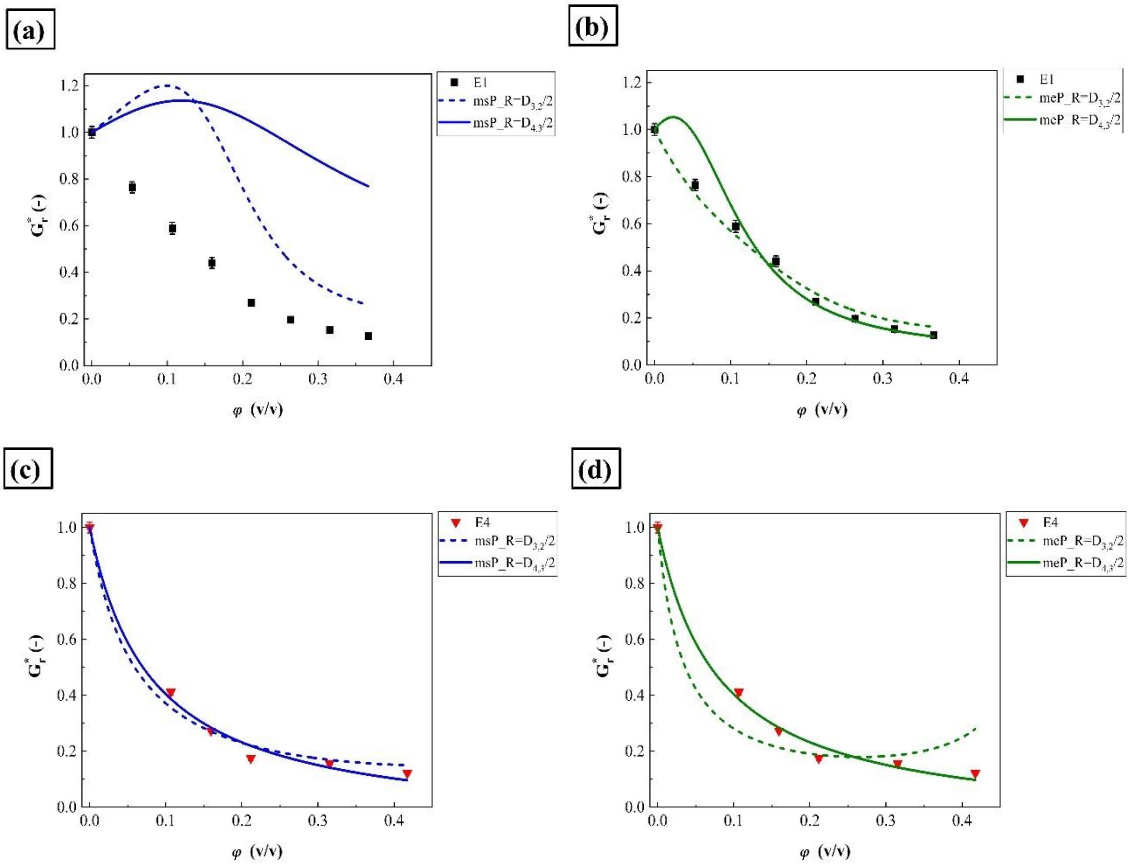

Fig.8. Rheological modelling results with interfacial tension and moduli contributions and different estimation of microstructure ($R = D_{3,2}/2$ and $R = D_{4,3}/2$): (a) fitting with msP of set of samples E1, (b) fitting with meP of set of samples E1, (c) fitting with msP of set of samples E4 and (d) fitting with meP of set of samples E4. Lines report the data fitting.

5. Application of the modified Kerner model for food design prediction

The ability of modified Kerner model to predict the consistency of emulgels-like food products was tested by using it to design (i.e., to estimate the formulation in terms of oil and fiber content) emulgels having a complex modulus value (G^*) equal to commercial products chosen as benchmarks. In this work a light mayonnaise (named B1) and a light spreadable cheese (named B2) were chosen. The emulgels prepared according to model estimates were named EM_P1, EM_P2 and contained an oil phase volume fraction (soy lecithin and EVO oil, x_l = 0.15) of ϕ = 0.26 (φ = 0.27) and ϕ = 0.12 (φ = 0.13) respectively (corresponding to the values of the commercial benchmarks).

For the validation of modified Kerner model, the fitting parameters (A) found for the different sets of samples E1, E2, E3 and E4 were plotted as a function of the fiber fraction x_f and a fitting equation was used to describe this dependence. The data are reported in Fig.S3 and the fitting equation and parameter values in Eq.S1. The method proposed for food consistency design is based on an iterative procedure which used the aforementioned equations and can be summarized as follows. The volume oil fraction of the emulgel φ, was assumed equal to the benchmark oil content, and x_f was assumed in the first iteration, consequently the value of A, from Eq.S1, and the value of G_r^*, from Eq.13 and Eq.5, were estimated. Assuming the value of G_E^* equal to benchmark value (obtained with the rheological characterization, reported with that of EM_P1, EM_P2 in Fig.8b), G_C^* was calculated from Eq.1. Then, using the inverse form of Eq.15, the fiber fraction was calculated. The calculated and esteemed x_f were then compared and, if different, the new value of x_f was used for a further iteration. The procedure was stopped when a difference lower than 1% was found. According to the procedure described, the following values of fiber fraction, x_f = 0.0055 and x_f = 0.0453 were found for EM_P1 and EM_P2, respectively. The error on the estimation found from the iteration was 0.7% for EM_P1 and 0.2% for EM_P2. The samples were prepared and characterized, and the results of their frequency sweep tests are compared to those of benchmarks in Fig.9, data of complex moduli of emulgels and benchmarks almost overlap whereas slight differences are observed for the phase angle.

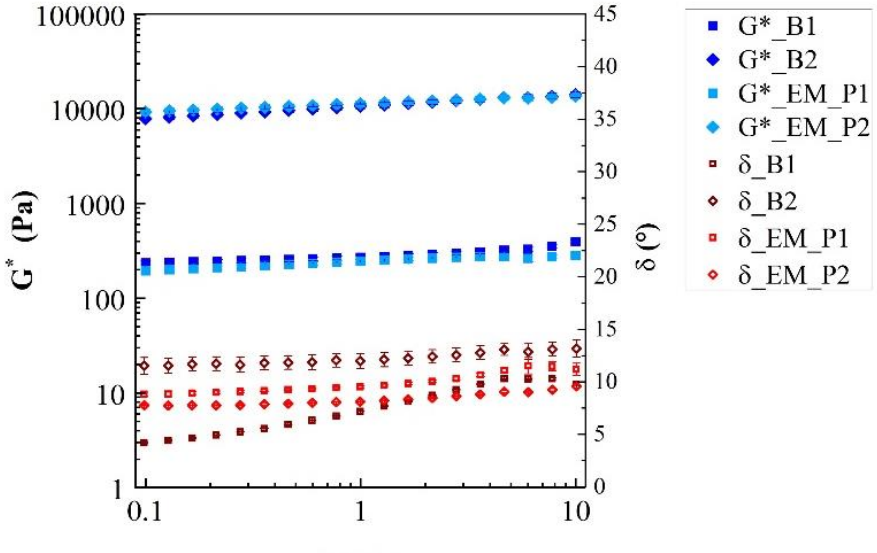

Fig.9. Rheological modelling of emulgel consistency: comparison of complex modulus and phase angle of emulgel prototype and benchmark.

Sample ID	G_r^* (-)	G^*@1Hz (Pa)	δ@1Hz (°)
EM_P1	0.307	250 ± 10	9.53 ± 0.09
EM_P2	0.365	11300 ± 700	8.10 ± 0.03
B1	-	270 ± 10	7.19 ± 0.03
B2	-	10600 ± 600	12.0 ± 0.7

Tab.6. Comparison between the rheological parameters of model prediction, emulgel prototype and benchmarks.

The data of complex relative modulus, complex modulus and phase angle at 1 Hz of emulgels and benchmarks are reported in Tab.6. The complex moduli of the emulgels were very close to those of the benchmarks, since complex modulus of EM_P1 underestimates that of B1 by only 8.9% whereas the complex modulus of EM_P2 overestimates that of B2 by only 6.4%. It is interesting to observe that all the discrepancies are quite small (lower than 10%), especially by noting that both the fiber fractions calculated (0.0055 and 0.0453) are outside of the investigated fiber range ($0.01 < x_f < 0.04$).

6. Conclusions

Emulgel samples with rheological properties similar to those of food products were successfully produced by microfluidization. For hydrogel the complex modulus increases with the increasing fiber fraction. An increasing trend in the consistency of emulgel with increasing fiber fraction was also found whereas the increase of the oil phase, in general,

yields a reduction of the consistency. The microstructure and the morphology of emulgels are strongly influenced by composition, i.e., fiber concentration and oil phase fraction. Droplet size depends on both fiber fraction and oil phase volume fraction. Droplet size seems to decrease with the increasing oil phase volume fraction. For high oil phase volume fraction, morphological changes like the formation of bi-continuous microemulsion can be observed. The quantification and mathematical description of the microstructure (droplets radius) as a function of oil phase volume fraction is strictly dependent on fiber fraction and non-linear empirical equation can be necessary to model droplets size as fiber content.

The theoretical rheological models without introducing a corrective parameter yield values significantly different with respect to the experimental data, confirming relevant non-ideality factors in the studied systems. The modified Kerner model agrees quite well with experimental data, and it was found to be suitable to design food-type emulgels containing citrus fiber as structuring agent.

From a first analysis of the fitting results, aware of the complexity in identifying a rational estimation of droplets radius, using the modified simplified Palierne model and modified extended Palierne model it is possible to conclude that both of them are extremely affected by the estimation of the droplets radius and that a different choice of this parameter can change the model results. Consequently, from these initial results, it is not clear which is the best choice for the estimation of the droplets radius (i.e., it is relating it to the surface mean diameter of to the volume mean diameter), and further microstructural considerations and analysis will be necessary to make possible the use of advanced rheological models for food consistency design purposes. For instance, a clearer and deeper view of the system could be obtained starting with these results and by using the Palierne approach in its original form, i.e., by taking into account the polydispersity of the droplets. Finally, further insights, aimed at better understanding the physical meaning of the fitting parament and their relation to composition and properties of the systems may contribute to raise the impact of the present research work.

References

[1] Kavya, M.; Ranjit Jacob, A.; Nisha, P. Pectin Emulsions and Emulgels: Bridging the Correlation between Rheology and Microstructure. *Food Hydrocoll.* **2023**, *143*, 108868, doi:10.1016/j.foodhyd.2023.108868.

[2] Milutinov, J.; Krstonošić, V.; Ćirin, D.; Pavlović, N. Emulgels: Promising Carrier Systems for Food Ingredients and Drugs. *Polymers (Basel).* **2023**, *15*, doi:10.3390/polym15102302.

[3] Dickinson, E. Emulsion Gels: The Structuring of Soft Solids with Protein-Stabilized Oil Droplets. *Food Hydrocoll.* **2012**, *28*, 224 – 241.

[4] Raeisi Estabragh, M.A.; Sajadi Bami, M.; Dehghannoudeh, G.; Noudeh, Y.D.; Moghimipour, E. Cellulose Derivatives and Natural Gums as Gelling Agents for Preparation of Emulgel-Based Dosage Forms: A Brief Review. *Int. J. Biol. Macromol.* **2023**, *241*, 124538, doi:10.1016/j.ijbiomac.2023.124538.

[5] Van Aken, G.A.; Oliver, L.; Scholten, E. Rheological Effect of Particle Clustering in Gelled Dispersions. *Food Hydrocoll.* **2015**, *48*, 102–109, doi:10.1016/j.foodhyd.2015.02.001.

[6] Lupi, F.R.; Shakeel, A.; Greco, V.; Oliviero Rossi, C.; Baldino, N.; Gabriele, D. A Rheological and Microstructural Characterisation of Bigels for Cosmetic and Pharmaceutical Uses. *Mater. Sci. Eng. C* **2016**, *69*, 358–365, doi:10.1016/j.msec.2016.06.098.

[7] Oliver, L.; Berndsen, L.; van Aken, G.A.; Scholten, E. Influence of Droplet Clustering on the Rheological Properties Ofemulsion-Filled Gels. *Food Hydrocoll.* **2015**, *50*, 74–83, doi:10.1016/j.foodhyd.2015.04.001.

[8] Alfaro-Rodríguez, M.C.; Prieto, P.; García, M.C.; Martín-Piñero, M.J.; Muñoz, J. Influence of Nanoemulsion/Gum Ratio on Droplet Size Distribution, Rheology and Physical Stability of Nanoemulgels Containing Inulin and Omega-3 Fatty Acids. *J. Sci. Food Agric.* **2022**, *102*, 6397–6403, doi:10.1002/jsfa.12005.

[9] Muñoz, J.; Prieto-Vargas, P.; García, M.C.; Alfaro-Rodríguez, M.C. Effect of a Change in the CaCl2/Pectin Mass Ratio on the Particle Size, Rheology and Physical Stability of Lemon Essential Oil/W Emulgels. *Foods* **2023**, *12*, doi:10.3390/foods12061137.

[10] Bruno, E.; Lupi, F.R.; Mammolenti, D.; Mileti, O.; Baldino, N.; Gabriele, D. Emulgels Structured with Dietary Fiber for Food Uses : A Rheological Model. *Foods* **2022**, *11*.

[11] Bruno, E.; Lupi, F.R.; Mammolenti, D.; Baldino, N.; Gabriele, D. Development and Rheological Modeling of Dietary Fiber and Policosanol Plant-Based Bigels for Potential Food Applications. *Food Hydrocoll.* **2024**, *150*, 109733, doi:10.1016/j.foodhyd.2024.109733.

[12] Lupi, F.R.; De Santo, M.P.; Ciuchi, F.; Baldino, N.; Gabriele, D. A Rheological Modelling and Microscopic Analysis of Bigels. *Rheol. Acta* **2017**, *56*, 753–763, doi:10.1007/s00397-017-1030-3.

[13] Saffold, A.C.; Acevedo, N.C. Development of Novel Rice Bran Wax/Gelatin-Based Biphasic Edible Gels and Characterization of Their Microstructural, Thermal, and Mechanical Properties. *Food Bioprocess Technol.* **2021**, *14*, 2219–2230, doi:10.1007/s11947-021-02719-7.

[14] FROHLICH, H.; SACK, R. Theory of the Rheological Properties of Dispersions. *Proc. R. Soc. Lond. A. Math. Phys. Sci.* **1946**, *185*, 415–430, doi:10.1098/rspa.1946.0028.

15] Kerner, E.H. The Elastic and Thermo-Elastic Properties of Composite Media. *Proc. Phys. Soc.*

Sect. B **1956**, *69*, 808–813, doi:10.1088/0370-1301/69/8/305.

[16] Lewis, T.B.; Nielsen, L.E. Dynamic Mechanical Properties of Particulate-filled Composites. *J. Appl. Polym. Sci.* **1970**, *14*, 1449–1471, doi:10.1002/app.1970.070140604.

[17] Palierne, J.F. Linear Rheology of Viscoelastic Emulsions with Interfacial Tension. *Rheol. Acta* **1990**, *29*, 204–214, doi:10.1007/BF01331356.

[18] Pal, R. Linear Viscoelastic Behavior of Multiphase Dispersions. *J. Colloid Interface Sci.* **2000**, *232*, 50–63, doi:10.1006/jcis.2000.7185.

[19] Lozano-Castellón, J.; López-Yerena, A.; Domínguez-López, I.; Siscart-Serra, A.; Fraga, N.; Sámano, S.; López-Sabater, C.; Lamuela-Raventós, R.M.; Vallverdú-Queralt, A.; Pérez, M. Extra Virgin Olive Oil: A Comprehensive Review of Efforts to Ensure Its Authenticity, Traceability, and Safety. *Compr. Rev. Food Sci. Food Saf.* **2022**, *21*, 2639–2664, doi:10.1111/1541-4337.12949.

[20] He, Y.; Wang, B.; Wen, L.; Wang, F.; Yu, H.; Chen, D.; Su, X.; Zhang, C. Effects of Dietary Fiber on Human Health. *Food Sci. Hum. Wellness* **2022**, *11*, 1–10, doi:10.1016/j.fshw.2021.07.001.

[21] Fernández-Fernández, A.M.; Dellacassa, E.; Medrano-Fernandez, A.; Castillo, M.D. Citrus Waste Recovery for Sustainable Nutrition and Health. In *Food Wastes and By-products: Nutraceutical and Health Potential*; Rocio Campos-Vega, B. Dave Oomah, and H.A.V.-C., Ed.; John Wiley & Sons Ltd., 2020; pp. 193–222.

[22] Jimenez-Lopez, C.; Gallardo-Gomez, M.; Simal-Gandara, J.; Carpena, M.; Lorenzo, J.M.; Lourenço-Lopes, C.; Barba, F.J.; Prieto M.A. Bioactive Compounds and Quality of Extra Virgin Olive Oil. *Foods* **2020**, 135–142.

[23] Mangrulkar, S. V.; Kulkarni, S.S.; Nanepag, P. V.; Neje, P.S.; Chaple, D.R.; Taksande, B.G.; Umekar, M.J. A Comprehensive Review on Pleiotropic Effects and Therapeutic Potential of Soy Lecithin. *Adv. Tradit. Med.* **2024**, doi:10.1007/s13596-024-00770-1.

[24] Morales-Medina, R.; Dong, D.; Schalow, S.; Drusch, S. Impact of Microfluidization on the Microstructure and Functional Properties of Pea Hull Fibre. *Food Hydrocoll.* **2020**, *103*, 105660, doi:https://doi.org/10.1016/j.foodhyd.2020.105660.

[25] Poel, van der On the Rheology of Concentrated Dispersions. *Rheol. Acta* **1958**, *1*, 198–205, doi:10.1002/actp.1984.010350801.

[26] Smith, J.C. Simplification of van Der Poel's Formula for the Shear Modulus of a Particulate Composite. *J. Res. Natl. Bur. Stand. Sect. A Phys. Chem.* **1975**, *79A*, 419, doi:10.6028/jres.079a.007.

[27] McClements, D.J. *Food Emulsions-Principles, Practices, and Techniques*; Third Edit.; CRC Press Taylor & Francis Group, 2016; ISBN 9781498726696.

[28] McClements, D.J. Critical Review of Techniques and Methodologies for Characterization of

Emulsion Stability. *Crit. Rev. Food Sci. Nutr.* **2007**, *47*, 611–649, doi:10.1080/10408390701289292.

[29] Mileti, O.; Baldino, N.; Lupi, F.R.; Gabriele, D. Interfacial Behavior of Vegetable Protein Isolates at Sunflower Oil/Water Interface. *Colloids Surfaces B Biointerfaces* **2023**, *221*, 113035, doi:10.1016/j.colsurfb.2022.113035.

[30] Bruno, E.; Lupi, F.R.; Martin-Piñero, M.J.; Girimonte, R.; Baldino, N.; Muñoz, J.; Gabriele, D. Influence of Different Dispersing Systems on Rheological and Microstructural Properties of Citrus Fiber Suspensions. *Lwt* **2021**, *152*, doi:10.1016/j.lwt.2021.112270.

[31] Lupi, F.R.; Puoci, F.; Bruno, E.; Baldino, N.; Marino, R.; Gabriele, D. The Effects of Process Conditions on Rheological Properties of Functional Citrus Fibre Suspensions. *Food Bioprod. Process.* **2020**, *121*, 54–64, doi:10.1016/j.fbp.2020.01.018.

[32] Pakseresht, S.; Mazaheri Tehrani, M. Advances in Multi-Component Supramolecular Oleogels-a Review. *Food Rev. Int.* **2022**, *38*, 760–782, doi:10.1080/87559129.2020.1742153.

[33] Qi, J.; Song, L.; Zeng, W.; Liao, J. Citrus Fiber for the Stabilization of O/W Emulsion through Combination of Pickering Effect and Fiber-Based Network. *Food Chem.* **2021**, *343*, 128523, doi:https://doi.org/10.1016/j.foodchem.2020.128523.

[34] He, K.; Li, Q.; Li, Y.; Li, B.; Liu, S. Water-Insoluble Dietary Fibers from Bamboo Shoot Used as Plant Food Particles for the Stabilization of O/W Pickering Emulsion. *Food Chem.* **2020**, *310*, doi:10.1016/j.foodchem.2019.125925.

[35] Gutiérrez-Méndez, N.; Chavez-Garay, D.R.; Leal-Ramos, M.Y. Lecithins: A Comprehensive Review of Their Properties and Their Use in Formulating Microemulsions. *J. Food Biochem.* **2022**, *46*, 1–22, doi:10.1111/jfbc.14157.

[36] Tchakalova, V.; Bailly, C.; Fieber, W. Food-Grade Bicontinuous Microemulsions. *Flavour Fragr. J.* **2014**, *29*, 67–74, doi:10.1002/ffj.3181.

Supplementary Material

The rheological modeling of food emulgels: application and insights on the interfacial contribution and estimation of droplets radius

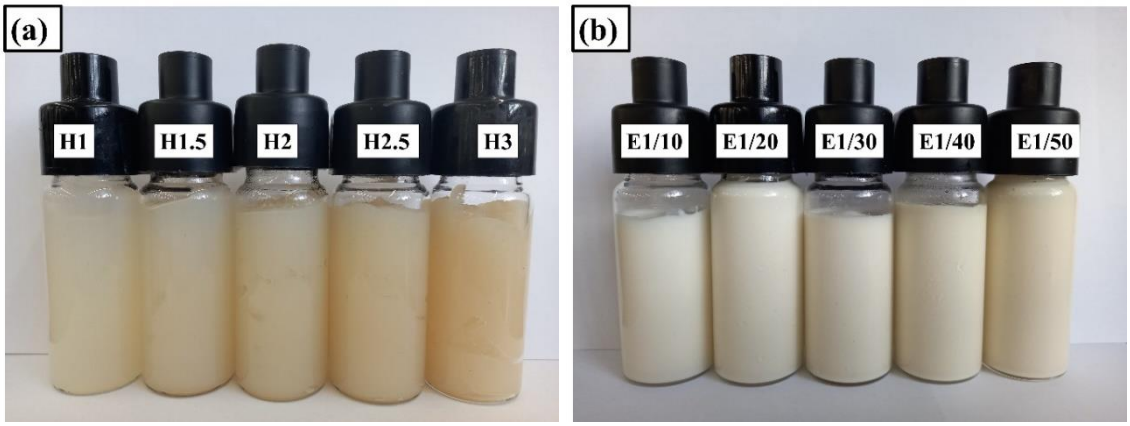

Fig.S1. Picture of samples: (a) hydrogel samples and (b) emulgel samples.

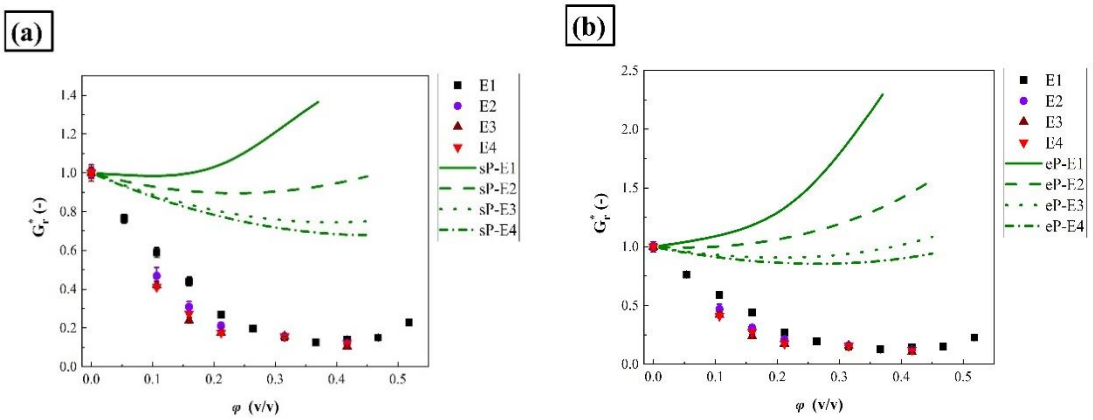

Fig.S2. Rheological modelling results with interfacial tension: (a) simplified Palierne model, sP and (b) extended Palierne model, eP. Droplets diameter was estimated using the surface mean diameter. Lines report the data fitting.

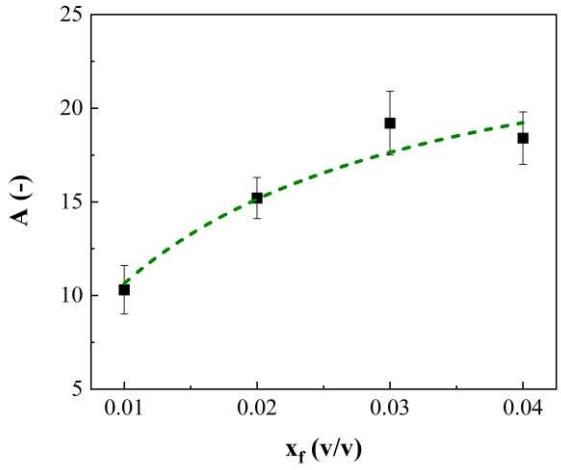

Fig. S3. Fitting of A parameter as function of fiber fraction, x_f. Dashed line reports the data fitting

Fitting equation used for the correlation of A parameter with x_f, Eq.1S.

$$A = \frac{b * x_f}{c + x_f} \tag{1S}$$

with

$b = 26.3 \pm 3.3$

$c = 0.015 \pm 0.005$

CHAPTER 4

Microfluidized hydrogel and emulgels structured with citrus fiber: effect of processing cycles and channels on rheology and microstructure

Microfluidized hydrogels and emulgels structured with citrus fiber: effect of processing cycles and channels on rheology and microstructure

Abstract

The incorporation of dietary fibers obtained from revaluation of by-products or wastes from food industry is receiving a lot of attention from both academy and industry because of their health benefits, sustainability, and technological performances in both water-based and O/W systems. Recently, the application of novel high-pressure homogenization techniques, such as microfluidization, to dietary fiber-based systems, is being faced. In this work the effect of microfluidization conditions, i.e., processing cycles and channel geometry, on the rheological and microstructural properties of hydrogels and emulgels structured with citrus fiber are investigated. Hydrogel and emulgel samples were produced with different compositions using both Z-z and y-Z chambers and processing them by one and two passes. Rheological investigations were carried out in linear condition, limit stress and strain (τ_L and γ_L), critical stress and critical strain (τ_C and γ_C) were obtained from stress sweep test while plateau modulus and minimum viscous modulus (G_N^0 and G''_{min}) were obtained from frequency sweep test. Rheological tests and parameters, supported by particle/droplets size and morphological investigation highlighted that fiber network is affected by processing condition in both hydrogel and emulgels production. For the latter, a competitive stabilization action between fiber network and Pickering effect was found although all the samples showed a marked physical stability

Keywords

Insoluble Dietary Fibers; microfluidization; structured emulsion; food microscopy; microrheology; Turbiscan;

1. Introduction

In recent years the incorporation in foodstuff of dietary fibers obtained from agri-food industry by-products or wastes is receiving a growing interest because of its success in providing simultaneously health benefits, texture and stability and guaranteeing food production with reduced environmental impact [1–3]. Among all, citrus fiber is one of the most completive ingredients in formulation of foods thanks to its physiological properties, excellent technical performances and sustainability [4]. Under the action of machinal shear stress, citrus fiber aqueous suspension typically gives rise to particle hydrogel [1,5,6]. The introduction of an oil phase in a citrus-fiber-based hydrogel through a simple homogenization, leads to water-structured systems typically called emulgels [7], if the oil phase is not viscoelastic, or bi-structured systems called bigels [8] if the oil phase is viscoelastic. Citrus fiber in O/W can even generate Pickering emulsions as reported in literature [9] in the case of bamboo roots fiber [10], by strongly pre-homogenizing the systems. In any case, citrus fiber can improve the stability of foods by promoting the formation of an emulsion-type microstructure. Process (both technology and condition) influences particle/droplets size and morphology of the systems structured with dietary fibers which, consequently, exhibit different rheological properties and commercial stability [5,9,11,12]. A lot of recent research works are aimed at investigating both the effect of conventional processes on the properties of fiber and fiber-based systems, and the development of new processing technologies. For instance, the effect of process conditions (both pressure and cycle) and dietary fiber concentration in high pressure homogenization (HPH) was deeply discussed by several authors [13–15], as well as the combination of HPH with size-reduction pretreatments like cryogenic ball-milling [16] or the adoption of new technologies like high hydrostatic pressure and cavitation jet-process [17,18]. Among the homogenization techniques, dynamic high pressure microfluidization (microfluidization) is receiving more and more attention [19,20]. Nowadays, if, on the one hand, the effect of process parameters in high-pressure homogenization on dietary fiber and dietary fiber-base systems is well known [12–15], there is a lack of investigation related to the effects of microfluidization conditions on food systems containing insoluble dietary fibers (IDFs). Consequently, because of the advantages of microfluidization, there is a growing interest focused on the effects of microfluidization process on systems with insoluble dietary fibers [19]. For instance, a comparison study between high-speed homogenization (HSH) and microfluidization for the production of gelled suspension structured with citrus fiber was recently carried out [5], as well as the effect of microfluidization pressure and cycles on

suspensions of pea hull fiber [11]. The effect of microfluidization cycles on multiphasic systems like structured emulsion was recently explored for nanoemulgels structured with xanthan gum and inulin [21].

In the present work, after a preliminary analysis of the structuration ability of fiber, the effects that microfluidization channels type and cycles exert on consistency and microstructure of both hydrogel and emulgel structured with insoluble dietary fiber and on the physical stability of the latter is proposed. Both the hydrogels and emulgels where structured with citrus fiber, and an oil phase made by soy lecithin in extra virgin olive oil was used as dispersed phase, with a composition typical of food applications according to literature on similar system [8]. The adopted approach is aimed at highlighting the stabilization mechanism of the emulgels structured with citrus fiber, and it is based on rheological and microstructural considerations supported by morphological accreditments.

2. Material and methods

2.1.Materials

Citrus fiber (trade name Vitacel CF 312 ®) was kindly provided by JRS Silvateam Ingredients S.r.l. (Italy). Organic soy lecithin was purchased from IVOVITAL GmbH (Germany). Distilled water and extra virgin olive oil, (EVO, DeSantis, Italy), were used for the preparation of the aqueous and oil phase, respectively. All chemicals were used as received without any manipulation.

2.2.Hydrogel samples preparation

Hydrogel samples with 0.0010 w/w of fiber were prepared by high-speed homogenization followed by one or more cycles of microfluidization. Sample was pre-treated using Ultraturrax T50 (IKA-Werke, Germany) equipped with the G45F tool at 4000 rpm for 1 min. Subsequently the coarse system was homogenized using Microfluidizer M110P (Microfluidics Int. Corp., USA) at 25000 psi (345 W) through a series of two Z-type interactions chambers (H30Z and G10Z). A further sample of hydrogel was cycled twice. In all the preparations, the material coming out of the homogenizer was thermostated by an ice bath. Samples were stored in fridge at 4°C for 24 hours before the characterizations. With the aim of investigating the effect of fiber amount on hydrogel viscoelasticity, further samples with different fractions of fiber (0.015 w/w, 0.020 w/w, 0.025 w/w, 0.030 w/w, 0.035

w/w, 0.040 w/w) were prepared using one pass and the configuration based on the series of two Z-type chambers. Sample ID and process conditions are reported in Tab. 1.

Sample ID	Citrus fiber fraction (w/w)	Number of cycles	Interaction chamber configuration	Microfluidization diameters (µm)
H1_C1	0.010	1	Z-z	200-87
H1.5_C1	0.015			
H2_C1	0.0200			
H2.5_C1	0.025			
H3_C1	0.030			
H3.5_C1	0.035			
H4_C1	0.040			
H1_C2	0.010	2	Z-z + Z-z	
E1/20_C1	0.010	1	Z-z	200-87
E2/20_C1	0.020			
E3/20_C1	0.030			
E4/20_C1	0.040			
E1/20_C2	0.010	2	Z-z + Z-z	
E1/20_C3	0.010	1	y-Z	75-200
E1/20_C4	0.010	2	y-Z + y-Z	

Tab1. Sample ID and process configuration. The letter Z indicates the interaction chamber H30Z with a microfluidization channel diameter of 200 µm, z indicates the interaction chamber G10Z with a microfluidization channel diameter of 87 µm and y indicates the interaction chamber F12Y with a microfluidization channel diameter of 75 µm.

2.3.Emulgel samples preparation

Emulgel samples with 1% w/w of fiber and 20% w/w of oil phase were prepared similarly to hydrogel by high-speed homogenization followed by one or more cycles of microfluidization. Samples was pre-treated using Ultraturrax T50 (IKA-Werke, Germany) equipped with the G45F tool at 4000 rpm for 1 min. The oil phase was added to the water phase with a flow rate of 11-14 g/min during the pre-treatment. Then, tharse system was homogenized using Microfluidizer M110P (Microfluidics Int. Corp., USA) at 25000 psi (345 W) though a series of two interactions chambers. Different configurations of chamber were used, particularly series of two Z-type chambers (H30Z and G10Z, denoted as Z-z) and series of Y-type followed by Z-type chamber (F12Y and H30Z, denoted as y-Z) were used to produce sample by both one and two passes. Schematic representations of microfluidization channels and configuration are reported in Fig. S1 and Fig. S2, respectively. In all the preparation the outlet of the homogenizator was thermally controlled by thermostatic ice

bath. Samples were stored in fridge at 4°C for 24 hours before the characterizations. For the emulgel preparation, oil phase containing 15% w/w of soy lecithin was prepared according to our previous work [7]. With the aim of investigating the effect of fiber fraction on their viscoelastic properties, further samples of emulgel with different fractions (0.020 w/w, 0.030 w/w and 0.040 w/w) were prepared using one pass and the configuration based on the series of two Z-type chambers. Sample ID, citrus fiber fraction and process conditions (number of cycles, configuration of the interaction chamber and diameter of the microfluidization channels) are reported in Tab. 1.

2.4.Functional properties

As functional properties the oil holding capacity (OHC) were determined according to the procedures of literature with slight modifications [22,23]. Briefly, 1 g of fiber was manually mixed with 40 g of oil and left for 24 h at 25°C. The mixture was then centrifugated (5810, Eppendorf, Germany) at 4000 rpm (relative centrifugal force 3220 x g) for 20 min. The supernatant was removed, and the wet solid mass was determined by weighting. The OHC was calculated according to Eq.1.

$$OHC = \frac{m_w - m_d}{m_d} \quad (1)$$

where m_w and m_d are the mass (in g) of wet and dry fiber, respectively. The OHC was determined for both EVO oil and EVO oil with lecithin. The OHC measurements were carried out in duplicate, and the results averaged.

2.5.Rheological characterization and analysis

Rheological characterizations of the hydrogel and emulgels were carried out using the stress-controlled rotational rheometer Haake MARS 40 (Thermo Fisher Scientific, Germany) equipped with parallel serrated plate (diameter 35 mm, gap 1.6 ± 0.2 mm). Stress sweep tests were carried out varying the stress from 0.1 to 1000 Pa to identify the linear viscoelastic region. Frequency sweep tests were carried out between 0.01 and 10 Hz using the stress values in the linear viscoelastic region previously obtained from the stress sweep test. In order to limit the evaporation of water from the sample during the measurements a wet sealing bell was used. All the measurements were carried out at 25°C and repeated three times. The results are shown in terms of average value and standard deviation. Rheological data were interpreted in terms of elastic and viscous moduli, G^' and G^" respectively.

Different parameters were obtained from both frequency and stress sweep test and used for the quantitative comparison of hydrogel and emulgels. For all samples, the limit stress (τ_L) and limit strain (γ_L), i.e. the stress/strain coordinates behind which the material response is not linear, were defined according to Eq.2 and Eq.3 as the value of stress and strain at which the elastic modulus decreases of 5% from the value of the linear region, similarly to what done in previous works on comparable systems [24,25].

$$\tau_L = \tau|_{G' = 0.95\ G'_{LIN}} \quad (2)$$

$$\gamma_L = \gamma|_{G' = 0.95\ G'_{LIN}} \quad (3)$$

In particular, G'_{LIN} (Pa) was calculated through the moving average of the elastic modulus data, and τ_L (Pa) and γ_L (dimensionless) were determined as the value at which the deviation of the measured elastic modulus from the moving average was 5%. For samples produced with different process configuration, stress and strain were also evaluated in the crossover condition, similarly to what reported in previous work on soluble fiber-based systems [26]. Specifically, the critical stress, τ_c (Pa), and the critical strain, γ_c (dimensionless), were defined according to Eq.4 and Eq.5 as the value of stress and the value of strain measured when $G' = G''$.

$$\tau_c = \tau|_{G' = G''} \quad (4)$$

$$\gamma_c = \gamma|_{G' = G''} \quad (5)$$

As quantitative parameters for the description of the viscoelastic properties of the samples, the plateau modulus, G_N^0 (Pa), defined as the elastic modulus evaluated at the minimum value of viscous modulus, Eq.6 [27–29], and the minimum of viscous modulus, G''_{min} (Pa), were used.

$$G_N^0 = G'|_{G''_{min}} \quad (6)$$

In analogy to the literature on food emulsions stabilized with biopolymers, [27, 28], on compressed emulsions [29] and on colloidal suspensions close the glass transition [30], high value of G_N^0 indicates and increasing of interaction in the systems. For the tested samples, in first instance, it can be assumed to be proportional to the physical interactions in the particle network.

2.6.Laser diffraction analysis

Particles/droplets size distribution (P/DSD) of fiber powder, hydrogel, and emulgel was determined by the laser diffraction technique through Mastersizer 2000 (Malvern, UK),

using the Hydro2000G accessory for wet dispersions. For hydrogel sample laser diffraction, is due only to particles (citrus fibers), on the contrary for emulgels both citrus fiber particles and oil phase droplets generate diffraction. In light of these observations, for hydrogel samples, the size distribution is indicated as Particle Size Distribution (PSD); whereas for emulgels samples the size distribution is indicated as Particle/Droplets Size Distribution (P/DSD).

Both dry fiber particles, hydrogel and emulgels were dispersed and diluted in distilled water before carrying out the analysis. Every P/DSD acquisition was the result of computations of three signals, and, for each sample, three independent acquisitions were collected, and the results averaged. As quantitative indicator of sample microstructure both surface and volume diameter and span index, $D_{3,2}$, $D_{4,3}$ and $SPAN$ respectively, defined according to Eq. 7 – 9, were used [21].

$$D_{3,2} = \frac{\sum_{i=1}^{N} n_i {d_i}^3}{\sum_{i=1}^{N} n_i {d_i}^2} \tag{7}$$

$$D_{4,3} = \frac{\sum_{i=1}^{N} n_i {d_i}^4}{\sum_{i=1}^{N} n_i {d_i}^3} \tag{8}$$

$$SPAN = \frac{d_{90} - d_{10}}{d_{50}} \tag{9}$$

where n_i is the number of droplets/particles with a diameter of d_i (μm), and d_{90} (μm) and d_{10}(μm) are the 90th and 10th percentile diameter and d_{50} (μm) the median diameter. The first computation of diameter is more affected by small particles of fiber and small droplets, whereas the second is more influenced by large fiber particles, large droplets, droplets aggregate, fiber-droplets aggregates. Finally, the span index quantifies the width of the distribution.

2.7.Multiple light scattering analysis

The physical stability of emulgels was evaluated through a Turbiscan Lab Expert (Formulaction SAS. France). By scanning the samples using multiple light-scattering, the optical profiles along the height of the test cell can be obtained at different times. The Turbiscan analysis was carried out on the samples immediately after the preparation and after different periods of time (48 h, 1 week and 2 weeks). Every scanning set at different times was organized in a monitoring of 10 minutes with 1 scan per minute. Samples were stored in fridge at 4°C for the entire time of observation and thermally equilibrated to

ambient conditions before the measure. The data obtained were interpretated in terms of backscattering signal in delta mode (ΔBS%) to better highlight the variations in the optical profile of the samples and to provide a more significant measure of the stability [28,31,32].

2.8.Contrast phase optical microscopy (CPOM)

Optical microscopy investigations were carried out on selected hydrogels using Axio Scope A1 (Carl Zeiss, Germany) in contrast phase mode with a magnification of 20X.

2.9.Confocal laser scanning microscopy (CLSM)

Confocal laser scanning microscopy (CLSM) investigations were carried out on emulgels samples by using Stellaris 8 (Leica microsystem, Germany) microscope equipped with 63X immersion object (1.4 oil). Micrographs were taken according to sample autofluorescence without any stainer addition. Both reflectance and emission signal were used in the morphological investigation. For reflectance analysis the excitation wavelength was 631 nm and the spectral position 619 – 647 nm, for water phase morphology the excitation was at 405 nm and the spectral position of emission at 410 – 605 nm, whereas for oil phase the excitation was 638 nm and the spectral position of emission at 648 – 833 nm. Images were acquired with a scanning speed of 400 Hz, a resolution of 512 X 512 pixels and processed by LAS X software (Leica).

2.10. Cryo-SEM

Scanning electron microscopy in cryogenic mode (Cryo-SEM) were carried out on selected emulgels through a FlexSem 1000 II (Hitachi, Japan). Images were acquired at 1000X in low vacuum condition (70 Pa) using the signal of backscattered electron (BSE) with an accelerating voltage of 10kV. No metallization of the samples surface was applied for observation.

2.11. Statistical analysis

Data fitting and statistical analysis were performed with the software Origin Pro (Version 2021b; OriginLab Corporation, USA). A one-way ANOVA test was used to compare the value of rheological parameters and P/DSD parameters. Differences were considered statistically significant for $p < 0.05$ and Fisher test was used to compare the average values.

3. Results and discussion

3.1.Functional properties

The OHC of EVO oil was found to be 1.62 ± 0.02 g/g, this result is rather similar to what found for other oils in previous papers [22,23]. The addition of lecithin to the EVO oil made the oil phase more suitable for binding to the fiber. The addition of lecithin to the EVO oil made the oil phase more suitable for binding to the fiber. Indeed, the OHC in the case of EVO oil with lecithin resulted markedly increased, 4.75 ± 0.08 g/g. The increase of OHC due to lecithin addition can be explained by the significant decrease of the surface tension of oil phase with respect to EVO oil [7]; this improves oil's ability to wet polar surfaces such as that of citrus fiber particles.

3.2.Linear viscoelasticity and microstructure of hydrogels

The values of limit stress (τ_L) and limit strain (γ_L) of particle hydrogel samples with different fractions of citrus fiber (x_f) are reported in Fig.1a.

The limit stress increases with the increasing of fiber fraction, indicating a strengthening of particle network. Particularly, it follows a sigmoidal trend in which two plateau conditions can be appreciated, the first one (low limit stress) below the mass fraction xf = 0.015 w/w and the other one (high limit stress) for xf > 0.03 w/w. In between, the stress increases about 4 times from 22.1 ± 3.5 Pa to 80 ± 3 Pa. The limit strain undergoes a decrease with the increasing of citrus fiber fraction, indicating a stiffening of the particles network. This trend in γ_L is rather in agreement with what reported in literature for carrot reconstituted suspension with a low particle size (40 μm) [24]. However, to best of our knowledge, no results are present in literature concerning the effect of concentration on τ_L, although it was studied in similar systems containing different types of dietary fibers at fixed fraction [25].

The plateau modulus and minimum viscous modulus of particle gel samples with different fiber fractions are reported in Fig.1b. Both dynamic moduli increase with increasing citrus fiber mass fraction. The plateau modulus (G_N^0) follows the typical trend of elastic modulus of dispersions with a fractal-based microstructure, as already observed for elastic shear modulus (G') at 1 Hz for similar systems [7,8] and for nanoemulsions [28]. Also, the minimum viscous modulus (G''_{min}) follows a power low type trend.

It is worth to note that, for these samples, the rheological outcomes on fiber network are only function of fiber content since, as reported in Fig.1c, the hydrogel samples at different fiber fractions exhibited almost the same particle size distribution.

According to ANOVA analysis (data not shown) no significant changes can be found in $D_{3,2}$, $D_{4,3}$ and $SPAN$ of hydrogels at different fiber fraction and the following mean values $D_{3,2}$ = 22.2 ± 0.1, µm, $D_{4,3}$ = 48.9 ± 2.1 µm and $SPAN$ = 2.60 ± 0.01 (-) can be considered representative of all the samples.

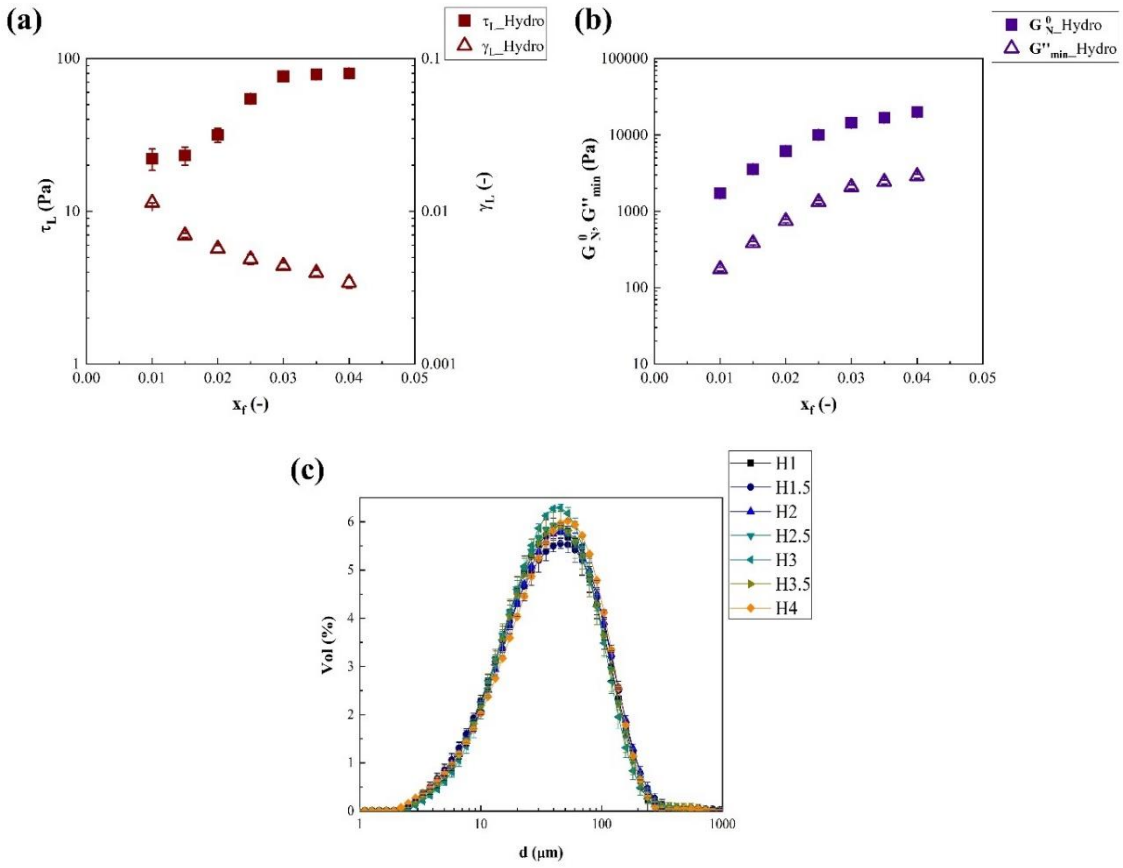

Fig.1. Rheology and microstructure of hydrogel with different fraction of citrus fiber: (a) limit stress and limit strain of hydrogels, τ_L_Hydro and γ_L_Hydro, respectively, (b) plateau modulus and minimum viscous modulus of hydrogels, $G_N^0\_Hydro$ and G''_{min}_Hydro, respectively and (c) particle size distribution of hydrogel samples with different fiber fractions.

3.3.Linear viscoelasticity and microstructure of emulgels

The values of τ_L and limit strain γ_L of emulgel samples with different fractions of citrus fiber (x_f) are reported in Fig.2a. The values of τ_L of emulgel samples at different x_f are lower than that of the corresponding hydrogels, in fact τ_L values range from 4.9 ± 1.2 Pa to 19.1 ± 1.7 Pa, although they follow a similar trend, indicating a weaking of the gel network due to the presence of oil phase droplets. On the contrary, γ_L values of emulgels at different

x_f are rather similar to those of the hydrogel samples, ranging from 0.0119 ± 0.0008 (-) to 0.0038 ± 0.0008 (-) for the emulgel and from 0.0114 ± 0.0002 (-) to 0.0034 ± 0.0003 (-) for the hydrogel. From this last result, it seems that no changes in the linear deformability of gel network took place by oil phase incorporation.

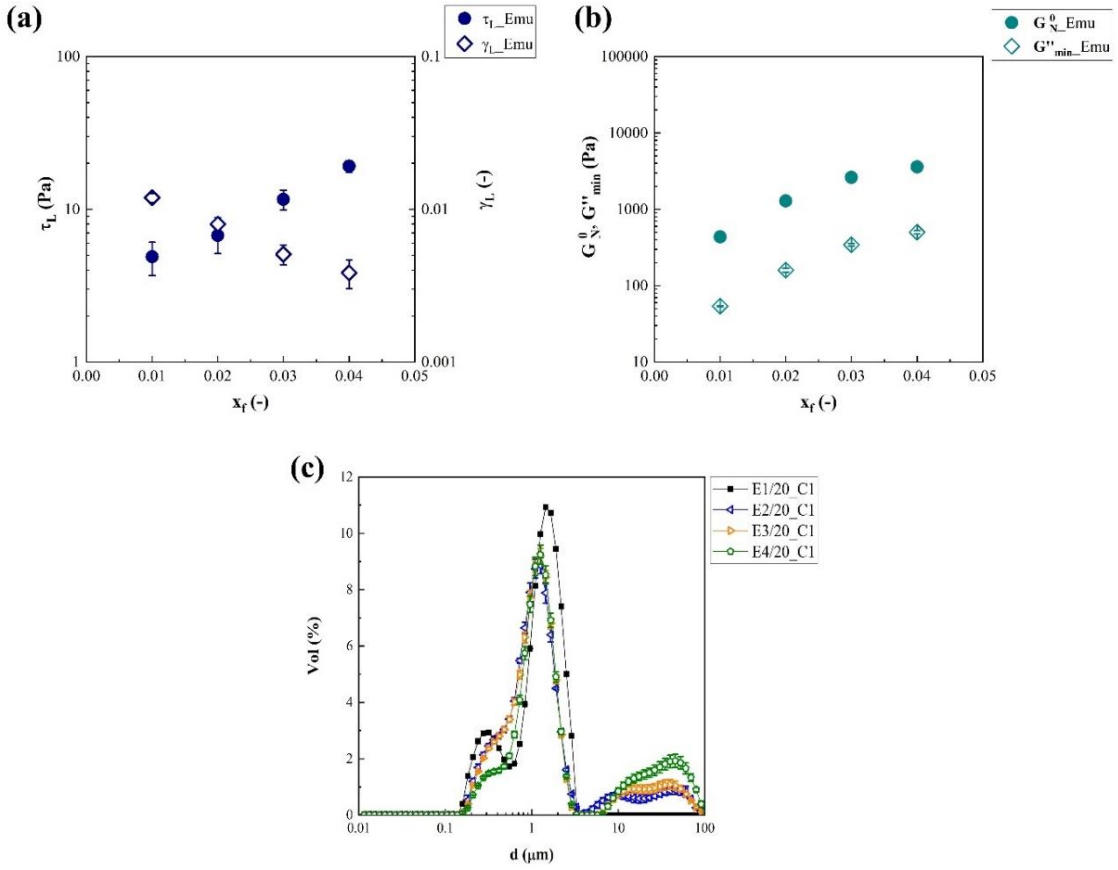

Fig.2. Rheology and microstructure of emulgels with different fractions of citrus fiber: (a) limit stress and limit strain of emulgels, τ_L_Emu and γ_L_Emu, respectively and (b) plateau modulus and minimum viscous modulus of emulgels, $G_N^0\_Emu$ and G''_{min}_Emu, respectively and (c) particle/droplets size distribution of emulgel samples with different fiber fractions.

Looking at Fig.2b, the weakening action induced by oil phase droplets can also be observed in terms of dynamic moduli. Indeed, despite G_N^0 and G''_{min} of emulgel samples follow the same trend of hydrogels, their values are lower (i.e., from 436 ± 18 Pa to 3602 ± 163 Pa for G_N^0 and from 53.8 ± 1.1 Pa to 501 ± 25 Pa for G''_{min} against the G_N^0 and G''_{min} of hydrogels which ranges from1719 ± 21 Pa to 19945 ± 205 Pa and from 175.2 ± 9.2 Pa to 2892 ± 172.

The particle/droplets size distribution of emulgel at different fiber fraction are reported in Fig.2.c. A main peak linked to droplets size is present at around 1 μm. Furthermore, a peak between 10 μm and 100 μm, given by the fiber size, appears and increases with increasing of fiber fraction form 0.02 w/w to 0.04 w/w.

3.4.Effect of number of cycles on viscoelasticity and microstructure of hydrogels

The results of stress sweep test and frequency sweep test on samples obtained with different process configuration (one and two passes with Z-z chamber) are reported in Fig.3a and Fig.3b, respectively. Hydrogels exhibited solid-like behavior ($G' > G''$) and, can be considered as weak gels ($G'/G'' \sim 1$) in agreement with the literature on similar materials [5,7,11,22,23]. From Fig.3a, it is possible to observe that reprocessed hydrogel samples have a slightly narrower linear region (in terms of stress) and from both Fig.3a and Fig.3b also lower values of dynamic moduli. Furthermore, looking at Fig.3b it is possible to see a minimum value of G'' at around 0.316 Hz and the corresponding plateau condition of G'. As reported for similar systems, the minimum of G'' is rather shallow and the plateau condition G' can be identified by an inflection point rather than a rigorous constant trend [27,29].

The PSD of hydrogel samples produced using one and two cycles of microfluidization is reported in Fig.3c and compared with that of citrus fiber powder (simply named Powder) and that of the pre-hydrogel., i.e., the suspension after the high-speed homogenization and before the microfluidization. From the decrease in particle size observed between the pre-hydrogel, which shows PSD comparable to the one of fiber powder, and the microfluidized sample, it is possible to verify how microfluidization process, responsible for the defibrillation-activation of citrus fiber-based systems [11], dramatically reduces the particle size of fibers [5,11] similarly to high pressure homogenization [9,10]. Furthermore, an increasing number of microfluidization cycles for hydrogels implies the formation of smaller fibers; this reduces the average size of the particles from tens of microns to approximately 10 μm, and results in the appearance of a second peak in the distribution curve at diameters of the order of 0.1 μm, indicating that a second defibrillation step induced by mechanical shear can generate a second population of small particles, confirming literature [9, 10,11].

The changes in particle size of the hydrogel samples, quantified though $D_{3,2}$, $D_{4,3}$ and $SPAN$, are reported in Tab.2.

From the data found it is possible to observe how a second microfluidization step on hydrogel decreases the size of particle ($D_{3,2}$ decreases of one order of magnitude and $D_{4,3}$

undergoes roughly a halving) and how citrus fiber powder and pre-hydrogel exhibited substantially the same microstructural parameters, indicating that the preliminary high speed homogenization step simply suspends the fibers without inducing relevant fiber breakage and gelification.

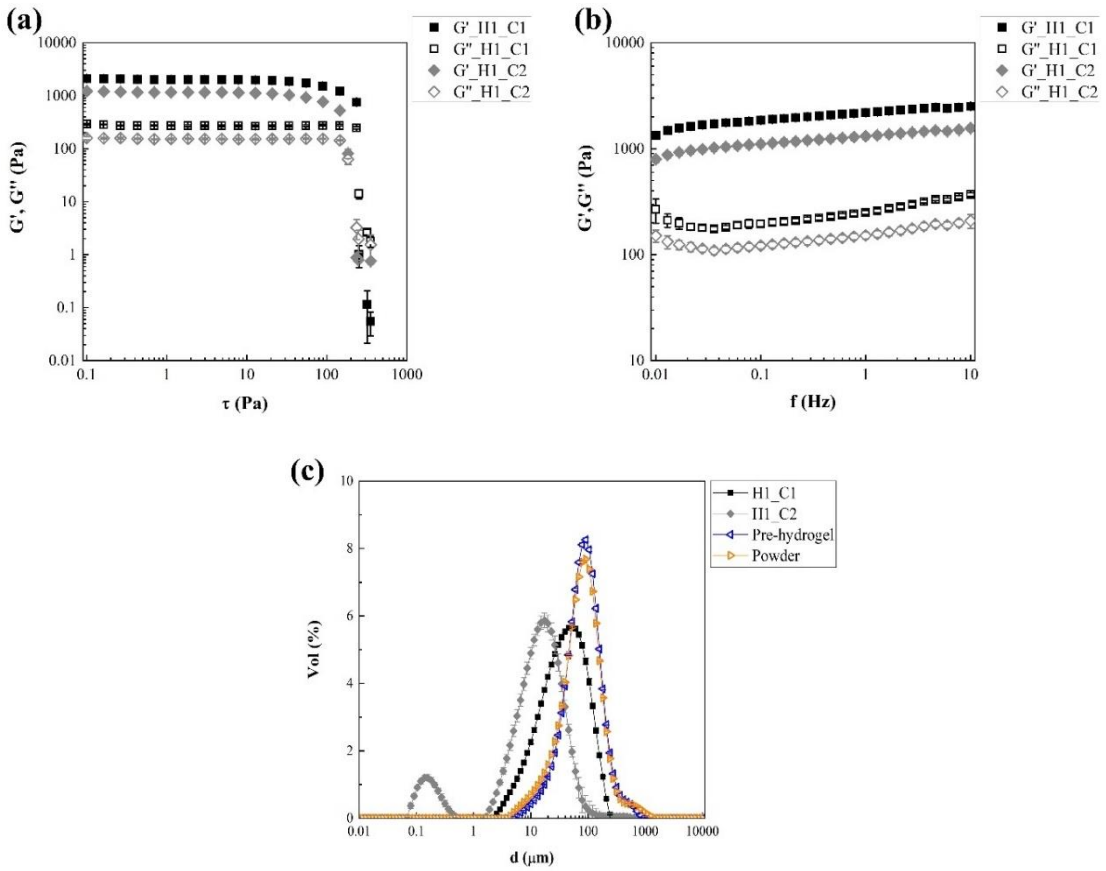

Fig.3. Rheology and microstructure of hydrogel samples in different process conditions: (a) stress sweep test, (b) frequency sweep test and (c) particle size distribution.

Sample ID	$D_{3,2}$ **(µm)**	$D_{4,3}$ **(µm)**	***SPAN*** **(-)**
Powder	45.6 ± 0.2[a]	98.7 ± 2.0 [a]	2.14 ± 0.02 [a]
Pre-hydrogel	44.1 ± 0.6 [b]	98.1 ± 1.2 [a]	2.22 ± 0.03 [a]
H1_C1	21 ± 1[c]	46.7 ± 1.5 [b]	2.64 ± 0.03 [b]
H1_C2	1.27 ± 0.08[d]	18.4 ± 3.8 [c]	2.9 ± 0.3 [b]

Tab.2. Microstructural parameters of hydrogel samples and process intermediate. Different letters, for the same parameters, refer to significantly different values.

Matching the rheological and microstructural results, it turns out that the decreasing of consistency due to process cycles is connected to a decreasing of particle size, or more precisely by the formation of a second population of small particles. This result is in contrast with those obtained by other authors of similar systems, for which the decreasing of particle size was associated with an increase of consistency according to the classical behavior of suspensions [5,10,11]. This decreasing of consistency could be explained by the fact that these systems are gelled suspensions rather than simply suspension, in which large particles (size ~10 μm) give a greater contribution to the strength of the network compared to that of small particles (size ~10 0.1 μm). Consequently, as a result of particle size reduction due to reprocessing, fiber network is destroyed and reforms weaker

3.5.Effect of number of cycles on viscoelasticity and microstructure of emulgels

The stress sweep test and frequency sweep test on emulgel samples obtained with different process configuration (one and two passes with Z-z chamber and one and two passes with the y-Z chamber) are reported in Fig.4a and Fig.4b, respectively. Emulgel samples also behave as solid-like material ($G' > G''$) with weak gel properties ($G'/G'' \sim 1$) in agreement with the literature [7,31]. Similarly to what found for hydrogels, reprocessing, using both Z-z and y-Z chamber configuration, lead to a decrease of linear region and of dynamic moduli. Looking at Fig.4b it is possible to note that the minimum value of G'' and the corresponding plateau condition for emulgel samples is also located at around 0.316 Hz and to draw the same considerations reported for hydrogels about its identification, association of inflection point (plateau) to the minimum of viscous modulus [27,29].

Form Fig.4c, for all emulgel samples produced with different process configurations (one and two passes with Z-z chamber and one and two passes with the y-Z chamber), the main peak at around 1 μm is reasonably more linked to droplets than to citrus fiber particles, since fiber particles (much larger) should be better represented by a peak between 10 μm and 100 μm, whereas the peak appearing at smaller sizes (0.3 – 0.4 μm), probably describes both small particle and small droplets. However, for this set of samples the volume of oil droplets in the systems is much greater than that of fiber: for this reason, no peaks between 10 μm and 100 μm were detected, as instead reported in Fig.2c for emulgels with higher fiber. Consequently, the P/DSD curves of emulgel with 0.01 w/w of fiber in Fig.4c, produced with different process cycles and configurations, can be considered representative of the droplets distribution since they are not affected by fiber particles. Overall, from the DSD in Fig.4c,

no substantial difference in droplets distribution due to process cycles can be observed. A rather similar results were obtained for nanoemulsion for which no differences in DSD were found after 3 passes of microfluidization [21].

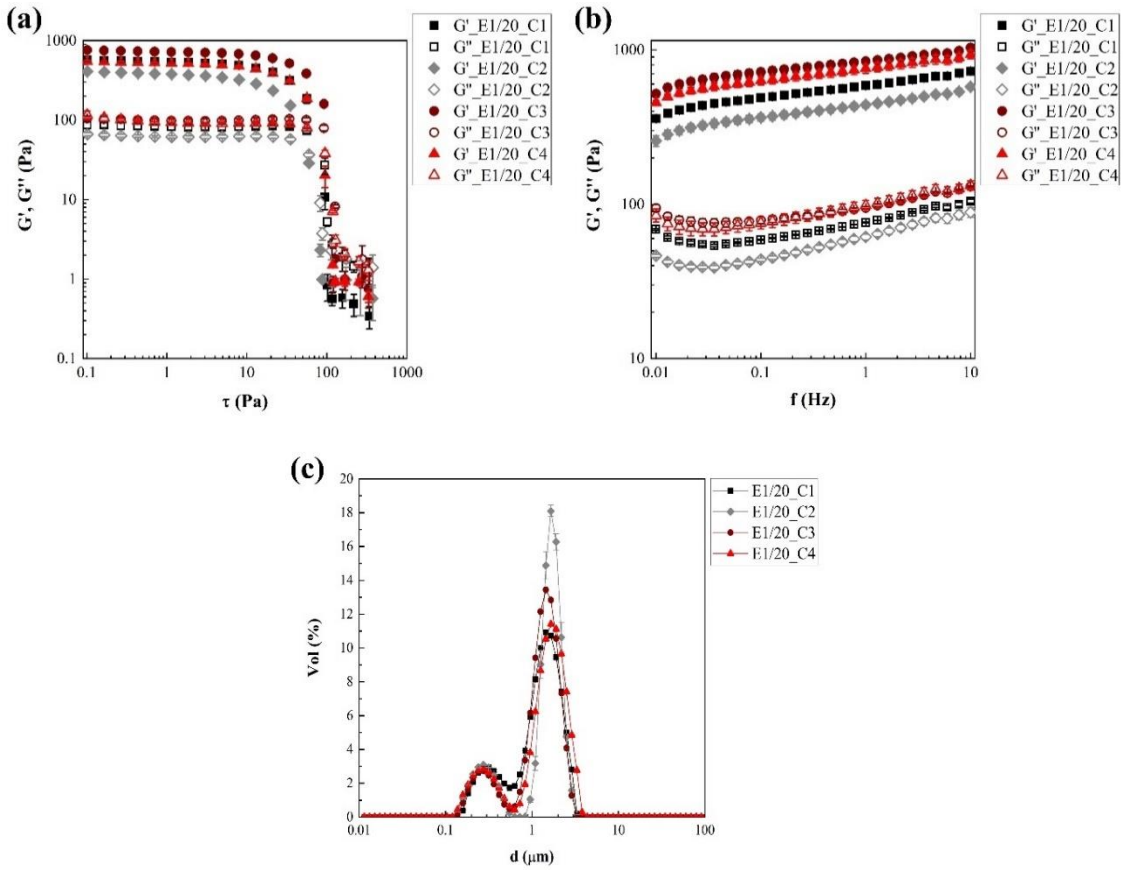

Fig.4. Rheology and microstructure of emulgel samples in different process conditions: (a) stress sweep test, (b) frequency sweep test and (c) droplets size distribution.

In Tab. 3 the microstructural parameters of emulgel samples are reported. As far as the width of the distribution, quantified through $SPAN$ index it decreases by a second microfluidization cycle and resulted slightly higher for emulgel processed with y-Z configuration.

Since no relevant differences in DSD were recorded for emulgels obtained with one or two cycles, it is reasonable to assume that also for emulgels the decrease of the linear region and of the dynamic moduli is due to the weakening of the fiber network induced by the production of sub-micron fiber particles as suggested by the decrease of $SPAN$. It is interesting to observe that emulgels produced with y-Z configuration exhibited slightly higher values of G' and G''in comparison to emulgels produced with Z-z configuration,

despite the similar values of average diameters The higher consistency is probably due to the higher value of $SPAN$ index of samples microfluidized by y-Z chambers. However, rheological and microstructural data on hydrogel samples produced by one and two passes with y-Z are necessary to confirm this hypothesis.

Sample ID	$D_{3,2}$ (µm)	$D_{4,3}$ (µm)	$SPAN$ (-)
E1/20_C1	0.721 ± 0.005 [a]	1.209 ± 0.005 [a]	1.510 ± 0.006 [a]
E1/20_C2	0.737 ± 0.004 [b]	1.35 ± 0.02[b]	1.237 ± 0.009[b]
E1/20_C3	0.7267 ± 0.0006 [a]	1.391 ± 0.001[c]	1.5350 ± 0.0001[c]
E1/20_C4	0.7427 ± 0.0006 [c]	1.229 ± 0.001 [a]	1.3727 ± 0.0006 [d]

Tab.3. Microstructural parameters of emulgel samples. Different letters, for the same parameters, refer to significantly different values.

3.6.Effect of number of cycles on viscoelastic parameters

Rheological parameters defined according to Eq.2 – 6, i.e., limit stress, limit strain, critical stress, critical strain, plateau modulus, respectively and minimum viscous modulus of samples are reported in Tab.4. The limit stress, τ_L, and the critical stress, τ_C, decreases with processing cycle in all cases (hydrogel and emulgel). A decrease of approximately 45% and 30% were found on τ_L and τ_C respectively. Emulgel samples produced via y-Z chambers exhibited higher values of both τ_L and τ_C comparing to emulgel proceeded via Z-z chamber, indicating a stronger network. It is interesting to observe how limit strain, γ_L, is almost the same for all sample regardless of whether they are hydrogels or emulgels, similar to what found for hydrogel and emulgel samples with different x_f in Fig.1a.

Sample ID	τ_L (Pa)	γ_L (-)	τ_C (Pa)	γ_C (-)	G_N^0 (Pa)	G''_{min} (Pa)
H_C1	22.1 ± 0.5[a]	0.01138 ± 1.4 10^{-5}[a]	275 ± 4[a]	1.71 ± 0.01[a]	1719 ± 21[a]	177.2 ± 9.2[a]
H_C2	13.9 ± 0.6[b]	0.012 ± 0.001[a]	206 ± 7[b]	1.79 ± 0.09[a]	1017 ± 42[b]	109.2 ± 8.5[b]
E_C1	4.9 ± 1.4[c]	0.010 ± 0.002[a]	75.3 ± 1.8[c]	0.96 ± 0.06[b]	402.5 ± 9.9[c]	46.2 ± 1.2[c]
E_C2	2.5 ± 0.2[d]	0.0092 ± 6.6 10^{-4}[a]	53 ± 1.3[d]	0.87 ± 0.09[b]	334 ± 19[d]	39.1 ± 1.2[c]
E_C3	6.889 ± 0.002[e]	0.009 ± 0.003[a]	103.0 ± 0.9[e]	0.88 ± 0.03[b]	665 ± 27[e]	77.1 ± 1.8[d]
E_C4	3.6 ± 0.2[cd]	0.010 ± 3.1 10^{-4}[a]	70.9 ± 4.5[c]	1.0 ± 0.1[b]	578 ± 33[f]	67.5 ± 5.2[d]

Tab.4. Viscoelastic and microstructural parameters. Different letters, for the same parameters, refer to significantly different values.

A common meaning value of γ_L equal to 0.010 ± 0.002 (-) can be considered representative for all samples. On the contrary, the critical strain, γ_C, of hydrogels results around 1.75 (-) which is more than double that of emulgels, 0.93 (-). The plateau modulus (G_N^0) decreases with increasing process cycles for all systems. A decrease of approximately 40% was obtained for hydrogel samples while for emulgel samples produced using Z-z chambers or y-Z chambers a decrease of about 15% was found. The minimum viscous modulus G''_{min} of the hydrogel decreases by applying a second pass while that of emulgels resulted independent from the number of passes. In general, emulgels produced via y-Z chamber exhibited higher values of both G_N^0 and G''_{min} in comparison with emulgel proceeded via Z-z chamber, indicating once again a stronger network.

3.7.Morphological investigations

Some representative samples were chosen for morphology investigation, specifically the morphology samples H1_C1, H1_C2, E1/20_C1 and E1/20_C2 is reported in Fig.5. From the optical micrographs in Fig.5a and Fig.5d no particular changes between the morphology of hydrogel samples produced with one and two microfluidization cycles can be appreciated, besides the presence of smaller citrus fiber particles, as previously discussed and observed by other authors [11].

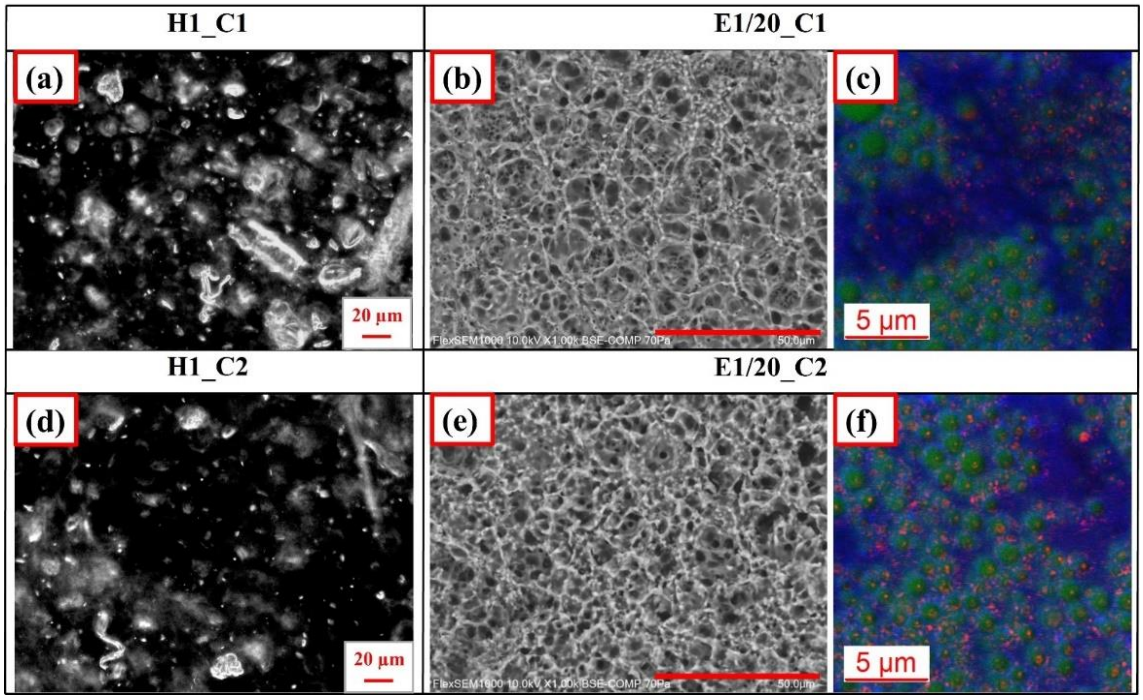

Fig.5. Morphology of hydrogel and emulgel samples. In SEM images bar refers to 50 µm.

In Fig.5b and Fig.5e the SEM images, acquired in cryo-mode of sample E1/20_C1 and E1/20_C2 respectively, are reported. SEM images show a uniform distribution of droplets in the matrix indicating good effectiveness of both processing configurations. In micrographs in Fig.5c and Fig.5f the morphology of samples E1_C1 and E1_C2 obtained by CLSM is reported, particularly the oil phase (648 – 833 nm) is reported in green, the water phase containing citrus fiber (410 – 605 nm) is reported in blue and the reflection signal is reported in red. Looking at the figures, it is possible to observe that a double cycle of microfluidization leads to the formation of more cellulose nanocrystals, reds dots observed by reflectance signal (619 – 647 nm) which adsorb at the O/W interfaces exerting Pickering effects [33] as already observed for similar O/W emulsion obtained by different processes [9,10]. This morphological result is rather reasonable, indeed considering the PSD of hydrogel in Fig.3c a population of small particle with a size of around 0.1 μm was formed following two passes and from the DSD of emulgel in Fig.4c the size of droplets was around 1-2 μm, then the condition for Pickering effects is fulfilled.

3.8.Physical stability of emulgels structured with citrus fiber

The percentage backscattering (BS%) profile of emulgel samples is reported in Fig.6. All samples reported similar values of BS%, around 80% in the central part. From the figure, it is possible to see how the BS% signal oscillates during the time (up and down) and some distortion of the profile in the central part of the samples can be seen in some samples, attributable to some voids in measuring cells due to the high consistency of samples. It is worth mentioning that the high consistency of samples does not also allow the formation of an optimal meniscus in the measuring cell. In general, looking at Fig.6, no relevant distortion of the profile can be observed, the BS% signal remains almost constant along the samples heigh during time, then the produced systems can be considered substantially stable. In addition, as reported in of Fig. 7, all the emulgel samples exhibited a change in the ΔBS% profile lower than 5% which can be considered a more than reliable proof of the physical stability of the systems. Indeed, according to literature works, no particle/droplets size changes can be speculated if the ΔBS% values is lower than 2%, while values higher than 10% some destabilization phenomena could be expected [32,34]. In light of this and taking into account the previous results on similar systems [32], no phase separations or changes in the particle size and emulsion droplets size can be expected along the samples within 14 days. Overall, all the emulgels are physically stable, independently from the differences in

morphology, i.e., the presence of very sub-micron particles and a greater Pickering effect indicating that, despite the occurrence of Pickering effect hindered network strength it does not affect the general physical stability of the systems.

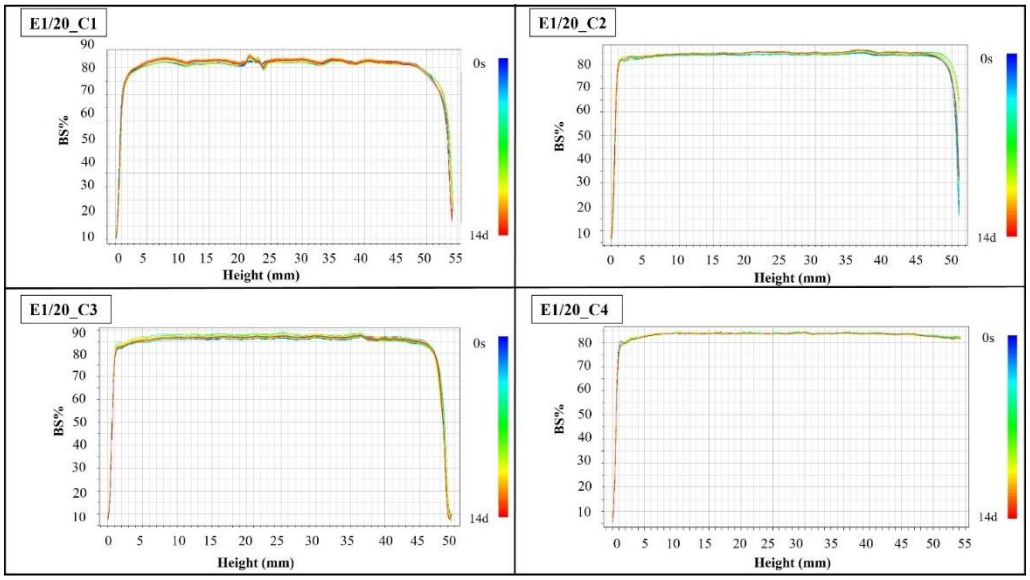

Fig.6. Backscattering profile of emulgel samples.

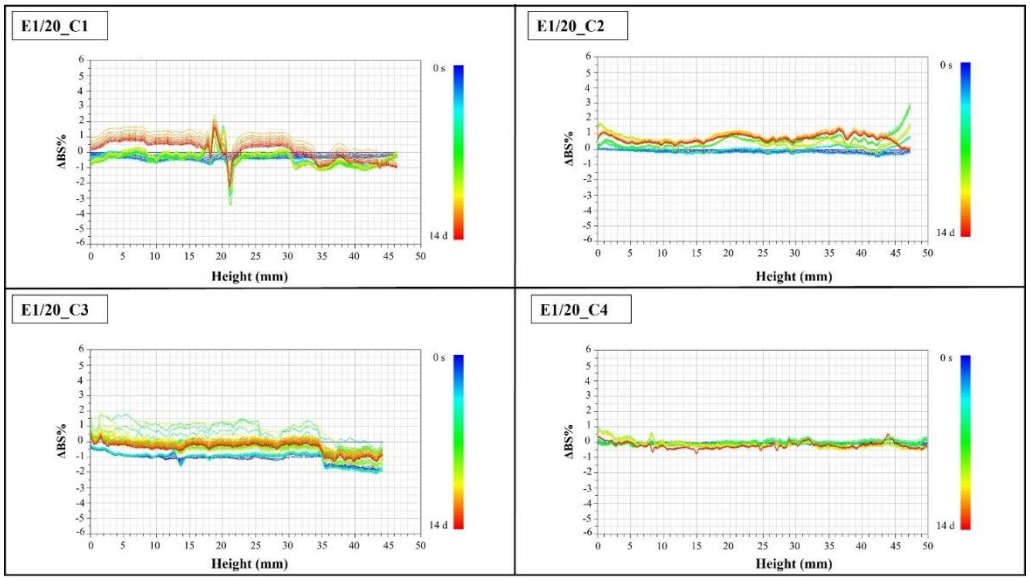

Fig.7. Delta backscattering profile of emulgel samples.

4. Conclusions

Hydrogels and emulgels structured with citrus fiber were successfully produced by microfluidization and the effect of process cycles and chamber configuration on rheological properties and microstructure was investigated. All the microfluidization conditions used,

one and two passes with Z-z configuration for hydrogels and one and two passes with Z-z and y-Z configuration for emulgels, allowed the preparation of samples with good structure and stability. The number of microfluidization cycles and the type of interaction chamber were found to change the particle size of citrus fiber and the rheology of both hydrogels. Particle size reduction was associated with the formation of a weaker gel network; this reasonably means that larger fiber mainly contributes to network structure. As for emulgels, the investigated process conditions do not affect *de facto* the droplets size distribution, and the rheological properties are substantially due to fiber size modifications. For emulgels a second cycle was also found to produce small fiber particles which do not contribute to particle gel network and because of the presence of droplets they adsorb to the interface generating Pickering effects. Both the networking and the Pickering effect provide stability to emulgel samples, but an increase of the latter was wound to decrease the consistency of emulgel. Morphology observations and PSD/DSD gave a clear analysis of the microstructure and proved that the most relevant stabilization mechanism is due to formation of the network. Despite the presence of smaller particles due to extra processing, network formation is still prevalent for the stabilization of droplets at the expense of Pickering stabilization. Overall, it seems that network formation and Pickering effects are microstructurally competitive since the formation of small particles, around 0.1 μm, reduced the linear region and the dynamic moduli of both hydrogels and emulgels. Rheological parameters linked to network structure, τ_L, γ_L, τ_C, γ_L, G_N^0, G''_{min} are good indicators for monitoring process effects on this type of system. In all cases, both hydrogels and emulgels showed a consistency that could be suitable for food applications and also a remarkable physical stability. Future attractive insights that could be integrated in the preset research are: (i) the preparation and characterization of hydrogel samples using the y-Z configuration with one and two passes, possible samples H_C2 and H_C3, (ii) preparation of emulgels and hydrogels with high number of cycles (8 cycles for example) and characterization by stress and frequency sweep test and PSD, (iii) the acquisition of PSD of pre-emulsion and (iv) the preparation and the characterization of two O/W emulsions microfluidized without citrus fiber (as reference).

References

[1] Gidley, M.J.; Yakubov, G.E. Functional Categorisation of Dietary Fibre in Foods: Beyond 'soluble' vs 'Insoluble.' Trends Food Sci. Technol. 2019, 86, 563–568, doi:10.1016/j.tifs.2018.12.006.

[2] Ye, S.; Shah, B.R.; Li, J.; Liang, H.; Zhan, F.; Geng, F.; Li, B. A Critical Review on Interplay

between Dietary Fibers and Gut Microbiota. Trends Food Sci. Technol. 2022, 124, 237–249, doi:10.1016/j.tifs.2022.04.010.

[3] He, Y.; Wang, B.; Wen, L.; Wang, F.; Yu, H.; Chen, D.; Su, X.; Zhang, C. Effects of Dietary Fiber on Human Health. Food Sci. Hum. Wellness 2022, 11, 1–10, doi:10.1016/j.fshw.2021.07.001.

[4] Fernández-Fernández, A.M.; Dellacassa, E.; Medrano-Fernandez, A.; Castillo, M.D. Citrus Waste Recovery for Sustainable Nutrition and Health. In Food Wastes and By-products: Nutraceutical and Health Potential; Rocio Campos-Vega, B. Dave Oomah, and H.A.V.-C., Ed.; John Wiley & Sons Ltd., 2020; pp. 193–222.

[5] Bruno, E.; Lupi, F.R.; Martin-Piñero, M.J.; Girimonte, R.; Baldino, N.; Muñoz, J.; Gabriele, D. Influence of Different Dispersing Systems on Rheological and Microstructural Properties of Citrus Fiber Suspensions. Lwt 2021, 152, doi:10.1016/j.lwt.2021.112270.

[6] Lupi, F.R.; Puoci, F.; Bruno, E.; Baldino, N.; Marino, R.; Gabriele, D. The Effects of Process Conditions on Rheological Properties of Functional Citrus Fibre Suspensions. Food Bioprod. Process. 2020, 121, 54–64, doi:10.1016/j.fbp.2020.01.018.

[7] Bruno, E.; Lupi, F.R.; Mammolenti, D.; Mileti, O.; Baldino, N.; Gabriele, D. Emulgels Structured with Dietary Fiber for Food Uses : A Rheological Model. Foods 2022, 11.

[8] Bruno, E.; Lupi, F.R.; Mammolenti, D.; Baldino, N.; Gabriele, D. Development and Rheological Modeling of Dietary Fiber and Policosanol Plant-Based Bigels for Potential Food Applications. Food Hydrocoll. 2024, 150, 109733, doi:10.1016/j.foodhyd.2024.109733.

[9] Qi, J. ru; Song, L. wen; Zeng, W. qi; Liao, J. song Citrus Fiber for the Stabilization of O/W Emulsion through Combination of Pickering Effect and Fiber-Based Network. Food Chem. 2021, 343, 128523, doi:10.1016/j.foodchem.2020.128523.

[10] He, K.; Li, Q.; Li, Y.; Li, B.; Liu, S. Water-Insoluble Dietary Fibers from Bamboo Shoot Used as Plant Food Particles for the Stabilization of O/W Pickering Emulsion. Food Chem. 2020, 310, doi:10.1016/j.foodchem.2019.125925.

[11] Morales-Medina, R.; Dong, D.; Schalow, S.; Drusch, S. Impact of Microfluidization on the Microstructure and Functional Properties of Pea Hull Fibre. Food Hydrocoll. 2020, 103, 105660, doi:https://doi.org/10.1016/j.foodhyd.2020.105660.

[12] Van Buggenhout, S.; Wallecan, J.; Christiaens, S.; Debon, S.J.J.; Desmet, C.; Van Loey, A.; Hendrickx, M.; Mazoyer, J. Influence of High-Pressure Homogenization on Functional Properties of Orange Pulp. Innov. Food Sci. Emerg. Technol. 2015, 30, 51–60, doi:10.1016/j.ifset.2015.05.004.

[13] Willemsen, K.L.D.D.; Panozzo, A.; Moelants, K.; Debon, S.J.J.; Desmet, C.; Cardinaels, R.; Moldenaers, P.; Wallecan, J.; Hendrickx, M.E.G. Physico-Chemical and Viscoelastic Properties of High Pressure Homogenized Lemon Peel Fiber Fraction Suspensions Obtained after

Sequential Pectin Extraction. Food Hydrocoll. 2017, 72, 358–371, doi:10.1016/j.foodhyd.2017.06.020.

[14] Su, D.; Zhu, X.; Wang, Y.; Li, D.; Wang, L. Effect of High-Pressure Homogenization on Rheological Properties of Citrus Fiber. Lwt 2020, 127, 109366, doi:10.1016/j.lwt.2020.109366.

[15] Su, D.; Zhu, X.; Wang, Y.; Li, D.; Wang, L. Effects of High-Pressure Homogenization on Physical and Thermal Properties of Citrus Fiber. Lwt 2019, 116, doi:10.1016/j.lwt.2019.108573.

[16] Van Audenhove, J.; Bernaerts, T.; Putri, N.I.; Van Rooy, L.; Van Loey, A.M.; Hendrickx, M.E. The Role of Mechanical Collapse by Cryogenic Ball Milling on the Effect of High-Pressure Homogenization on the Microstructural and Texturizing Properties of Partially Pectin-Depleted Tomato Cell Wall Material. Food Res. Int. 2022, 155, 111033, doi:10.1016/j.foodres.2022.111033.

[17] Wu, C.; Teng, F.; McClements, D.J.; Zhang, S.; Li, Y.; Wang, Z. Effect of Cavitation Jet Processing on the Physicochemical Properties and Structural Characteristics of Okara Dietary Fiber. Food Res. Int. 2020, 134, doi:10.1016/j.foodres.2020.109251.

[18] Gu, Y.; Niu, L.; Song, J.; Liu, C.; Zhang, Z.; Liu, C.; Li, D.; Xiao, L. Effect of Pretreatment and High Hydrostatic Pressure on Soluble Dietary Fiber in Lotus Root Residues. J. Food Qual. 2022, 2022, doi:10.1155/2022/5565538.

[19] Chen, J.; Gao, D.; Yang, L.; Gao, Y. Effect of Microfluidization Process on the Functional Properties of Insoluble Dietary Fiber. Food Res. Int. 2013, 54, 1821–1827, doi:10.1016/j.foodres.2013.09.025.

[20] Guo, X.; Chen, M.; Li, Y.; Dai, T.; Shuai, X.; Chen, J.; Liu, C. Modification of Food Macromolecules Using Dynamic High Pressure Microfluidization: A Review. Trends Food Sci. Technol. 2020, 100, 223–234, doi:10.1016/j.tifs.2020.04.004.

[21] Alfaro-Rodríguez, M.C.; Prieto, P.; García, M.C.; Martín-Piñero, M.J.; Muñoz, J. Influence of Nanoemulsion/Gum Ratio on Droplet Size Distribution, Rheology and Physical Stability of Nanoemulgels Containing Inulin and Omega-3 Fatty Acids. J. Sci. Food Agric. 2022, 102, 6397–6403, doi:10.1002/jsfa.12005.

[22] Chen, B.; Cai, Y.; Liu, T.; Huang, L.; Deng, X.; Zhao, Q.; Zhao, M. Improvements in Physicochemical and Emulsifying Properties of Insoluble Soybean Fiber by Physical-Chemical Treatments. Food Hydrocoll. 2019, 93, 167–175, doi:10.1016/j.foodhyd.2019.01.058.

[23] Zhang, Y.; Qi, J.; Zeng, W.; Huang, Y.; Yang, X. Properties of Dietary Fiber from Citrus Obtained through Alkaline Hydrogen Peroxide Treatment and Homogenization Treatment. Food Chem. 2020, 311, 125873, doi:10.1016/j.foodchem.2019.125873.

[24] Moelants, K.R.N.; Cardinaels, R.; Jolie, R.P.; Verrijssen, T.A.J.; Van Buggenhout, S.; Zumalacarregui, L.M.; Van Loey, A.M.; Moldenaers, P.; Hendrickx, M.E. Relation Between

Particle Properties and Rheological Characteristics of Carrot-Derived Suspensions. Food Bioprocess Technol. 2013, 6, 1127–1143, doi:10.1007/s11947-011-0718-0.

[25] Bengtsson, H.; Wikberg, J.; Tornberg, E. Physicochemical Characterization of Fruit and Vegetable Fiber Suspensions. II: Effect of Variations in Heat Treatment. J. Texture Stud. 2011, 42, 281–290, doi:10.1111/j.1745-4603.2010.00276.x.

[26] Suresh, H.; Ho, V.; Zhou, J. Rheological Characteristics of Soluble Fibres during Chemically Simulated Digestion and Their Suitability for Gastroparesis Patients. Nutrients 2020, 12, 1–22, doi:10.3390/nu12082479.

[27] Franco, J.M.; Berjano, M.; Gallegos, C. Linear Viscoelasticity of Salad Dressing Emulsions. J. Agric. Food Chem. 1997, 45, 713–719, doi:10.1021/jf9605355.

[28] Martin-Piñero, M.J.; García, M.C.; Santos, J.; Alfaro-Rodriguez, M.C.; Muñoz, J. Characterization of Novel Nanoemulsions, with Improved Properties, Based on Rosemary Essential Oil and Biopolymers. J. Sci. Food Agric. 2020, 100, 3886–3894, doi:10.1002/jsfa.10430.

[29] Weitz, D.A.; Mason, T.G.; Bibette, J. Elasticity of Compressed Emulsions. Phys. Rev. Lett. 1995, 75, 2051–2054.

[30] Mason, T.G.; Weitz, D.A. Linear Viscoelasticity of Colloidal Hard Sphere Suspensions near the Glass Transition. Phys. Rev. Lett. 1995, 75, 2770–2773, doi:10.1103/PhysRevLett.75.2770.

[31] De Paola, M.G.; Mammolenti, D.; Lupi, F.R.; De Santo, M.P.; Gabriele, D.; Calabrò, V. Formulation and Process Investigation of Glycerol/Starch Suspensions for Edible Films Production by Tape Casting. Chem. Pap. 2022, 76, 1525–1538, doi:10.1007/s11696-021-01956-6.

[32] Muñoz, J.; Prieto-Vargas, P.; García, M.C.; Alfaro-Rodríguez, M.C. Effect of a Change in the CaCl2/Pectin Mass Ratio on the Particle Size, Rheology and Physical Stability of Lemon Essential Oil/W Emulgels. Foods 2023, 12, doi:10.3390/foods12061137.

[33] Abdullah; Weiss, J.; Ahmad, T.; Zhang, C.; Zhang, H. A Review of Recent Progress on High Internal-Phase Pickering Emulsions in Food Science. Trends Food Sci. Technol. 2020, 106, 91–103, doi:10.1016/j.tifs.2020.10.016.

[34] Celia, C.; Trapasso, E.; Cosco, D.; Paolino, D.; Fresta, M. Turbiscan Lab® Expert Analysis of the Stability of Ethosomes® and Ultradeformable Liposomes Containing a Bilayer Fluidizing Agent. Colloids Surfaces B Biointerfaces 2009, 72, 155–160, doi:10.1016/j.colsurfb.2009.03.007.

Supplementary Material

Microfluidized hydrogel and emulgels structured with citrus fiber: effect of processing cycles and channels on rheology and microstructure

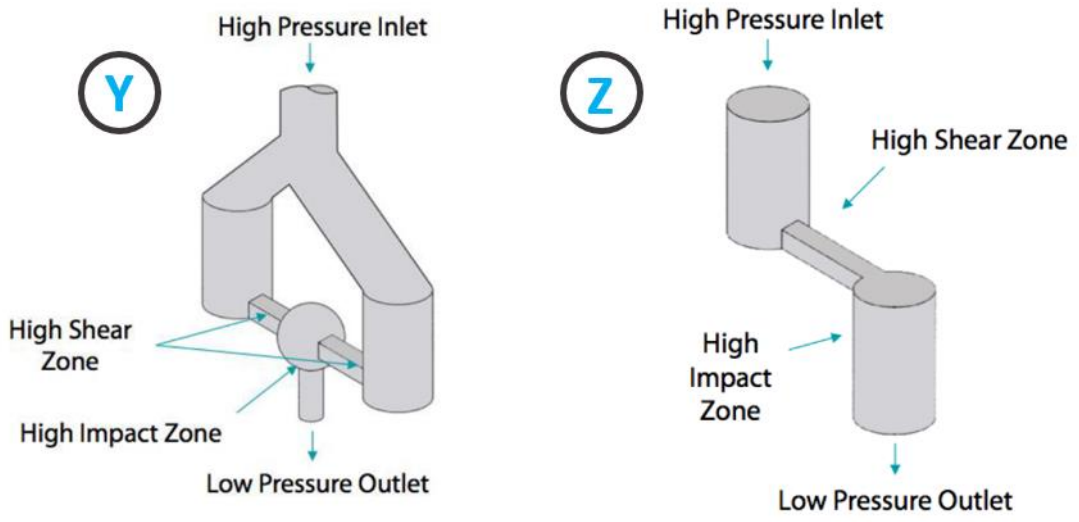

Fig.S1. Microfluidization interaction chamber geometries. Picture taken from: https://www.skyepharma.com/bioavailability-is-a-matter-of-size-microfluidization/.

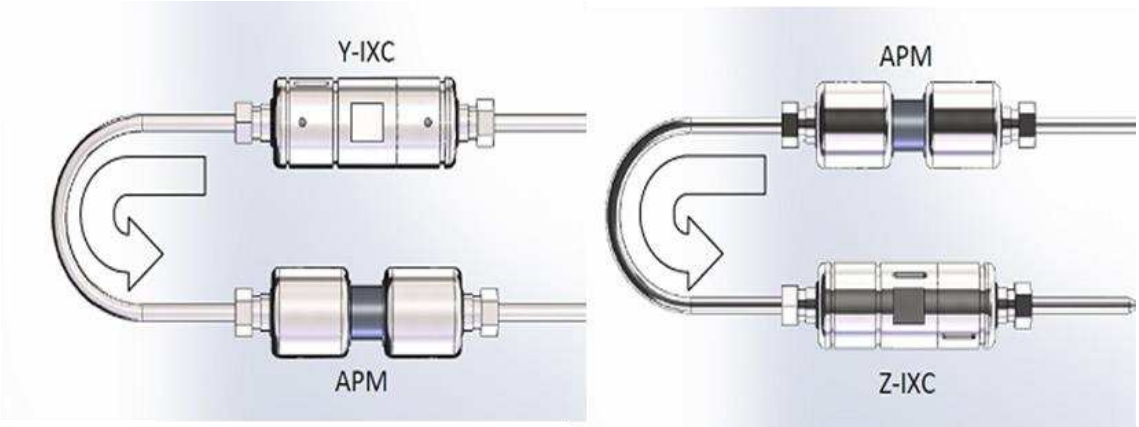

Fig.S2. Microfluidization interaction chambers configurations. APM is a Z-type chamber with large diameter. Picture taken from: https://www.microfluidics-mpt.com/microfluidizer-interaction-chambers.

CHAPTER 5

Industrial application of citrus fiber in food products

Production of homogenized orange juice clean label and source of fiber stabilized by inulin/citrus fiber blends

Assessment of structuring and stability of clean label vegan mayonnaise stabilized by citrus fiber and plant proteins

Production of homogenized orange juice clean label and source of fiber stabilized by inulin/citrus fiber blends

Abstract

The present work represents a scientific report containing an industrial application of citrus fiber in a water-based food system, in particular orange juice. The research activities were carried out in the laboratory of JRS Silvateam Ingredients s.r.l. during the internship held from 15/01/2024 to15/10/2024 and concerns the formulation and development of orange juice from concentrated juice, source of fiber and with improved stability properties comparing to common orange juices from concentrate.

1. Introduction

Orange juice is one of the most consumed fruit juice worldwide showing and interesting global market [61,62]. A particular category of orange juice is obtained from the dilution of concentrated juice with water to obtain reconstituted orange juice. Concentrate orange juice is a commercial form of industrial orange juice able to guarantee satisfying commerciality and nutritional characteristics [63]. However, being a suspension of particle, the reconstituted orange juice from its concentrate yields a physically unstable systems, since it undergoes to phase separation, i.e., particle sedimentation.

In general, the physical stability of suspensions like fruit juice can be enhanced by acting on both processes and on the addition of stabilizers. In the first case, the result is a finer dispersion, whereas, in the second, an increase of the consistency or a structuration of the continuous phase, or even other more complex mechanisms are promoted. These two strategies can be also coupled to achieve the best properties with a moderate change of composition, dispersions and microstructure of the systems.

In the present work the formulation of commercial grade orange juices from concentrated juice with improved stability was developed by the application of high-pressure homogenization (HPH) and the addition of dietary fiber mixture made of citrus fiber and inulin with the aim to increase consistency. The effect of pressure, dietary fiber blending ratio and citrus fiber type was investigated. The addition of total amount of fiber was set to 1.5% w/w which grossly represent more than the double of the minimum value required for the nutritional claim “source of fiber” according to EU regulation No 1924/2006 [64], .i.e., 1.5 g of fiber per 100 kcal, and by considering that a commercial orange juice from

concentrate have an energetic content ranging from 30 to 50 kcal every 100 ml (roughly 100 g). This choice is based on both cost saving issues and a technical reason related to an over thickening due to fiber action which can make orange juice unacceptable to consumers. The ratio between inulin and citrus fiber was changed, and citrus fibers with different properties were tested. It must be highlighted that the addition of citrus fiber and inulin as stabilizers make the formulation suitable for adopting the commercial claim "clean label", since both of them are E-number free food components, i.e., not listed as food additives in EU regulation No 1129/2011 [65]. The analysis was based on rheological characterization and stability evaluation. In particular frequency sweep tests in the linear region and steady state flow tests were carried out with the aim of characterizing the microstructure and the flow properties of samples, whereas Turbiscan analysis, i.e., multiple light scattering, was used to monitor their destabilization process due to sedimentation.

2. Material and methods

2.1. Materials

Citrus fibers with different amount of soluble (SDF) and insoluble (IDF) fiber fractions and different functional and physical-chemical properties were provided by JRS Silvateam Ingredients (Italy). Sample details, such as water holding capacity (WHC), color (L*, a*, b*), pH, percentage humidity ($H_{\%}$), particle diameter (D50), Span index (SPAN) and SDF/IDF ratio are reported in Tab.1. Inulin samples (purity ≥ 90%, average DP ≥ 10%, $H_{\%}$ = 1, pH = 5 – 7) was kindly provide by LBG Sicilia (Italy). Concentrated orange juice (66° brix) was provided by Louis Dreyfus Company-LDC (Netherlands). Tap water was used for the dilutions of samples. Commercial orange juices, named B1 ("Succo d'arancia da concentrato", Solevita, Italy), B2 ("Bevanda all'arancia senza zuccheri aggiunti", Conad, Italy), were bought in local supermarkets and used as benchmarks for a comparison of produced samples in terms of color and physical stability.

2.2.Orange juice preparations

The concentrated orange juice was manually mixed with tap water to obtain suspended reconstituted orange juice. The obtained suspension (500 g) was then homogenized using high pressure homogenizer Twin Panda 600 lab homogenizer (GEA, Germany). Orange juice samples without fibers were produced at different homogenization pressures (0-80-120 Pa) whereas samples with 1.5% w/w of dietary fibers, i.e., sample with 1.5% w/w of inulin

and sample with 1.5% w/w of inulin/citrus fiber blends were produced at 80 bar. Different types of citrus fibers samples were used, Tab.1. Inulin and inulin/citrus fiber blends were added to reconstituted orange juice and manually dispersed before homogenization process. For each samples the amount of juice contrate and water was calculated to keep the minimum vale of soluble solid allowed for orange juice from concentrate to 11.2 Brix (checked by hand-held refractometer (master-20α, Atago, Japan)) and by considering the contribution of soluble fraction of the dietary fibers added, i.e., the Brix degrees due to the soluble part of citrus fiber and that due to the inulin. Sample ID, composition and pressure of all orange juice samples are reported in Tab. 2.

Properties	**CF1**	**CF2**	**CF3**	**CF4**	**CF5**
WHC (g/g)	22.7	23.7	19.1	15.4	21.2
H% (-)	8.20	7.66	7.06	6.36	8.73
pH (-)	3.95	4.65	4.01	4.63	4.68
L*	83.4	85.1	86.5	81.38	81.63
a*	0.45	0.38	0.31	1.59	1.23
b*	18.75	19.12	18.9	18.62	18.99
D_{90} (µm)	204	163	148	237	274
SDF%/IDF%	15/85	20/80	20/80	40/60	40/60

Tab.1. Functional and physical-chemical properties of citrus fiber samples. Data provided by the supplier.

Orange Juice ID	**Citrus Fiber ID**	**%w/w Inulin**	**%w/w Citrus Fiber**	**Inulin/Citrus Fiber in blend**	**SDF%/IDF% in blend**	**Pressure (Pa)**
OJ_0	-	-	-	-	-	0
OJ_80	-	-	-	-	-	80
OJ_120	-	-	-	-	-	120
OJ-I_80	-	1.50	-	1	1	80
OJ-CF1-1_80	CF_1	0.90	0.60	0.60	0.77	80
OJ-CF1-2_80	CF_1	0.75	0.75	0.50	0.64	80
OJ-CF1-3_80	CF_1	0.60	0.90	0.40	0.51	80
OJ-CF2-1_80	CF_2	0.90	0.60	0.60	0.72	80
OJ-CF3-1_80	CF_3	0.90	0.60	0.60	0.72	80
OJ-CF4-1_80	CF_4	0.90	0.60	0.60	0.54	80
OJ-CF5-1_80	CF_5	0.90	0.60	0.60	0.54	80

Tab.2. Sample ID, composition (%w/w of single fibers, inulin/citrus fiber in blend and SDF%/IDF% in blend) and process conditions (pressure) of homogenized orange juice sample.

2.3. pH measurements

The pH of samples was carried out at 25°C using pH meter S400 (Mattler Toledo, USA). All measures were taken at 25°C in duplicate, and the results averaged.

2.4. Color measurements

Color analysis was performed by colorimeter Croma Meter CR-400 (Konica Minolta, Japan). Color coordinates, L* (axis of lightness), a* (axis of red/green transition) and b* (axis of yellow/blue transition), in the CieLab space were determined. The color sampling was run twice, using the white standard plate as background.

2.5. Water activity measurements

Water activity of dietary fiber powder was measured using the water activity meter AwTherm (Rotronic, Switzerland). All measures were taken in duplicate, and the results averaged.

2.6. Multiple light scattering analysis

The physical stability of sample was evaluated using Turbiscan Tower (Formulaction SAS, France). The data were interpreted in terms of destabilization kinetics, i.e., by monitoring the Turbiscan stability index (TSI) defined according to Eq.1, in the time.

$$TSI = \sum_{i} \frac{\sum_{h} |scan_i(h) - scan_{i-1}(h)|}{H} \quad (1)$$

where $scan_i(h)$ and $scan_{i-1}(h)$ are the values of the profile for a given scan "i" and the previous one "i-1" assessed at a given height "h", respectively whereas H is the total high of the sample. Turbiscan analysis was used to monitor the stability of samples for 24 h and for 72 h. According to the connections between the TSI values and stability provided by the Turbiscan manufacturer, the stability criteria of orange juice samples was fixed to a stricter condition for the first 24 h, TSI < 1, which corresponds to an extremely good visually appearance in which particle migration and optical changes undetectable by human eye, to a softer condition for the 72 h, TSI < 3, which represent the start of a visually phase separation, detectable by human eyes.

Samples were gently mixed manually before filling the cell, and an equilibration time of 30 minutes before the scanning was adopted. The scanning frequency was fixed at 1 scan every 10 min to monitor the samples for the first 24 h, whereas, for the following 48 h, the profile of samples was scanned every 30 min. For the long-time scanning series (72 h), after filling

and sealing, the Turbiscan cells were immersed in boiling water for 1 min and cooled in fresh water (10-12 °C) in order to carry out the observation safer from possible microbiological instability. This procedure was also adopted to in the assessment of the stability of benchmarks. With the aim of evaluating the effect of thermal treatment on stability analysis for benchmark samples, a further scanning set of 72 h was carried out without using the thermal treatment and the results were compared with that obtained for the same sample after immersion of cell in boiling water.

2.7. Rheological analysis

Rheological tests were carried out with MCR 102e rheometer (Anton Paar, Austria) equipped with parallel serrated plate geometry (diameter 50 mm, gap 1 ± 0.2 mm) and Peltier systems for thermal control. Frequency sweep tests were carried out, in linear region previously determined by amplitude sweep test, in the frequency range (0.1 – 10 Hz). Flow curve tests were carried out in the shar rate range of 0.1 – 100 s^{-1}. All measurements were carried out at 25°C in duplicate and the results averaged.

2.8. Statistical analysis

Statistical analysis was performed with the software Origin Pro (Version 2021b; OriginLab Corporation, USA). A one-way ANOVA test was used to compare the value of color parameters, pH and water activity. Differences were considered statistically significant for $p < 0.05$ and Tukey test was used to compare the means.

Results and discussion

3.1. Effect of pressure and blending ratio on rheological properties and stability

Frequency sweep test of neat OJ samples (OJ_0) homogenized at different pressures are reported in Fig.1a. A comparison of sample OJ_0 with OJ_80 and OJ_120, denotes that a pressure variation form 0 bar to 80 MPa results in significant rheological modifications of samples, that vary from liquid-like to solid like; in fact, δ moves from 80 – 40° to 5 – 30° and there is also a variation of G^*. In particular, the slope of G^*drastically decreases. No appreciable differences were found between samples produced with 80 and 120 bar in terms of both G^* and δ. The flow curve of samples produced at different pressures are reported in Fig.1b; it is evident that the flow behavior is independent from process pressure, since very close curves were obtained. Considering the dynamic and steady state flow behavior induced

by homogenization pressure and with the aim of keeping a cost-saving approach, a value of 80 bar was chosen as a satisfying pressure able to induce substantial rheological modifications and used to produce samples with different fiber blending ratio and citrus fiber type.

The results of the frequency sweep tests of samples produced at 80 bar with different blending ratio are reported in Fig.2a. From the graphs it is possible to see that all samples exhibited solid-like behavior, and that a more than linear increase in complex modulus curves G^* by increasing the citrus fiber fraction in the blending from 0 to 0.6 is encountered. On the contrary the structuration degree (deductible from the trend of δ) seems to be less affected by inulin/citrus fiber ratio and only the phase angle δ of sample OJ-I exhibited a different trend. As reported in the Fig.2b., the viscosity of OJ samples increased with the increasing of citrus fiber fraction in the blending from 0 to 0.5 than no relevant differences were found.

The destabilization kinetic in 24 h (84600 s) is reported in Fig.3a. All systems exhibited a TSI value higher than 2, and, after 24 h, were then considered unstable. On the contrary, from Fig. 3b., samples containing fibers exhibited lower TSI and the stability criterion, i.e., $TSI < 1$, was obtained for all the samples containing citrus fiber.

Considering these outcomes, with the aim of preparing a stable system by inducing the minimum changes in systems rheology, the blending ratio was fixed to 0.60 inulin/citrus fiber %w/w.

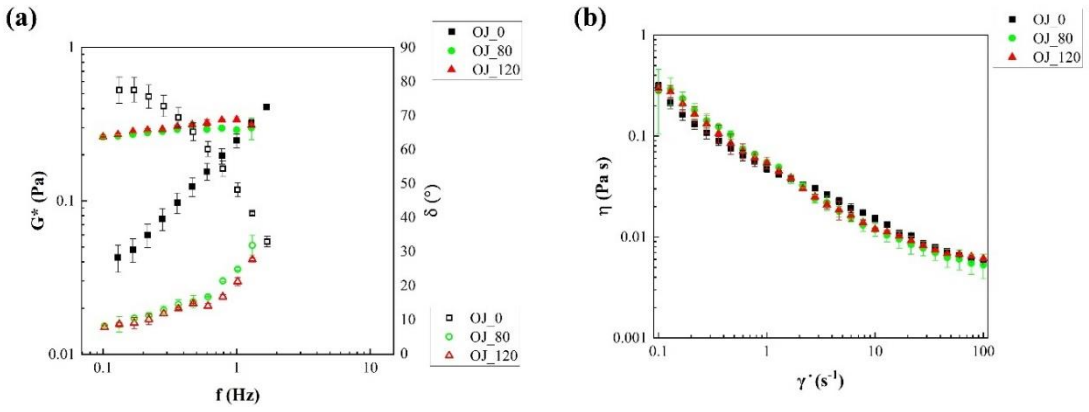

Fig.1. Rheological properties of samples at different pressure: (a) complex modulus (filled symbols) and phase angle (empty symbols) and (b) viscosity.

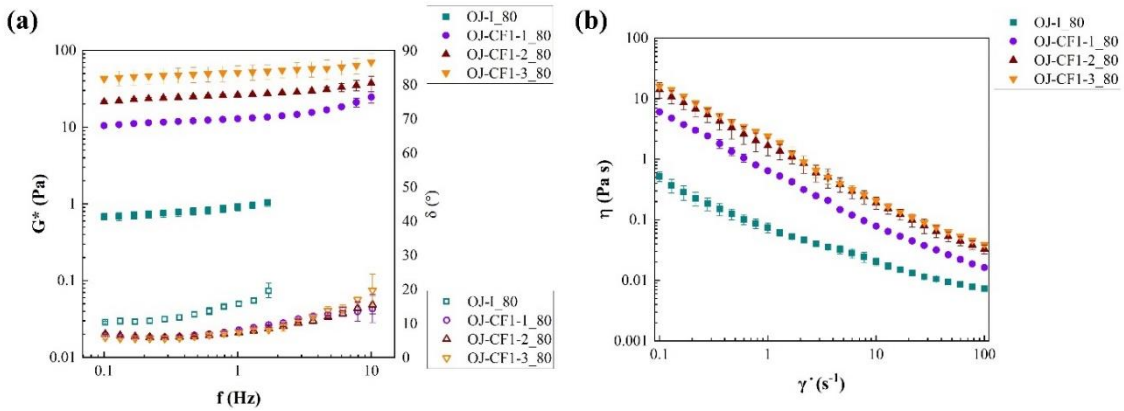

Fig.2. Rheological properties of samples at different blending ratios: (a) complex modulus (filled symbols) and phase angle (empty symbols) and (b) viscosity.

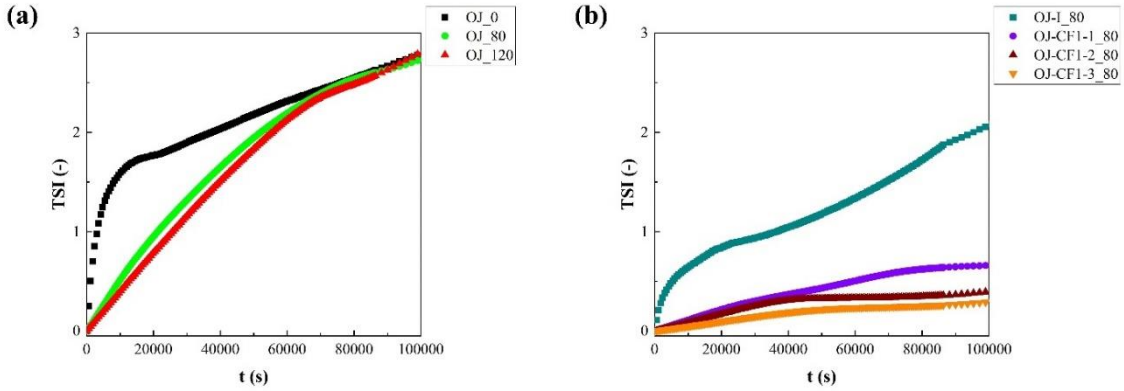

Fig.3. Destabilization kinetics at 24 h: (a) TSI of sample produced with different pressure and (b) TSI of sample produced with different blending ratio.

3.2. *Physical chemical properties of orange juice samples*

Physical-chemical properties of orange juice samples are reported in Tab. 3. The values of pH and water activity suggest they are independent from blending ratio, pressure and fiber type and an average value of pH of 3.74 ± 0.02 and water activity of 0.962 ± 0.004 (-) are representative of all the produced systems. In addition, no statical differences were found in pH and activity values between the produced samples and the benchmarks, as reported by the ANOVA analysis.

Similarly, no differences were found comparing the lightness, L*, of samples and benchmarks. The other color parameters, the red/green axis, a*, and the yellow/blue axis, b*, depend on processing and composition of the system. Specifically, the presence of inulin/citrus fiber in the orange juice decreases the red and yellow component of the color of samples. Indeed, orange juice with fibers showed values slightly lower in a* and b* than

that of unstructured samples. However, color is not affected by pressure since there are no differences within the unstructured samples produced with different homogenization pressure. Furthermore, no differences related to fiber type can be appreciated as suggested by the statistical analysis.

For homogenized samples without fibers, values of L*, a* and b* were approximately 55.6 ± 1.8 (-), -6.3 ± 0.2 (-) and 38.1 ± 2.0 (-) respectively, whereas for samples structured with inulin/citrus fiber blends the same parameters were found equal to 54.1 ± 1.7, -6.9 ± 0.1 and 31.8 ± 1.7. Looking at the color parameters associated with benchmarks B1 and B2, it is possible to observe that b* value is higher (double) than that of the samples; however, it is reasonable to assume that this parameter is more related to the color of the starting concentrate rather than to homogenization processing and to fiber addition.

The images of orange juice samples produced with different pressure, blending ratio and citrus fiber type are reported in Fig.4a-c. As can be observed, it is not possible to detect substantial differences in the appearance and quality of the samples by visual inspection.

Sample ID	L*	a*	b*	pH	Water activity
OJ_0	57.1 ± 1.6^{a}	-6.2 ± 0.1^{a}	38.7 ± 1.2^{a}	3.74 ± 0.01^{a}	0.955 ± 0.004^{a}
OJ_80	55.0 ± 0.6^{a}	-6.30 ± 0.06^{a}	38.4 ± 0.7^{ad}	3.76 ± 0.01^{a}	0.959 ± 0.002^{a}
OJ_120	54.8 ± 1.7^{a}	-6.4 ± 0.1^{a}	37.3 ± 2.5^{acd}	3.75 ± 0.01^{a}	0.962 ± 0.004^{a}
OJ-I_80	55 ± 3^{a}	-6.6 ± 0.1^{ab}	35.0 ± 1.7^{acd}	3.75 ± 0.03^{a}	0.963 ± 0.003^{a}
OJ-CF1-1_80	53 ± 1^{a}	-6.8 ± 0.2^{bc}	30.8 ± 1.1^{b}	3.71 ± 0.01^{a}	0.960 ± 0.003^{a}
OJ-CF1-2_80	53.5 ± 0.3^{a}	-6.9 ± 0.1^{bc}	30.8 ± 0.7^{b}	3.73 ± 0.01^{a}	0.964 ± 0.002^{a}
OJ-CF1-3_80	52.6 ± 0.8^{a}	-7.0 ± 0.1^{c}	30.2 ± 1.3^{b}	3.74 ± 0.01^{a}	0.964 ± 0.001^{a}
OJ-CF2-1_80	53.6 ± 1.7^{a}	-6.81 ± 0.02^{bc}	33.4 ± 1.8^{abcd}	3.74 ± 0.02^{a}	0.963 ± 0.003^{a}
OJ-CF3-1_80	54.4 ± 1.8^{a}	-6.83 ± 0.03^{bc}	33.5 ± 2.5^{abcd}	3.75 ± 0.03^{a}	0.967 ± 0.003^{a}
OJ-CF4-1_80	55.2 ± 1.6^{a}	-6.89 ± 0.03^{bc}	32 ± 1^{bcd}	3.74 ± 0.02^{a}	0.963 ± 0.001^{a}
OJ-CF5-1_80	56 ± 3^{a}	-6.90 ± 0.04^{bc}	32.5 ± 1.2^{bcd}	3.75 ± 0.03^{a}	0.960 ± 0.001^{a}
B1	50.7 ± 1.6^{a}	-3.00 ± 0.02^{d}	33.9 ± 1.6^{bcd}	3.74 ± 0.02^{a}	0.961 ± 0.007^{a}
B2	55.8 ± 0.7^{a}	-3.76 ± 0.03^{e}	32.5 ± 0.9^{bcd}	3.76 ± 0.04^{a}	0.962 ± 0.005^{a}

Tab.3. Physical-chemical properties of orange juice samples. Different letters, for the same parameters, refer to significantly different values.

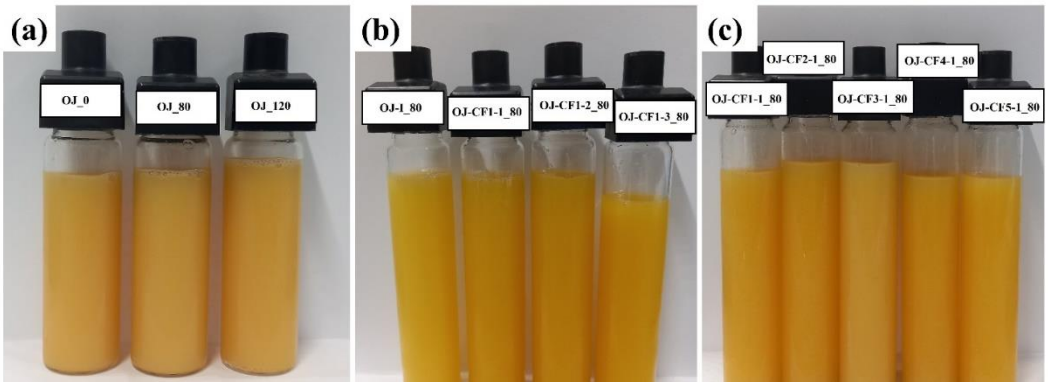

Fig.4. Picture of orange juice samples: (a) samples produced with different pressure, (d) samples with different bland ratio, (c) samples produced with different type of citrus fiber.

3.3. Rheology of homogenized orange juice with different types of citrus fibers

The consistency and structuration of orange juice samples with different types of citrus fiber and benchmarks are reported in Fig 5a. and Fig.5b, respectively. All samples exhibited weak gel behavior and sample OJ-CF4-1_80 showed a slightly lower consistency and structuring compared to that of other samples.

A shear thinning behavior was found for samples with different types of fibers as reported in Fig. 6a and Fig. 6b. No substantial differences in the flow behavior were found between samples with the different fibers as reported in Fig.6 in terms of steady state viscosity.

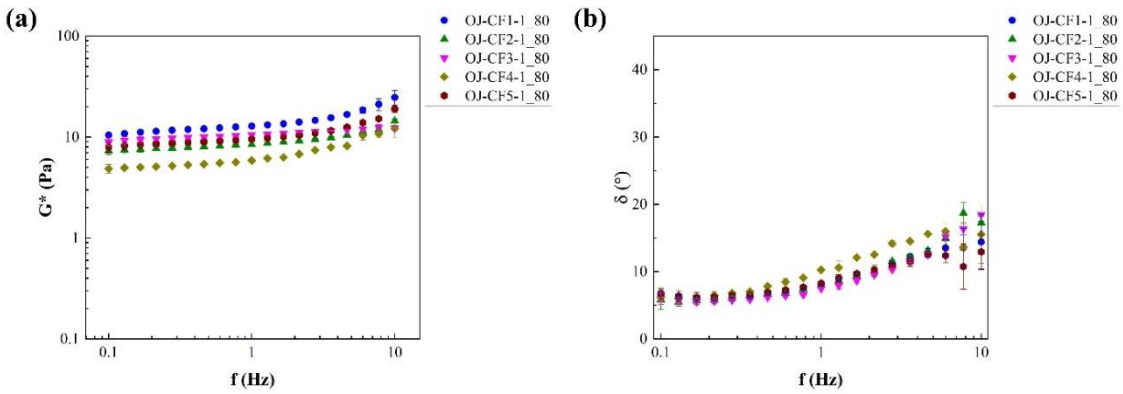

Fig.5. Frequency sweep test of samples with different types of citrus fiber: (a) complex modulus and (b) phase angle

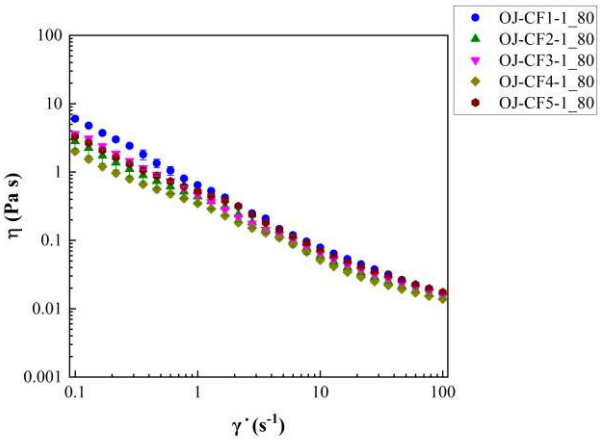

Fig.6. Steady state flow of samples with different types of citrus fiber.

3.4. Physical stability of homogenized orange juice with different types of citrus fibers

From Fig.7a. it is possible to observe that all the samples enriched with fiber exhibited a higher stability ($TS < 3$) within 72 h whereas the benchmarks showed higher values, around 6.5 for B1 and 9.5 for B2. This notable difference in physical stability is practically due to the networking action of the citrus fiber in the formulation, although as already discussed, modest improvement of the stability can be associated to homogenization process and to inulin thickening action.

Comparing the destabilization kinetics of benchmarks with (B1 and B2) and without (B1* and B2*) the thermal treatment used to limit the microbiological instability (Fig.7b), it is possible to conclude that the thermal treatment does not exert relevant changes in the transmission/backscattering profile during time.

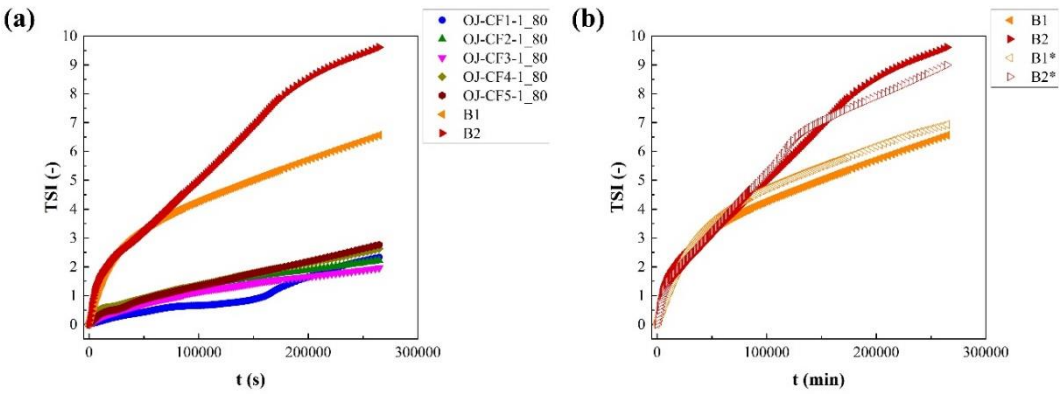

Fig.7. Destabilization analysis of orange juice samples: (a) destabilization kinetic of samples and benchmarked 72 h and (b) effect of thermal treatment on destabilization kinetics of benchmarks.

3. Conclusion

Orange juice samples with improved physical stability and nutritional profile were successfully produced by dilution of concentrated juice, fiber addition and high-pressure homogenization treatments.

Homogenization process increases consistency, modifying the system behavior form liquid-like to solid like, but not viscosity and physical stability. The fiber addition allows the production of consistent, viscous and physically stable juices. Stable systems can be obtained starting from the lowest citrus fiber fraction, and an increase of citrus fiber fraction in the fiber blend led to a relevant increase of consistency and viscosity of stable samples. The physical chemical parameters of samples such as pH and water activity resulted independent from process and composition. The color of samples turned out to be dependent on compositions, but it is comparable to commercial benchmarks. No substantial differences were found in the viscoelasticity and flow behavior of orange juice samples produced with different types of citrus fiber. According to Turbiscan analysis, the homogenized and fiber-added samples resulted stable in contrast to benchmarks. It is worth mentioning that homogenized orange juice samples with different citrus fiber were sent to external analysis, to a specialized laboratory, for the evaluation of commerciality and acceptability and all were found suitable for marketing and consumption.

Assessment of consistency, structuring and stability of clean label vegan mayonnaise stabilized by citrus fiber and plant proteins

Abstract

The present work represents a scientific report containing an industrial application of citrus fiber in a biphasic food system, in particular a plant-based mayonnaise. The research activities were carried out in the laboratory of JRS Silvateam Ingredients s.r.l. during the internship held from 15/01/2024 to15/10/2024 and concerns the rheological and stability characterizations of vegan mayonnaise structured with citrus fiber and different types of plant proteins.

1. Introduction

Mayonnaise is one of the most consumed sauces. From a physical point of view, it is a biphasic system, typically stabilized by egg proteins, consisting of a dispersed phase of oil droplets, surrounded by a water-based continuous phase.

Recently, consumers are more oriented towards consumption of plant-based products, including mayonnaise, and food companies are investigating the design of vegan formulations, i.e., without eggs. This yields the need to use either emulsifiers or vegetal protein. Although, emulsifiers are typically much more effective than plant protein in reducing interfacial tension, the use of plant protein allows the improvement of the nutritional profile and utilization of the claim “clean label”. Moreover, as discussed in previous chapters, biphasic systems can be effectively stabilized by the addition of citrus fiber that is able to modify both the bulk and the interfacial rheological properties of these systems further improving the nutritional profile of the final product.

Therefore, starting from the results obtained in simple biphasic systems (i.e. oil water, emulsifier and fiber), in the present work, clean label vegan mayonnaises stabilized by plant proteins and citrus fiber were produced and characterized. Specifically, three plant proteins were used: pea protein, carob protein and Tara germ.

In addition to the taste, the quality control and the development of mayonnaise formulation is strictly related to the texture, appearance and commercial stability. For these reasons rheological and stability evaluations are necessary for the industrial development of such a product.

Frequency sweep tests were carried out with the aim of investigating the microstructure of mayonnaise samples, while their flow properties were evaluated by steady state flow tests. Dynamic temperature ramp test was used to evaluate the effects of temperature on sample microstructure. Finally, the stability of samples was assessed by multiple light scattering methods by monitoring the sample for a given time and at different temperatures.

2. Material and methods

2.1. Samples

Different samples, named M1 M2 and M3 (see table 1), of vegan mayonnaise were prepared according to a base formulation, proposed by the company, and using the food processing systems Qbo3540 (Roboqbo, Italy). Owing to confidentiality agreements on company procedures, the exact adopted method cannot be reported in detail, whereas the list of the ingredients other than water is provided in table 1. In particular, samples were prepared using sunflower oil (De Santis, Italy), vinegar (Ponti, Italy), sugar (Eridania, Italy), salt (Italkali, Italy), pea protein (Ingredion, USA), carob protein (LBG Sicilia, Italy), Tara germ (JSR Silvateam ingredients, Italy), Citrus fiber (JSR Silvateam ingredients, Italy) and soluble native starch (Ingredion, USA).

	M1	**M2**	**M3**
Ingredients	**% w/w**		
Fats (sunflower oil)	50	50	50
Carbohydrates	8	8	6.5
Sugar	5	5	5
Salt	1.2	1.2	1.2
Plant Protein	1.5	1.5	0.5
Pea protein	*1.5*	-	-
Carob protein	-	*1.5*	-
Tara germ	-	-	*0.5*
Fibers	***0.8***	***0.8***	***0.8***
Citrus fibers	*0.8*	*0.8*	*0.8*

Tab1. Sample ID and composition.

According to results obtained during the characterization of simple biphasic systems through microfluidization, mechanically stable samples were obtained already at 0.55% w/w of fiber in water, in an emulgel miming a light mayonnaise with 26% w/w of fats. However, according to the industrial knowledge and previous preliminary tests developed in the R&D laboratory of the company, taking into account that the present samples have higher fats

(oils) content and that the effectiveness of Qbo3540 food processing system is lower than that of microfluidizer, the amount of fiber was fixed at 0.8% w/w on the total amount of emulsion. In a similar way, on the basis of preliminary industrial internal tests, the amount of soluble native starch and protein (Tara germ) in sample M3 were than those of samples M1 and M2.

2.2.Rheological characterization

Rheological tests were carried out with MCR 102e rheometer (Anton Paar, Austria) equipped with parallel sandblasted plate geometry (diameter 50 mm, gap 1.2±0.1) and Peltier system for temperature control. Frequency sweep tests were carried out, in linear conditions previously determined by amplitude sweep test, in the frequency range 0.1 – 10 Hz. Flow curve tests were carried out in the shear rate range of 0.01 – 100 s^{-1}. Both frequency sweep test and flow curve measurements were carried out at 25 °C. Whit the aim of investigating the rheological stability of samples as a function of the potential temperature fluctuations during shipping and storage, cyclic dynamic temperature ramp tests were carried out at 1 Hz in linear conditions decreasing the temperature from 25 °C to 5 °C, then increasing the temperature up to 45 °C and finally by cooling the sample down to 25 °C. Adopted ramp rate was 4 °C/min, in absolute value, for all steps. The lower and upper temperatures were chosen according to the information provided by the company as the minimum (5 °C) and maximum (45 °C) temperature to which the mayonnaise can be subjected during shipping and storage.

2.3. Multiple light scattering analysis

The physical stability of samples was evaluated using Turbiscan Tower (Formulaction SAS, France). Data were interpreted in terms of destabilization kinetics, i.e., by monitoring the Turbiscan stability index (TSI) defined according to Eq.1.

$$TSI = \sum_{i} \frac{\sum_{h} |scan_i(h) - scan_{i-1}(h)|}{H} \quad (1)$$

where $scan_i(h)$ and $scan_{i-1}(h)$ are the values of the profile for a given scan "i" and the previous one "i-1" assessed at a given height "h", respectively, whereas H is the total height of the sample. With the aim of determining stability over time, samples were monitored for 48 h by scanning them every 30 min. It is expected that sample temperature can change during storage and shipping, therefore, to further investigate the potential mechanical

stability of samples during these steps, tests were performed also at the lowest and greatest expected temperatures, i.e. 5° and 45°C, chosen according to company experience. Therefore, TSI was determined by monitoring the sample for 3 h at 5 °C and 45°C, the profile was scanned every 30 min and the TSI values were averaged with the aim of having a single representative value of TSI for each temperature (5°C and 45°C). In a similar way TSI at 25°C was determined within the first 3 h, to have a representative value of TSI at 25°C. An equilibration time of 30 min at each temperature was used before measuring.

3. Results

3.1. Dynamic behavior

The results of frequency sweep tests, in terms of complex modulus and phase angle, are reported in Fig.1a and Fig.1b, respectively. All samples exhibited a solid-like behavior, with a phase angle close to 10°, suggesting a weak gel behavior typical for such food systems. From Fig.1a. it is possible to see that carob protein increases consistency more than pea protein, but Tara germ resulted the most effective in increasing G*, even if it is present in lower amounts with respect to other proteins. Furthermore, it also slightly increases the structuring degree as can be seen from Fig.1b where a lower value of phase angle can be observed.

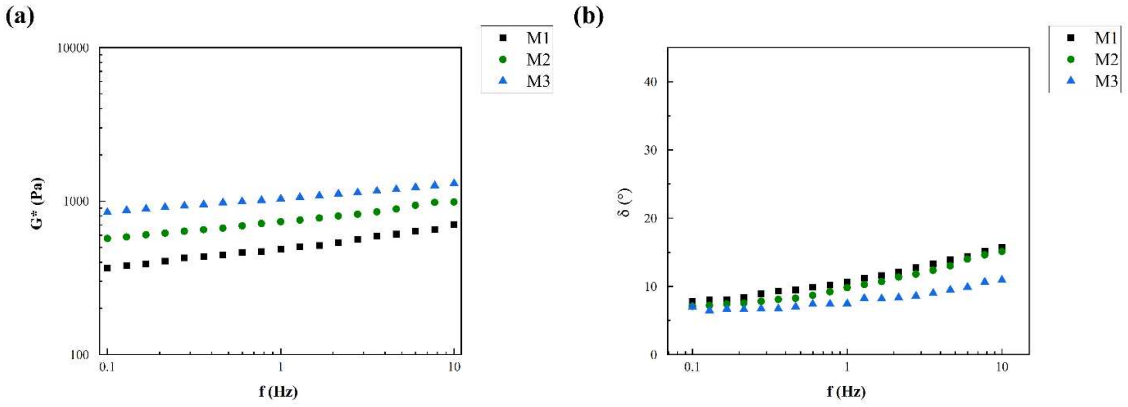

Fig.1. Frequency sweep test of vegan mayonnaise samples: (a) complex modulus and (b) phase angle.

3.2.Flow behavior

The result of steady state flow tests, in terms of viscosity, is reported in Fig.2. Shear thinning behavior was observed for all samples, although some differences arise, depending on the

formulation, indeed M1 and M2 have similar flow behavior and almost overlap, whereas sample M3 showed a different trend. In particular, it exhibits a more shear thinning behavior. It is worth noticing that for samples M1 and M3 the onset of Newtonian plateau can be observed, with M3 exhibiting a higher value of zero shear viscosity, in agreement with results obtained in small amplitude oscillations; on the other hand, for sample M3 it was not measured, probably owing to experimental issues.

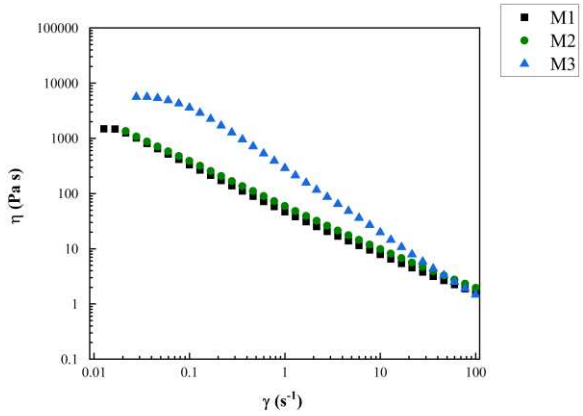

Fig.2. Steady state flow test of vegan mayonnaise samples

3.3. Temperature behavior

The results of temperature ramp tests of all samples, in terms of complex modulus and phase angle, are reported in Fig. 3a and Fig. 3b, respectively. Sample M3 is more consistent and structured than M2, which in turn is more consistent and structured than M1, in the whole range of temperature, whereas the phase angle follows the opposite trend since M3 resulted in the most structured sample. During the first step, cooling the sample from 25°C to 5°C, G* slightly increases, the subsequent heating from 5°C to 45°C leads to a slight decreasing of G*, during the last cooling from 45°C to 25°C the complex modulus increases again as can be seen from Fig.3. Looking at the G* data it is possible to conclude that the changes in consistency due to the imposed thermal process (cooling/heating/cooling at 4°C/min, between 5-45 °C) is reversible since cooling and heating curves are overlapped. Phase angle remains almost constant with temperature for all the samples as reported in Fig.3b, where it is shown that cooling and heating curves are overlapped. These results suggest that the samples do not experience irreversible transitions, within the temperature range investigated, and therefore mechanical stability can be expected.

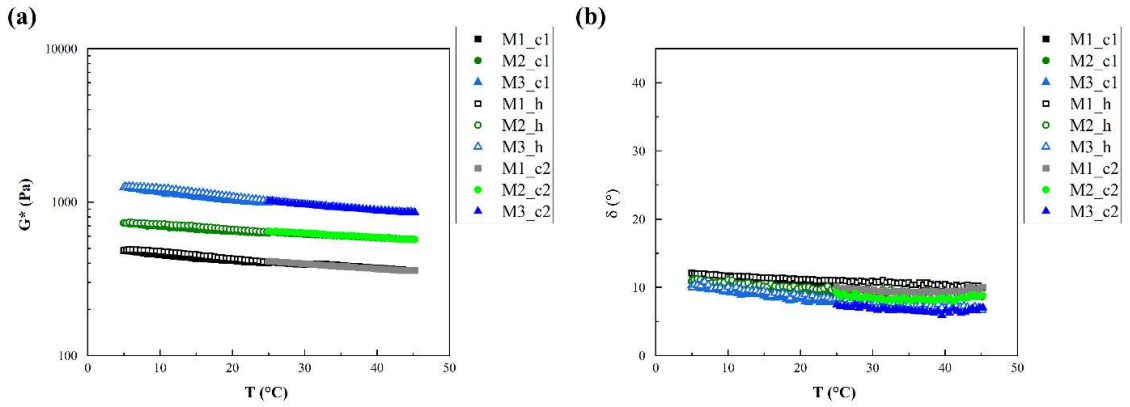

Fig. 3. Time cure test of vegan mayonnaise samples: (a) complex modulus and (b) phase angle.

3.4.Destabilization kinetics

Turbiscan destabilization kinetics, i.e., the TSI as function of time, of mayonnaise samples is reported in Fig.4a. All systems are very stable, according to the criteria suggested by Turbiscan manufacturer (Formulaction, Application note- Quantify stability with TSI scale), since TSI was lower than 0.5 within 48 h was found, independently of the formulation. Sample M3 seems to be the most stable since measured values are lower than those obtained for M2 and M1.

Aiming at better highlighting the differences in physical stability among the samples, the effect of temperature on TSI was investigated and it is shown in Fig.4b.

It is worth noticing that at low temperature (4° and 25°C) differences are not relevant (data almost overlap with the adopted scaling) whereas at 45°C differences seem more evident, and sample M3 seem the most stable with TSI = 3.1, followed by M2 with TSI = 4.2 and M1 with TSI = 4.4. It is worth noticing that the stability trend (see Fig.4a and, more evidently, Fig.4b) is in agreement with the consistency/structuration trend, in particular, the greater the consistency and the structuring degree (high G* and low δ) the greater the physical stability (low TSI).

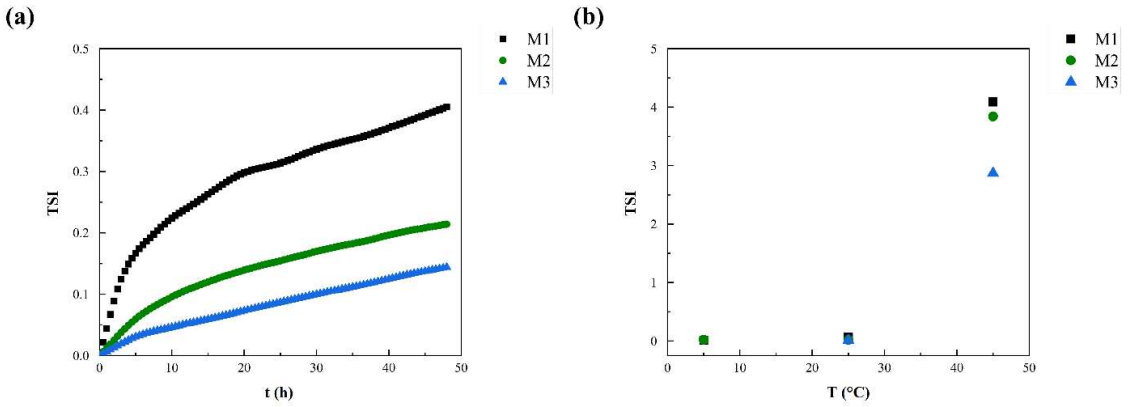

Fig. 4. Destabilization kinetics of vegan mayonnaise: (a) Turbiscan stability index during 48 h at 25°C and (b) Turbiscan stability index during 3 h at different temperatures.

4. Conclusion

Vegan mayonnaise containing pea protein, carob protein and Tara germ and structured with citrus fiber were successfully produced. Rheological tests such as frequency sweep test, steady stare flow test and temperature ramp test were carried out, resulting in very effective methods for the evaluation of the consistency, the viscosity and the effects of temperature on consistency. In addition, the destabilization kinetics and Turbiscan Stability Index at different temperatures offer powerful and objective tools in the investigation of physical stability of mayonnaise samples. Among all, samples with Tara germ exhibited the highest consistency, structuring degree and stability, although this protein is present in lower amounts with respect to proteins used in other samples.

CONCLUSIONS

The technological aspects related to the engineering and processing of food systems containing insoluble dietary fiber, such as that obtained from the industrial recovery of citrus peels, are receiving considerable interest from the scientific community. This interest is based on the already proven physiological benefits induced by fiber and, on the other hand, the interest in using a food ingredient able to meet the criteria of circularity and sustainability.

Dietary fiber obtained from the recovery of citrus processing by-products has proven to be a functional ingredient with a relevant ability to structure both monophasic and biphasic food systems. This ability has been observed and studied by varying different conditions, typical of the food industry, such as the presence of solutes and oils phases, the effect of temperature and the influence of processing methods. Matrices of both academic and industrial-commercial interests were analyzed into detail by rheological and physicochemical methods.

In water-based formulations, the solutes affect the interaction between citrus fiber and water, decreasing its structuring ability. As a consequence, in the applications in which a targeted consistency is requested, an extra-dosage of citrus fiber could be required in the product compared to that estimated by considering the neat fiber-water systems.

Biphasic systems structured with citrus fibers can exhibit a wide spectrum of morphologies (O/W systems, bi-continuous microemulsions, Pickering emulsions) and rheological properties linked to the consistency of single phases (emulgels, bigels) that depend on the composition, the presence of different agents in the oil phase (emulsifier, organogelator) and the processing conditions. Each of these systems has specific microstructural and rheological properties yielding the possibility to meet a wide range of consumers needs regarding consistency and texture.

Biphasic systems for food use, such as emulgels structured with citrus fiber, can be modelled from a rheological perspective, i.e., in terms of consistency, by using the different theories on the modelling of composite gels. The simultaneous modeling of monophasic (hydrogel) and biphasic (emulgel) systems, structured with fiber, allows the development of equations capable of predicting the amount of fiber known the texture of reference food systems. These models provide good accuracy in the reproduction of the texture of commercial biphasic food products, like light mayonnaise and light spreadable cheese. It is worth highlighting that for a deep rheological modelling a careful analysis of the microstructural properties is necessary, because of some difficulties in properly selecting an experimental (mean) diameter suitable for the representation of the value of droplets radius in the model .

Nowadays, different types of commercial foods are currently structured with citrus fibers, indicating good structuring ability. In particular, it is successfully employed in the formulation of both water-based and biphasic food products by effectively conferring texture and stability. It is worth to mention that its use as ingredient in food products is driving toward the most searched nutritional and marketing claims like “source of fiber”, “rich in fiber”, “clean label”, “vegan”, “plant-based”, “low calories”, “light”, “low-fat”, “fat-reduced” and so on. Furthermore, regarding industrial research, it is possible to say that the objectives are mainly oriented to the application of citrus fiber in mixture with other food ingredients like other dietary fiber or plant protein. Finally, it is worth noticing that, currently, the R&D sector of the food industry makes use of advanced characterization techniques and protocols such as rheological and stability analysis, especially in the field of new food product development.

SCIENTIFIC CONTRIBUTIONS

Publication in International Peer Reviewed Journals

- Bruno E., Lupi F.R., Mammolenti D., Baldino N., Gabriele D. Development and rheological characterization of dietary fiber and policosanol plant-based bigels for potential food applications. Food Hydrocolloids. 150 (2024) 109733, https://doi.org/10.1016/j.foodhyd.2024.109733.
- Bruno E., Lupi F.R., Mammolenti D., Mileti O., Baldino N., Gabriele D. Emulgels Structured with Dietary Fiber for Food uses: A Rheological Model. Foods. 11 (2022) 3866. https://doi.org/10.3390/foods11233866.

Publication in Book of Abstract of National and International Conferences

- Mammolenti D., Bruno E., Lupi F.R., Mileti O., Baldino N., Gaudio D., Cupone V., Gabriele D. Rheological properties of dietary fiber suspensions as a function of water solutes, XVIII National conference of Italian Society of Rheology – SIR, Capri Island, Naples (Italy), September 12-14, 2024.
- Mammolenti D., Mileti O., Bruno E., Lupi F.R., Baldino N., García M. C., Muñoz J., Gabriele D. Rheology of microfluidized emulgels structured with citrus fiber, XVIII National conference of Italian Society of Rheology – SIR, Capri Island, Naples (Italy), September 12-14, 2024.
- Alfaro M.C., Prieto P., García M.C., Mammolenti D., Lupi F.R., Baldino N., Gabriele D., Muñoz J. Ingeniería del producto para el disegño de emulgel formulados como salsa finas estructuradas por fibras alimentarias microfluidizadas (Spanish language), XXXVII Jornadas Nacionales de Ingeniería Quimica, Castellón (Spain), September 13-15, 2023,178-181.
- Mammolenti D., Bruno E., Lupi F. R., Baldino N., Gaudio D., Cupone V., Gabriele D., (2023), The influence of extrinsic factors on rheological properties of citrus fiber suspensions, XIX International Congress on Rheology – ICR 2023, Athens (Greece) July 29-August 4, 2023, 492.
- Bruno E., Lupi F. R., Mammolenti D., Mileti O., Baldino N., Gabriele D., (2023), Emulgels structured with dietary fiber: a rheological model, XIX International Congress on Rheology – ICR 2023, Athens (Greece) July 29-August 4, 2023, 491.

- Bruno E., Lupi F.R., Baldino N., Mammolenti D., Marino R., Gabriele D., (2022), Studio di bigel per applicazioni alimentari (Italian language), XVII National conference of Italian Society of Rheology – SIR, Genoa (Italy), June 19-22, 2022, 99-101.

Under submission to International Peer Reviewed Journals

- Mammolenti D., Lupi F.R., Bruno E., D'Agostino A., Mileti O., Baldino N., Gabriele D.; Impact of solutes and temperature on rheological and microscopic properties of particle gels from insoluble citrus-derived dietary fiber, submitted in Food Research International

Submission to International Conferences

- Mammolenti D., Bruno E., Lupi F.R., Baldino N., García M. C., Muñoz J., Gabriele D. Microfluidized hydrogels and emulgels structured with citrus fiber: effect of process conditions on rheology and microstructure, Annual European Rheology Conference (AERC) 2025 – ESR, Lyon (France), April 14-17, 2025.
- Mammolenti D., Mileti O., Bruno E., Lupi F.R., Baldino N., García M. C., Muñoz J., Gabriele D. Rheology of biphasic systems structured with dietary fiber, Annual European Rheology Conference (AERC) 2025 – ESR, Lyon (France), April 14-17, 2025.